Dynamics et thermodynamics of the NJL Lagrangian

David Fuseau

DOCTORAT MATIERE BRETAGNE MOLECULES LOIRE ET MATERIAUX

UNIVERSITÉ DE NANTES

THESE DE DOCTORAT DE

L'UNIVERSITE DE NANTES

ECOLE DOCTORALE N° 596
Matière, Molécules, Matériaux
Spécialité : Physique des particules, physique hadronique

Par
David FUSEAU

Dynamique et thermodynamique du Lagrangien NJL

Thèse présentée et soutenue à Nantes, le 09/11/2020
Unité de recherche : UMR6457

Rapporteurs avant soutenance :

Hubert Hansen	Maître de Conférence, Université Claude Bernard Lyon 1
Oleg Teryaev	Directeur de recherche, JINR Dubna

Composition du Jury :

Président :	Gines Martinez	Directeur de recherche, SUBATECH Nantes
Examinateurs :	Elena Bratkovskaya	Professeur, Université Goethe Francfort
	Pol Gossiaux	Professeur, IMTA, Nantes
Dir. de thèse :	Joerg Aichelin	Professeur, Université de Nantes

Table of Contents

Remerciements

Je remercie le CNRS et la région Pays de la Loire pour avoir financé ma thèse.

Je remercie les membres de mon jury de thèse Hubert Hansen, Oleg Teryaev, Elena Bratkovskaya, Pol-Bernard Gossiaux et Gines Martinez, pour les échanges pertinents lors de ma soutenance de thèse et des corrections post-soutenance qui m'ont permi d'avancer encore un peu plus sur la voie infinie de la compréhension de la QCD et des modèles effectifs, ainsi que mon encadrant Joerg Aichelin pour toute la liberté qu'il m'a laissé dans la conduite de ce travail et sa bonne humeur quotidienne. Je remercie doublement Elena et Hubert pour leur travail de membre CSI.

Je remercie les membres du laboratoire SUBATECH avec qui j'ai pu partager beaucoup, que ce soit lors des journées du labo ou des animations de vulgarisation (Fête de la science, nuit blanche des chercheurs). J'en profite pour remercier l'équipe com Richard, Farah, Tanja, Lilian, Jesus, Johhhhhannes, Bugnon, on s'est bien amusé à gonfler et monter tous ces ballons !! et les filles de l'administration et particulièrement Stéphanie, Séverine, Tanja, Farah, Sophie et Sophie pour avoir débloqué mon badge d'entrée (14 fois), ferraillé pour que j'ai mes contrats d'enseignements... Je joins à ces remerciements les gars du basket, du foot, du bad. C'était vraiment une super ambiance, on a bien rigolé tous ces midis, ça défoulait vraiment de la thèse !! Et pour les bières du basket, même si on y a jamais vu Kheops et ses nems légendaires..

Je remercie les membres du groupe théorie avec qui j'ai pu beaucoup interagir, apprendre énormément de choses plus ou moins reliées directement à mon sujet, mais qui m'ont beaucoup aidé dans la critique de mon travail et dans la production de ma recherche.

Je remercie le groupe des thésards, parce qu'on est rien sans l'espwit d'équipe et pour la bonne humeur générale pendant ces trois années de thèse: Loic Le Meur, Alexandre Parent du Châtelet, Pierre Moreau, Charmou, Ophélie Bugnon, Chloé, Kevin Micheneau, Dennys Arrebato Villar, Maria Stefaniak, Etienne Nigron, Flavien Ralite, David Hénaff, le Planck pour son soutien à la cause, Manu, Erwann, Loic Virone, Jesus, Johhhhannes, Claudia, La secrétaire, Michael, Mahbobbeh, Parastoo, Emeline, Anne-Laure, Anto, Rita, Thomas Lipreau, Yajing, Yuwei, Nathan et des postdoc, stagiaires que j'ai eu la chance d'encadré ou pas, Laurine, Jules, Manon l'alsacienne, Axel, Hugo, Benjamin, Ayoub, Thomas, Laurence, Fabien, François, Arthur (Bon anniversaire)... Je remercie chaleureusement Hamza Berrehrah et Rudy Marty pour tout ce que vous avez fait pendant ma thèse !! Je finis par le quatuor final du bureau, le magic 4 qui tenait éveillé Subatech jusqu'au bout de la nuit avec les battle du DJ psi Roland le chauvin jambon-beurre-rotteur et son rnb cambodgien opposé aux punchline du pizzaYollo trappiste Goigré

arbitré par Stéphane (le meilleur prof de Zumba) qui delormalisait la situation quand le tout commencait à diverger, et mes deux compagnons d'aventures Cougoulitch le croate et le chevelu greco-chti-champenois du cirque péruvien unique Gebrieul Sophys avec qui ont allé chasser le Graaaaand Theta+ avec une couillère, un marteau et un interprète. Après avoir affronté les ptits monsieurs sympathique, les caniches enragés, la Lorraine, les tacos XL (plus jamais !) et les 14000 relectures de mon manuscrit, l'histoire se cloture. Enfin le tome 1, dans le tome 2 à venir, il parait qu'il y aura beaucoup de pheuseuk !! Un gros merci aux potals des quatre coins de la France, François et les Traisnels, Cloé nianiania, Hernande, Marco, Mike Pons pour leur coup de pouce sur le manuscrit, avoir tenté de venir à la soutenance puis, faute de pouvoir venir, se l'être infligé en visio !!

Et enfin, je remercie mes parents et mes soeurs, pour m'avoir supporté à raler pendant toutes ces longues années universitaires et particulièrement les trois dernières et m'avoir pourtant toujours encouragé. Un soutien sans faille qui m'a vraiment porté dans cette longue dernière ligne droite qu'est la dernière année, le manuscrit et la soutenance. Merci.

Introduction

The title of this thesis is a quite short one and summarises very well the idea of this work: study an effective model for the strong interaction and explore how it can be improved and how it allows to better understand the strongly interacting matter. The world of particle physics have to reach very high energy to create new types of particles which are very rare and are not even observable naturally on earth. There are natural sources of such particles like cosmic rays, but also artificial ones like heavy ion collisions. The study of the strong interaction and the theory which describes it known as Quantum ChromoDynamics (QCD) are linked to the field of heavy ion collisions. Since the birth of QCD in 1973, heavy ion collisions have been performed to collect data which have been confronted with the predictions leading to a better understanding of QCD. Most experiments produce matter at very high energy, especially since the construction of the Large Hadron Collider (LHC) at CERN. The experiments at this collider have improved our understanding of the QCD matter at high temperature and small baryonic density, commonly known as the early universe matter. The way the matter behaves when it gets hot and dense requires the knowledge of the T and μ phase diagram of strongly interacting matter.

Nowadays, the trend is to decrease the energy of the collisions which decreases the temperature of the medium but increases its baryon density. Russia is building the NICA collider specialised to the study of compact matter, Germany is extending the already existing GSI accelerators into the FAIR accelerator to be at the edge of what technology can offer to study the dense phase of matter. Also the USA and Europe are running projects like the Beam Energy Scan (BES) program at RHIC or are using the old SPS collider at CERN to reach this area of the QCD phase diagram. In comparison to what was done previously for the early universe study where $\mu = 0$, these new accelerators will explore the T-μ plane. In other words, there are plenty of places to look at. Under those conditions, experiments need theoretical predictions in order to identify the region which merit detailed investigations.

However it is not the whole phase diagram of matter which can be covered experimentally and theoretically at the moment. In this kind of situation, effective models are useful. All along this work, it will be shown that, even though they are approximative models of QCD whose results have to be carefully studied, they are the only eyes one has at the moment through which one sees a quite important part of the phase diagram of strongly interacting matter and even though they are weaker than the so called first principles theories like perturbative QCD (pQCD) or Lattice QCD (lQCD), they must be

treated with respect for what they brought to this domain of research.

Those effective models usually cover a small part of the phase diagram according to the domain of validity of the approximations which are made. In this validity range, their results must match the experimental data or the theoretical predictions made by more consistent theories in order to prove they are trustworthy. In this work, the mathematical and physical formalism and formulas that will be used all along this thesis will be presented first, followed by a presentation of QCD and the tools to study it: pQCD and lQCD. Then, the model (P)NJL will be introduced as it is one of the few models capable of describing a medium with quark degrees of freedom at low temperature and finite chemical potential with a Lagrangian that has almost the same symmetries as the QCD Lagrangian. The first task will be to find possible improvements in order to match the results of lQCD, and especially its equation of state, at vanishing chemical potential. Then it will be possible to extend those results to a finite chemical potential and to make predictions of the phase transition of the QCD matter at large densities. After this work is done, the equation of state will be ready to be used for calculating the transport coefficients of the QGP at finite temperature and chemical potenial and to study dynamically the thermalisation of a QGP and its transition to a hadron gas occurring through a first order phase transition.

Part I

QCD and its low energy effective model NJL

Chapter 1

Group theory, thermodynamics and field theory

This first section is the opportunity to present a non standard formalism of group theory known as birdtracks. This diagrammatic representation of the group theory is introduced for two purposes. First to derive the Fierz transformation, the decomposition of the tensor product of the fundamental representation and its conjugate into its different irreducible representations. This will be done for the Special Unitary group SU(N) (especially in the case N = 3 giving the application for colour and flavour space) and the Dirac group. The Fierz transformation will be used in section 3.B.3 to build the Lagrangian of the Nambu-Jona-Lasinio model. The second purpose is to make connexion with another formalism, the Young Diagrams, which are a fast way of making the tensor product decompositions involved in the construction of the baryons. In addition, basic concepts and formulas of thermodynamics and finite temperature field theory are stated, waiting to be used in the main corpus.

1.A Group theory with birdtracks for SU(N)

This section emphasises a formalism of group theory not very spread in the community, although more natural for particle physicists than what can be found in standard textbook: the birdtracks [1]. The birdtracks are a diagrammatic approach of group theory and are particularly useful for color counting involving a massive (up to some points however) amount of internal gluons, because more visual than the usual algebraic calculations. Building our birdtracks interpretation of SU(N) starts from looking for primitive invariants of our vector space. Primitive invariants are a minimal list of the invariants required to describe a symmetry group. For SU(N), one wants to preserve the norm of the scalar product. The primitive invariant is then the Kronecker delta $\delta^a{}_b$ [1] with the convention of a being the index in and b being the index out. In diagrammatic representation, the Kronecker delta is a line:

Fig. 1.1: Diagrammatic notation of the Kronecker delta or fundamental representation

Let's take for example the tensor product of the defining space and its conjugate $V \otimes \bar{V}$, where V is a N_c-dimensional complex vector space in the fundamental representation. The fundamental representation is represented by a line, see Fig. 1.1. Its conjugate is also

represented by a line, but the arrow is in the other way. There are two invariant matrices that can be constructed from the tensor product $V \otimes \bar{V}$. The matrix one $\mathbb{1}^{a,c}_{b,d}$ with incoming indices a,c and outcoming indices b,d. Its corresponding diagram is:

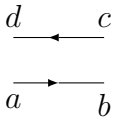

The second one is called the trace $T^{a,c}_{d,b}$ where the index b and d are permuted with respect to $\mathbb{1}^{a,c}_{b,d}$. The diagrammatic representation is

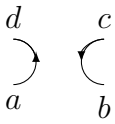

In standard group theory, the square of T is defined as

$$(T^2)^{a,c}_{d,b} = T^{a,f}_{d,e} T^{e,c}_{f,b} = \delta^a{}_d \delta^f{}_e \delta^e{}_f \delta^c{}_b = N_C T^{a,c}_{d,b}, \tag{1.A.1}$$

where the summation is done over repeated indices. Diagrammatically, the multiplication is done placing the tensors side by side and connecting the lines:

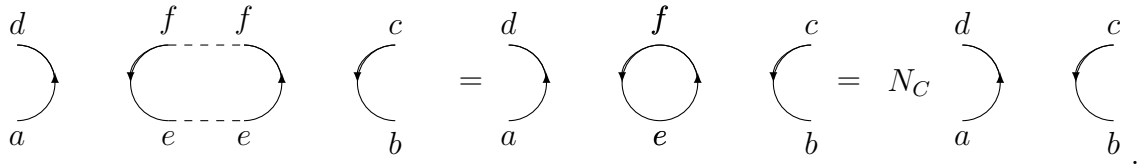

(1.A.2)

In diagrammatic notations, a loop is equivalent to the dimension of the defining space and the same result is obtained than in Eq.1.A.1. Eq.1.A.1 leads to the characteristic equation Eq. 1.A.3:

$$T(T - N_C \mathbb{1}) = 0 \tag{1.A.3}$$

The roots of the characteristic equation give the eigenvalues of the T matrix $\lambda_{1,2} = 0, N_C$.

$$T(T - N_C \mathbb{1}) = (T - 0\mathbb{1})(T - N_C \mathbb{1}) = \prod_i P_i = 0. \tag{1.A.4}$$

Projectors, normalised to the eigenvalues, can be constructed [1] and split the space into subspaces.

$$P_i = \prod_{i \neq j} \left(\frac{T - \lambda_j}{\lambda_i - \lambda_j} \right). \tag{1.A.5}$$

In terms of representation, the tensor product of the fundamental representation and its conjugate is then split by the projectors into the two possible irreducible representations (irreps). The first irrep is the adjoint representation P_A, associated to the eigenvalue $\lambda = N_C$:

$$P_A = \frac{T - N_C \mathbb{1}}{0 - N_C} = \mathbb{1} - \frac{1}{N_C} T, \tag{1.A.6}$$

P_A =

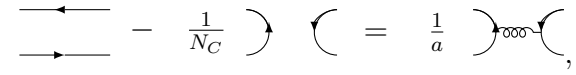

, (1.A.7)

where the diagram on the right hand side is the diagram representing the irrep P_A with the normalisation a. Here, the notation of [2] is used for the adjoint representation, to make connexion with the gluon diagrammatic notation of QCD. The second irrep is the singlet representation P_1, associated to the eigenvalue $\lambda = 0$ is:

$$P_1 = \frac{T - 0\mathbb{1}}{N_C - 0} = \frac{1}{N_C} T, \tag{1.A.8}$$

P_1 =

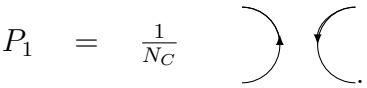

. (1.A.9)

The sum of the projectors verifies:

$$\sum_i P_i = \mathbb{1}. \tag{1.A.10}$$

Calculating the dimension (Dim) of each irrep is very easy using birdtracks, as tracing over the tensors is just connecting the initial and final legs.

$Tr(P_A)$ =

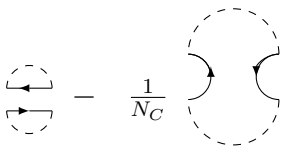

(1.A.11)

which gives:

$$\mathrm{Dim}(P_A) = N_C^2 - 1 \tag{1.A.12}$$

The dimension of P_1 is trivially:

$$\mathrm{Dim}(P_1) = 1 \tag{1.A.13}$$

For $N_C = 3$, the dimension of P_A is 8. And the adjoint representation can be written as:

$$P_A = \frac{1}{a} t_a t^a \tag{1.A.14}$$

where the t_a are the eight gluons of the adjoint representation with the normalisation a. The t_a are the Gell-Mann matrices, generators of the SU(3)group.

The diagrammatic notation of the generators t_a is:

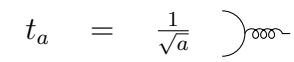

(1.A.15)

The overall normalisation is fixed by calculating P_A^2:

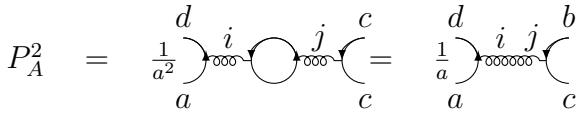

(1.A.16)

using:

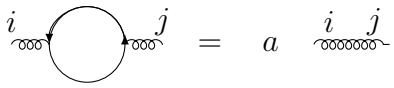

(1.A.17)

which corresponds to the orthogonality relation:

$$Tr(t_i t_j) = a\delta_{ij} \tag{1.A.18}$$

The convention traditionally used is $a = \frac{1}{2}$. The decomposition of Eq. 1.A.19

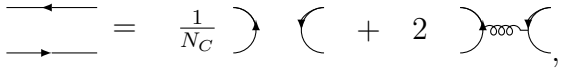

(1.A.19)

is called the Fierz Identity (or Fierz transformation) and will be used in the NJL model to go from the singlet representation to the adjoint representation in the SU(3) colour and flavour spaces.

Let's now apply this formalism to another simple group: the symmetric group and introduce the symmetric and antisymmetric operators and the formalism of the Young diagrams.

1.B The symmetric group S_n and the Young diagrams

In this section, birdtracks are read from right to left following [1] prescription. The symmetric group S_n is the group of permutations of n objects [2]. For S_2, the group is made of two elements: the identity

$$\mathbb{1}_{b,c}^{a,d} = \delta_b^a \delta_c^d \tag{1.B.1}$$

and the flip:

$$\langle \sigma_{(12)} \rangle_{c,b}^{a,d} = \delta_c^a \delta_b^d \tag{1.B.2}$$

In birdtracks notations, it becomes respectively:

(1.B.3)

For S_3, we have a product of three Kronecker deltas and 6 elements in the group: three elements for the flip (first line of diagrams), two for the cyclic permutation (first two of the second line of diagrams) and the identity:

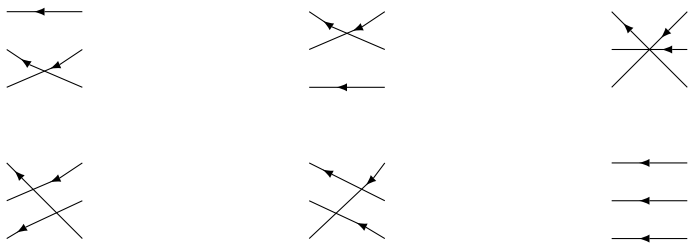

(1.B.4)

For example, the second flip is:

$$\begin{pmatrix} 1 & 2 & 3 \\ 2 & 1 & 3 \end{pmatrix} \tag{1.B.5}$$

and in birdtracks:

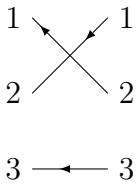

Labelling the group elements of Eq.1.B.4 from σ_1 to σ_6, the multiplication of $\sigma_4\sigma_3$ consists in putting both birdtracks side by side and connecting and stretching the lines:

$\sigma_4\sigma_3 =$  $= \sigma_2$

(1.B.6)

This shows how birdtracks simplify the calculations by making them much more visual and the multiplication tables of those groups becomes very easy to write down. The multiplication table of a group is actually a representation of a group and a smaller multiplication table inside a multiplication table is a subgroup. Now, let's go back to S_2 and calculate its projector to determine the irreps of the group. There are only two elements in the group, the identity and the flip. The square of the flip is:

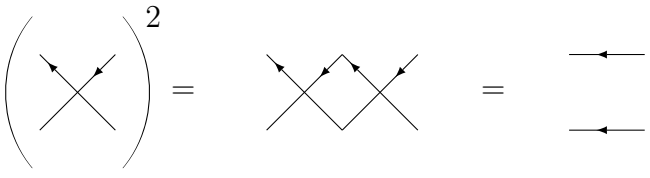

(1.B.7)

and then, using the characteristic equation:

$$\mathbb{1} - \sigma^2 = 0 = (\mathbb{1} - \sigma)(\mathbb{1} + \sigma) \tag{1.B.8}$$

The eigenvalues are $1, -1$ and the projectors associated are respectively:

$S_{12} = \frac{1}{2}\{$  $\}$ (1.B.9)

$A_{12} = \frac{1}{2}\{$  $\}$ (1.B.10)

Those projectors are known as symmetriser and an antisymmetriser. The birdtracks notations for symmetriser and antisymmetriser are respectively:

$S = \frac{1}{n!}$  (1.B.11)

and:

$A = \frac{1}{n!}$  (1.B.12)

where in the normalisation factor, n is the number of lines entering the (anti)symmetriser. The tensor products of symmetriser and antisymmetriser can be expressed in another formalism known as the Young Diagrams. For example, the $V \otimes V$ product in the birdtracks formalism reads:

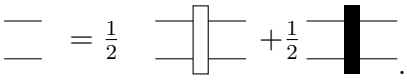 (1.B.13)

In Young Diagram formalism, it becomes:

$$\boxed{1} \otimes \boxed{2} = \boxed{1}\boxed{2} \oplus \begin{array}{|c|}\hline 1 \\ \hline 2 \\ \hline \end{array}. \tag{1.B.14}$$

The Young Diagrams are a very quick way to determine the decomposition of a tensor product into its irreducible representations using the possible permutations. They will be extremely useful to build the baryons in the NJL model.

A Young Diagram (YD) is a set of ρ connected boxes in r rows of non-increasing lengths as in Eq. 1.B.14. In this work, only top left align arrangement of boxes will be considered known as Regular YD [3]. The YD gives the shape of the arrangement of ρ boxes but the YD can be filled by a number. It becomes a Young Tableaux (YT) and obeys some rules:

- For a given row, numbers must increase from left to right
- For a given Columns, they must increase from top to bottom.
- Boxes from the tensor product must be placed side by side in all possible ways that fulfil the rules above.

An example following this rule is shown in Eq. 1.B.14. The set of possible YT can be restricted to the YT with numbers from 1 to ρ, each number appearing only once: they are called standard YT. One can notice that for two identical YD, YT can be different because of several possibilities when filling the ρ boxes with numbers.

Now that YD and YT have been defined, one can see how useful they are to calculate the decomposition of tensor product into irreps. Indeed, performing a tensor product consists in labelling the boxes of the YD of each tensor and connect them together for each possibility such that the YD is still valid as in Eq. 1.B.14. The different possible ways of building the YD are the different projectors of the tensor product.

For the SU(N) group, the properties of the group allow to give other rules simplifying the calculation.

- There is an additional invariant, the fully antisymmetric tensor of N indices in addition to the Kronecker delta tensor. Any columns of N boxes can be removed by contraction with the fully antisymmetric tensor. The consequence is that there are at most $N-1$ rows.

- The conjugate of a SU(N) Young diagram is constructed from the missing boxes needed to complete the rectangle of r rows.

Until now, no normalising factor have been mentioned for the YD. It is given by the shape of the YD [2]. The dimension of a YD is given by:

$$Dim = \frac{Num}{Den} \tag{1.B.15}$$

The numerator is given by labelling the boxes as follow:

N	$N+1$	$N+2$
$N-1$	N	

and multiplying the numbers in the boxes:

$$Num = N(N+1)(N+2)(N-1)N \tag{1.B.16}$$

The denominator is the normalising factor and is given by the hook length formula [3]. To label the box, you imagine a hook that would go from right to left and with the edge turned down. You count how many boxes you cross in order to have the right angle of the hook in a box and label the box with this number. For example, if you take the young diagram:

x	x	x
x		

for the top left boxe, a hook would cross the four boxes with a x. Finally, the number associated to each box is:

4	3	1
2	1	

Then you multiply the numbers in the boxes and obtain:

$$Den = 4 \times 3 \times 2 \times 1 \times 1 \tag{1.B.17}$$

In this work, the YD will be used only for tensor decomposition. However, it is also used to calculate the Quadratic Casimirs for example, see [3]. One can now introduce the SU(2) and the SU(3) groups and give some application of the YD formalism.

1.C SU(2) group

Using 1.A.12, they are three generators for the SU(2) group which are the famous Pauli matrices.

$$\sigma_1 = \begin{pmatrix} 0 & 1 \\ 1 & 0 \end{pmatrix}, \sigma_2 = \begin{pmatrix} 0 & -i \\ -i & 0 \end{pmatrix}, \sigma_3 = \begin{pmatrix} 1 & 0 \\ 0 & -1 \end{pmatrix} \tag{1.C.1}$$

For SU(2), the $V \otimes V$ and the $V \otimes \bar{V}$, corresponding to the tensor product of representations of a symmetry group appearing in a quark-quark and quark-antiquark bound states, are the same and the irreducible representations given by the Young tableau is:

$$\square \otimes \square = \square \otimes \bar{\square} = \begin{array}{|c|}\hline \\ \hline \\ \hline \end{array} \oplus \square\square = \bullet \oplus \square\square \tag{1.C.2}$$

After calculating the dimension of the irreps, we obtain:

$$2 \otimes 2 = 1 \oplus 3 \tag{1.C.3}$$

1.D SU(3) group

Using 1.A.12, there are eight generators associated to the SU(3) group. SU(2) being a subgroup of SU(3), the Pauli matrices are three of the eight generators :

$$\hat{\lambda}_1 = \begin{pmatrix} 0 & 1 & 0 \\ 1 & 0 & 0 \\ 0 & 0 & 0 \end{pmatrix}, \hat{\lambda}_2 = \begin{pmatrix} 0 & -i & 0 \\ -i & 0 & 0 \\ 0 & 0 & 0 \end{pmatrix}, \hat{\lambda}_3 = \begin{pmatrix} 1 & 0 & 0 \\ 0 & -1 & 0 \\ 0 & 0 & 0 \end{pmatrix} \tag{1.D.1}$$

Keeping the two non diagonal Pauli Matrices, the non zero part is moved of one row and one column :

$$\hat{\lambda}_4 = \begin{pmatrix} 0 & 0 & 1 \\ 0 & 0 & 0 \\ 1 & 0 & 0 \end{pmatrix}, \hat{\lambda}_5 = \begin{pmatrix} 0 & 0 & -i \\ 0 & 0 & 0 \\ i & 0 & 0 \end{pmatrix}, \hat{\lambda}_6 = \begin{pmatrix} 0 & 0 & 0 \\ 0 & 0 & 1 \\ 0 & 1 & 0 \end{pmatrix}, \hat{\lambda}_7 = \begin{pmatrix} 0 & 0 & 0 \\ 0 & 0 & -i \\ 0 & i & 0 \end{pmatrix} \tag{1.D.2}$$

For the last generator, a matrix that is diagonal with non vanishing coefficient is needed.

$$\hat{\lambda}_8 = \begin{pmatrix} \alpha & 0 & 0 \\ 0 & \alpha & 0 \\ 0 & 0 & \beta \end{pmatrix} \tag{1.D.3}$$

Using the relation :

$$\ln(Det(U)) = Tr(\ln(U)) \tag{1.D.4}$$

Trace needs to be zero as the determinant of special unitary group is 1.

$$\beta = -2\alpha \tag{1.D.5}$$

As the generator are hermitian, the coefficient have to be real. The constant α is chosen from the orthogonality relation :

$$Tr(\hat{\lambda}_a \hat{\lambda}_b) = 2\delta_{ab} \tag{1.D.6}$$

$$Tr(\hat{\lambda}_8 \hat{\lambda}_8) = Tr \begin{pmatrix} \alpha^2 & 0 & 0 \\ 0 & \alpha^2 & 0 \\ 0 & 0 & 4\alpha^2 \end{pmatrix} = 6\alpha^2 = 2 \tag{1.D.7}$$

Then we obtain:

$$\hat{\lambda}_8 = \frac{1}{\sqrt{3}} \begin{pmatrix} 1 & 0 & 0 \\ 0 & 1 & 0 \\ 0 & 0 & -2 \end{pmatrix} \tag{1.D.8}$$

For quark-antiquarks bound states, we have the following decomposition in irreps:

$$\square \otimes \bar{\square} = \square \otimes \begin{array}{|c|}\hline \\ \hline \end{array} = \bullet \oplus \begin{array}{|c|c|}\hline \\ \hline \end{array} \tag{1.D.9}$$

After calculating the dimension of the irreps, we obtain:

$$3 \otimes 3 = 1 \oplus 8 \tag{1.D.10}$$

The octet is the adjoint representation and contain the eight gluons, gauge fields of the strong interaction. For quark-quark bound states, we have:

$$\square \otimes \square = \begin{array}{|c|}\hline \\ \hline \end{array} \oplus \square\square \tag{1.D.11}$$

and the dimensions are:

$$3 \otimes 3 = \bar{3} \oplus 6 \tag{1.D.12}$$

The antitriplet representation is fully antisymmetric and the sextet is fully symmetric. The quark-quark-quark bound state is given by :

$$\square \otimes \square \otimes \square = \bullet \oplus \begin{array}{|c|c|}\hline \multicolumn{1}{c}{} \\ \hline \end{array} \oplus \begin{array}{|c|}\hline \multicolumn{1}{c}{} \\ \hline \end{array} \oplus \square\square\square \tag{1.D.13}$$

Leading to the following decomposition :

$$3 \otimes 3 \otimes 3 = 1 \oplus 8 \oplus 8 \oplus 10 \tag{1.D.14}$$

They are two octet, ie two adjoint representations, corresponding to the same YD. However they are two possible YT, $\begin{array}{|c|c|}\hline 1 & 2 \\ \hline 3 \\ \cline{1-1} \end{array}$ and $\begin{array}{|c|c|}\hline 1 & 3 \\ \hline 2 \\ \cline{1-1} \end{array}$, associated to the same YD which is the reason why both are conserved in the tensor decomposition.

Application to the NJL model

In the case of the NJL model, the baryons will be built from a quark-diquark bound state. The decomposition remains the same than for a three quark bound state but the tensor product of a quark and a diquark is given by multiplying a quark box by the two possible irreducible representations given by the right hand side of Eq.1.D.11:

$$\square \otimes \begin{array}{|c|}\hline \multicolumn{1}{c}{} \\ \hline \end{array} = \bullet \oplus \begin{array}{|c|c|}\hline \multicolumn{1}{c}{} \\ \hline \end{array} \tag{1.D.15}$$

and

$$\square \otimes \square\square = \begin{array}{|c|c|}\hline \multicolumn{1}{c}{} \\ \hline \end{array} \oplus \square\square\square \tag{1.D.16}$$

Comparing with equation 1.D.14, it leads to the following decomposition :

$$3 \otimes \bar{3} = 1 \oplus 8 \tag{1.D.17}$$

and

$$3 \otimes 6 = 8 \oplus 10 \tag{1.D.18}$$

The symmetric and antisymmetric properties of the sextet and the antitriplet will also be important to fulfil the Pauli principle: fermions must be in an antisymmetric overall product of the colour, flavour and Dirac representations.

1.E Dirac space, spinors and orthogonal group

Spinors are a representation of the orthogonal group SO(N) discovered by Cartan [1]. It is then naturally that it appears to describe a Lorentz invariant physics associated to the SO(3,1) group. Dirac introduced them along with the γ_μ matrices to linearise the

relativistic Klein-Gordon equation valid only for integer spins. The γ_μ matrices needed to be introduce to reach this purpose [4]

$$(-i\gamma^\mu\partial_\mu - m)(-i\gamma^\nu\partial_\nu - m)\psi = (\partial^2 + m^2)\psi = 0 \tag{1.E.1}$$

γ_μ being 4×4 matrices and ψ being a Dirac spinor. The Dirac equation has the form:

$$(i\gamma^\mu\partial_\mu - m)\psi(x) = 0 \tag{1.E.2}$$

which is the right relativistic equation of motion for spin $\frac{1}{2}$ free particles. To be relativistic, the Dirac equation must be invariant under Lorentz transformation. The Lorentz group has six generators which are the three boosts and the three rotations defined by the commutator of γ^μ matrices [4]. For interacting theories, Dirac field current:

$$j^\mu(x) = \bar{\psi}(x)\gamma^\mu\psi(x) \tag{1.E.3}$$

and bilinears

$$j^\mu(x)j^\mu(x) = \bar{\psi}(x)\gamma^\mu\psi(x)\bar{\psi}(x)\gamma^\mu\psi(x) \tag{1.E.4}$$

will be introduced, see Fig. 1.2.

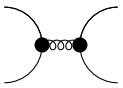

Fig. 1.2: Dirac bilinears for vector interaction

The vector interaction constructed from the γ^μ matrices can be expanded into a sum over the irreducible representations Γ^a: $\mathbb{1}$, γ^5, γ^μ, $\gamma^\mu\gamma^5$ of the Dirac space weighted by coefficients Eq. 1.E.5, as it was done for SU(3). This will be especially useful to describe the interaction in the NJL model where the vector interaction of QCD will be Fierz transformed into the sum of a scalar, pseudoscalar, vector and axial interaction, the scalar interaction adding a contribution to the mass which is most of the mass of the matter. To determine the coefficient associated to each irreps, the s channel bilinears Fig. 1.2 must be projected over each irreps in channel t. Only the case of scalar and vector projection will be shown here, the way to proceed being similar for the other cases. The vector interaction decomposition, in spinology, writes in birdtracks:

(1.E.5)

where $\frac{1}{\circ}$ is the birdtracks for the normalisation. To calculate the coefficient for scalar coupling, the right hand side and left hand side of Eq. 1.E.5 must be projected onto the scalar projector. This is done by acting on above and below.

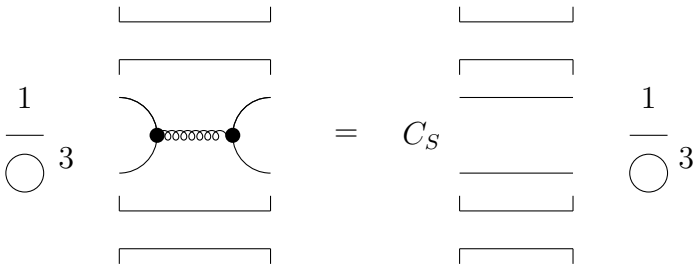

(1.E.6)

where:

(1.E.7)

is the scalar projector in the t channel and the factor $\frac{1}{O^3}$ is the overall normalisation. The scalar coefficient is determined by taking the trace of Eq. 1.E.6:

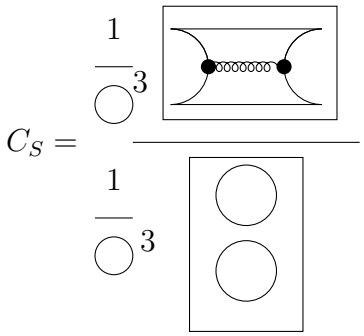

(1.E.8)

which is equal to:

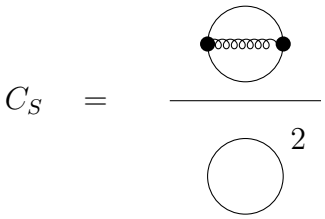

(1.E.9)

The diagram at the numerator cannot be reduced more and need to be calculated using the Birdtracks version of the Clifford algebra 1.E.10:

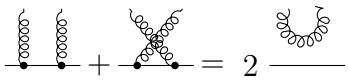

(1.E.10)

Rewriting the numerator of Eq. 1.E.9as:

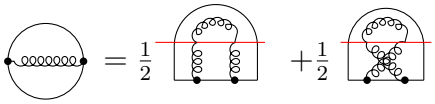

(1.E.11)

The red line on Eq. 1.E.11 shows how to cut the Birdtracks to make explicit the Clifford Algebra relation on the lower part. The simplification can be made using Eq. 1.E.10 and the final result for this diagram is:

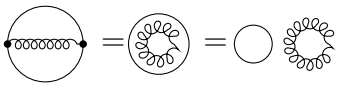

(1.E.12)

The scalar coefficient is then:

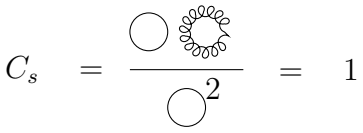

(1.E.13)

as the curly circle is $g^{\mu\nu}g_{\mu\nu} = 4$ and the full circle is $Tr[\mathbb{1}] = 4$.

Regarding the vector to vector coefficient, the projection must be with regard to the vector projector:

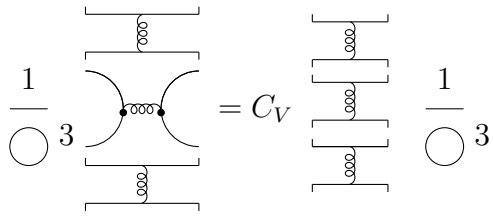

(1.E.14)

Eq.1.E.14 left hand side can be simplified using the Schur's lemma to cut (red lines)the upper and lower γ matrix (upper and lower coal) see Eq.1.E.15. As the indices of the upper γ_μ must be the same than the indices of the lower γ_ν and both γ matrices can be traced over reducing the Eq.1.E.14 to:

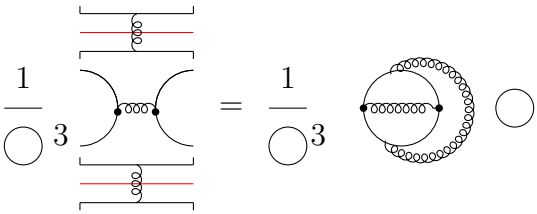

(1.E.15)

The right side of Eq. 1.E.14 is simplified using the fact that a square of the projector is itself. After connecting the lines, the expression for the C_V is:

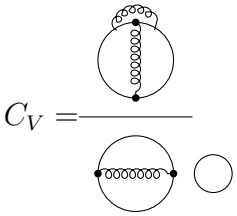

(1.E.16)

All diagrams have already been calculated for the denominator. The numerator, however needs to be simplified using the Clifford algebra:

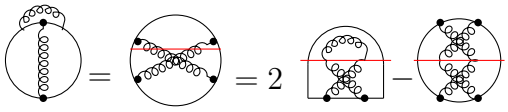

(1.E.17)

Where the upper part of the red cut is modified using the Clifford algebra. The final form of the numerator is:

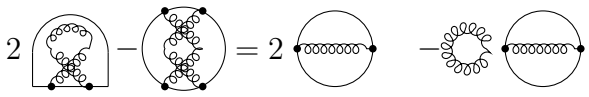

(1.E.18)

Eventually, the vector coefficient is:

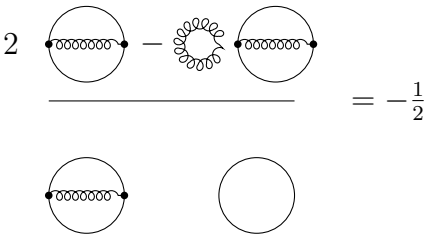

(1.E.19)

The final coefficient for vector to vector Fierz transformation is $C_V = -\frac{1}{2}$. The pseudoscalar coefficient is identical to the scalar coefficient considering that the coupling is $i\gamma^5$. The axial coefficient is equal to the vector coefficient. The calculations shows that the tensor coefficient is 0.

1.F Thermodynamics and statistical physics

All along this thesis, observables like pressure, entropy, speed of sound will need to be calculated. This section will give the main formulas and definitions that will be used in order to evaluate them and determine fundamental objects of a thermodynamical study like equations of state or phase diagrams.

Partition function, micro and macro states

The power of the statistical physics comes from the fact that the observables susmentionned are macroscopic and can be determined from summing over the microscopic states. The microscopic states are included in the Lagrangian density. Generally speaking, the first mathematical object which has to be determined in statistical physics is the partition function. The partition function is the sum of all the microstates possibly reachable by a system. In quantum field theory, it is a functional of the Lagrangian density integrated over the degrees of freedom of the theory (like quarks and gluons in the case of QCD):

$$Z = \int \mathscr{D}\psi \mathscr{D}\bar{\psi} \mathscr{D}A_\mu \exp(i \int d^4x \mathscr{L}_{QCD}) \tag{1.F.1}$$

The partition function Z relates the microscopic world to the macroscopic one expressed by the thermodynamical potential Ω [5]:

$$Z = Tr[\exp(-\beta\Omega)] \tag{1.F.2}$$

The thermodynamics of an isolated system can be described with three variables. The thermodynamic potentials are then functions of three variables which can be:

- Pressure P or volume V
- Entropy S or temperature T
- Chemical potential μ or Number of particles N

Only one variable of each couple can be chosen to characterise the system. They are called intensive and extensive variables. The intensive or extensive nature of the variable depends on how the variable react to a change of size of the system. If the size of the system double, the extensive variable will also double.The intensive variable will remain the same. There is a thermodynamic potential for each possible combination of variables the system depends on. They are calculated subsequently by performing a Legendre transformation of the internal energy U. The five most common are:

- The internal energy $U(S,V,N) = TS - PV + \mu N$ at constant T and P and μ giving $dU = TdS - pdV + \mu dN$.
- The Free energy is obtained by performing the Legendre transformation $F(T,V,N) = U(S,V,N) - TS$.
- The enthalpy is obtained by performing the Legendre transformation $H(S,P,N) = U(S,V,N) + PV$.
- The Gibbs free energy is obtain by performing the Legendre transformation $G(T,P,N) = U(S,V,N) + PV - TS$.
- The Grand Potential is obtained by performing the Legendre transformation $\Omega(T,V,\mu) = F - \mu N$.

All the extensive variables can be calculated by using partial differentiation of the thermodynamic potential with respect to the intensive variables whereas the other variables are kept fixed.

At thermodynamical equilibrium, the thermodynamical potential has a minimum. This can be seen from the fact that the system has reached the most probable state which means that the partition function is maximum. Eq.1.F.2 shows that there the potential must be minimal:

$$\frac{\partial \Omega}{\partial O} = 0 \tag{1.F.3}$$

where Ω is the chosen potential and O is a thermodynamic variable of interest. Those macroscopic variables are, however, calculated from microscopic states and different microscopic states can lead to the same macroscopic state.

The statistical physics introduces the concept of statistical ensemble to gather all the systems obeying the same rule in three ensemble:

- The microcanonical ensemble: the system is isolated and the energy is conserved. All the possible microstates have the same statistical weight ω:

$$P_l = \frac{1}{\omega} \quad \text{or} \quad 0 \tag{1.F.4}$$

- The canonical ensemble: the system has a temperature T and can exchange energy with a heat bath. The probability of a system to be in the state l of energy E_l is

$$P_l(T) = \frac{1}{Z} \exp\left(-\frac{E_l}{T}\right). \tag{1.F.5}$$

  Z is the partition function. It is the sum of all the possible states and is consequently the normalisation.

- The grand canonical ensemble: the system has a temperature T, a chemical potential μ and can exchange energy and particles with a reservoir. The probability of a system to be in the state l of energy E_l with the number of particles N_l is:

$$P_l(T,\mu) = \frac{1}{Z} \exp\left(-\frac{E_l - \mu N_l}{T}\right). \tag{1.F.6}$$

All the thermodynamic ensembles are equivalent in thermodynamic equilibrium. In this work, the systems studied will exchange energy and particles with a reservoir. The study will be then performed in the grand canonical ensemble with the grand potential.

$$\Omega(T,V,\mu) = F(T,V,N) - \mu N = U - TS - \mu N. \tag{1.F.7}$$

In addition, the volume will be infinite. Densities will then be evaluated and $\Omega = \frac{\Omega(T,\mu,V)}{V}$. The relation between the grand potential and the partition function is given by:

$$\Omega(T,\mu,V) = -T\ln(Z). \tag{1.F.8}$$

A short list of the thermodynamical quantities of interest in our work can be obtained from the expression of the grand potential 1.F.7. The differential form of Ω is:

$$d\Omega(T,\mu,V) = -SdT - PdV - Nd\mu. \tag{1.F.9}$$

The pressure is directly obtained from $\Omega(T,\mu,V)$ in infinite volume:

$$P(T,\mu) = -\frac{\Omega(T,\mu,V)}{V}. \tag{1.F.10}$$

Entropy has the following form:

$$S = -\frac{\partial\Omega}{\partial T} = \frac{\partial P}{\partial T}. \tag{1.F.11}$$

The energy is given by:

$$U = TS - P + N\mu = -T\frac{\partial\Omega}{\partial T} - P - \mu\frac{\partial\Omega}{\partial\mu} = T\frac{\partial P}{\partial T} - P + \mu\frac{\partial P}{\partial\mu}. \tag{1.F.12}$$

The interaction measure, defined as the trace of the energy-momentum tensor, is given by:

$$I = U - 3P. \tag{1.F.13}$$

The baryonic density is:

$$\rho = -\frac{\partial\Omega}{\partial\mu_B} = \frac{\partial P}{\partial\mu_B} \tag{1.F.14}$$

where μ_B is baryonic chemical potential. The speed of sound is given by [6]:

$$C_s^2 = \frac{\partial P}{\partial U} = \left(\frac{T}{S}\frac{\partial S}{\partial T} + \frac{\mu}{S}\frac{\partial N}{\partial T}\right)^{-1} \tag{1.F.15}$$

Another fact to be taken into account is that fermions and bosons do not have the same statistical properties, especially because of the Pauli exclusion principles, see section 2.A. The particularity of the fermions are now recalled.

Properties of fermions

For simplicity, only a free gas of fermions will be treated in this part. In the main chapter of the thesis, we treat an interacting gas of fermions. The fermions obey the Fermi-Dirac statistics, which means that the average occupation number of a state of energy E_λ is given by:

$$f_\lambda^F = \frac{1}{\exp(\beta(E_\lambda - \mu) + 1)} \tag{1.F.16}$$

with $\beta = \frac{1}{T}$ in natural units and μ is the chemical potential. Eq.1.F.16 reflects the fact that the occupation number is between 0 and 1, consequence of the exclusion principle. Fig. 1.3 shows the occupation number as function of the energy at T and μ fixed. The plot is symmetric with respect to $E = \mu$, which means that when $E_\lambda = \mu$, the probability of occupation is $\frac{1}{2}$. The temperature smooths the curvature of f_λ^F when going from 1 to 0. At zero temperature, the function has no curvature, this is a step function $\theta(\mu - E_\lambda)$.

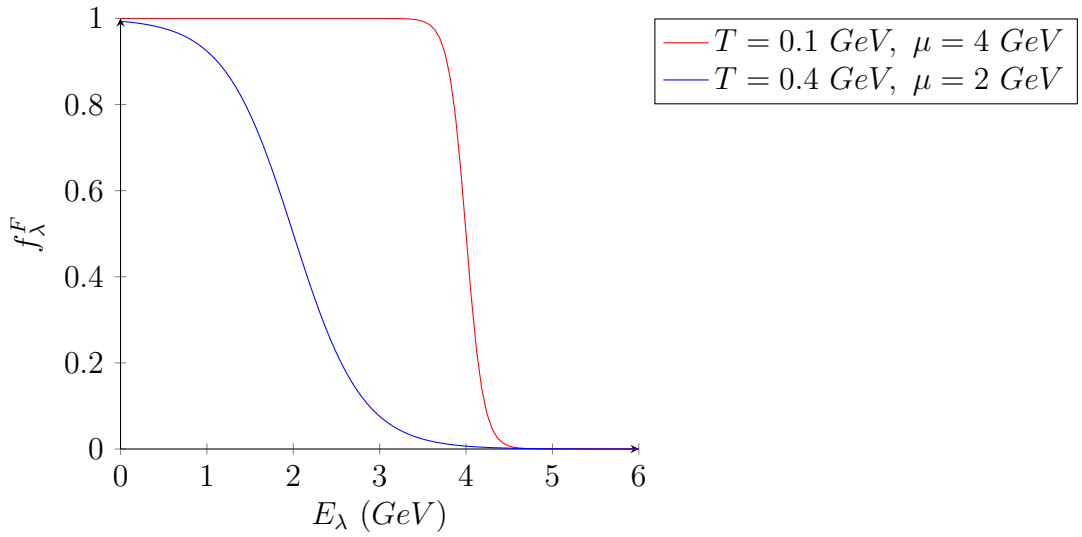

Fig. 1.3: Fermionic distributions

The average number of particles is given by summing up the probability of occupation for each state:

$$\bar{N} = \sum_\lambda f_\lambda^F. \tag{1.F.17}$$

When the size of the system becomes macroscopic, the discrete Eq.1.F.17 becomes continue. This is the thermodynamic limit:

$$\sum_\lambda \to \frac{V}{(2\pi)^3} \int d^3\vec{p}. \tag{1.F.18}$$

The number of particles becomes fixed and μ varies, which makes a fundamental difference with the grand canonical frame where N can vary but μ is fixed: if the system is not equilibrated, grand canonical and canonical ensemble are not equivalent. Literature can be found on the discussion of the equivalence of the canonical and grand canonical ensemble in the case of QCD and whether one should be preferred to the other in [7][8][9].

Let's explore the properties of the Fermi statistics in the limit of zero temperature. At $T = 0$ all the states λ of energy ϵ_λ lower than the Fermi Energy ϵ_F are occupied. The energy of a free Fermi gas is given by:

$$E = \frac{V}{2\pi}^3 \int_0^{k_f} d^3\vec{p} f_\lambda^F \epsilon_\lambda = \frac{1}{2m} \left(\frac{6\pi^2 N}{(2s+1)V} \right)^{\frac{2}{3}} = \frac{(k_F)^2}{2m} \tag{1.F.19}$$

k_F is the Fermi wave vector associated to ϵ_F. The sphere of radius k_F is called the Fermi surface and separates the empty states from the occupied states and the Fermi temperature is defined as:

$$T_F = \epsilon_f \tag{1.F.20}$$

If $T << T_F$, the approximation of zero temperature can be used. This feature is especially important for the study of the neutron star equation state in chapter 7. The temperature

in a neutron star is definitely much larger than 0 Kelvin, but it is however lower than its Fermi temperature which allows to calculate its equation of state at $T = 0$. Even at $T = 0$ the pressure does not vanish and there is a quantum pressure due to the Pauli principle. To calculate other thermodynamical quantities at $T = 0$, some precautions must be taken. The vanishing temperature limit is discontinuous and a series in power of T is required to be consistent and check the limit of validity of the $T = 0$ approximation. This series is called the Sommerfield series [5].

1.G Finite temperature field theory and Matsubara formalism

In quantum mechanics, the time evolution is Hamiltonian:

$$U(x', t', x, t) = \langle x'| \exp(-iH(t' - t))|x\rangle. \tag{1.G.1}$$

For thermodynamics purposes, a temperature evolution operator would better suit the situation than a time evolution operator. The temperature dependence of the system requires to involve the statistical physics and consequently the partition function:

$$Z(T) = Tr[\exp(-\beta\hat{H})] = \sum_n \exp(-\beta E_n) \tag{1.G.2}$$

The $\exp(-\beta\hat{H})$ can be brought to the same form than the $\exp(-i\hat{H}t)$ time evolution operator by performing a Wick rotation:

$$t \longrightarrow -i\tau \tag{1.G.3}$$

and $\beta = \tau$ The consequence of this is the imaginary time formalism. One can now directly use the Feynman diagram formalism developed for zero temperature to define finite temperature propagators just by performing this Wick rotation. This is a come back to the Euclidean space where the partition function has the form:

$$Z(\beta) = \int \mathscr{D}_{x(-i\tau)} \exp(-S_E(-i\beta)) \tag{1.G.4}$$

and depends now on the Euclidean action S_E which is real and $0 \leq \tau \leq \beta$ giving a periodicity in β to the system at thermal equilibrium.

The Fourier transform of the propagator $\Delta(\tau) = T\langle x(-i\tau_1)(x(-i\tau_2)\rangle$ is [10]:

$$\Delta(i\omega_n) = \int_0^\beta d\tau \exp(i\omega_n\tau)\Delta(\tau) \tag{1.G.5}$$

The periodicity constraint on $\Delta(\tau)$ implies that the continuous Fourier transform becomes a discrete Fourier series. The inverse Fourier transform has the form:

$$\Delta(\tau) = T\sum_n \exp(-i\omega_n\tau)\Delta(i\omega_n) \tag{1.G.6}$$

where the ω_n are discrete frequencies:

$$\omega_n = 2\pi n T = \frac{2\pi n}{\beta} \tag{1.G.7}$$

for bosons and:

$$\omega_n = \frac{2\pi(n+1)}{\beta} \tag{1.G.8}$$

for fermions. A consequence of the boundary condition is that energies are discrete and obey the Matsubara modes relations for fermions and bosons Eq. 1.G.7 and Eq. 1.G.8. The finite temperature and chemical potential propagator is then:

$$S(i\omega_n, \vec{p}) = \frac{i(\gamma^0(i\omega_n + \mu) - \gamma^i \vec{p} + m)}{(i\omega_n + \mu)^2 - E^2 + i\epsilon} \tag{1.G.9}$$

The fact that the energies are discrete induced that when evaluating loops, the four dimensional integral over the propagator becomes:

$$\int \frac{d^4p}{(2\pi)^4} \to T \sum_n \int \frac{d^3p}{(2\pi)^3} \tag{1.G.10}$$

and one needs to face the evaluation of what is called the Matsubara sum $\sum_n$. For the example of a one fermion loop, one can rewrite Eq. 1.G.9 in terms of the energy and use the complex integration formulas:

$$\frac{1}{\beta} \sum_n \frac{1}{(i\omega_n + \mu)^2 - E^2} = T \sum_n f(i\omega_n) = \oint \frac{dz}{2i\pi} f(z) P(z) \tag{1.G.11}$$

There are two poles in Eq.1.G.11 at $z = E - \mu$ and $z = -E - \mu$. One can use the residue theorem on the right half contour of the complexe plan see Fig. 1.4 [11]:

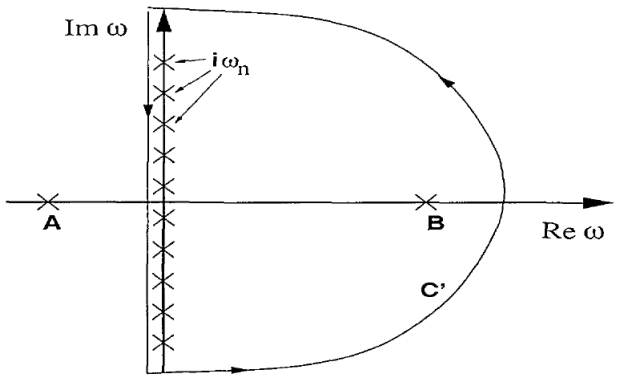

Fig. 1.4: Integration contour on the right half of the complex plan

and do the same on the left half contour of the complex plan. The P(z) function in Eq. 1.G.11 can be chosen to be:

$$P(z) = \frac{\beta}{\exp(\beta z) \pm 1)} \tag{1.G.12}$$

which are the the finite T and μ Fermi-Dirac or Bose-Einstein distributions . The contour integration can be performed in the case of fermions for example and is:

$$\oint \frac{dz}{2i\pi} \frac{1}{\exp(\beta z) - 1)} \frac{1}{(z+\mu)^2 - E^2} = \frac{1}{2E} \left(\frac{1}{\exp(\beta(E-\mu)) - 1)} - \frac{1}{\exp(\beta(-E-\mu)) - 1)} \right) \tag{1.G.13}$$

and the loop is now reduced to the evaluation of a three dimensional integral of the momentum $\vec{p}$.

It is now time to look at QCD, the properties of this theory and the tools that exist to study it and especially the phase diagram of strongly interacting matter.

Chapter 2

Strong interaction and Quantum ChromoDynamics

The existence of the NJL model is closely related to the complexity of studying QCD and the need of models easier to work with. The success and limitations of the tools we have to study the QCD phase diagram, the pQCD, the lQCD and the heavy ion collisions experiments, are presented in this section. The fundamentals of the QCD theory, the Lagrangian and the symmetries, will be emphasised as they are the building blocks of the NJL model.

2.A Strong interaction and the standard Model

The strong interaction is part of a more general theory called the Standard Model. The Standard Model considers two types of objects, fermions and bosons. Fermions are considered as the matter sector and bosons as the interaction sector: fermions interact with each other with a boson exchange.

Bosons and fermions:

They are two fundamental classes of particles which differs by a quantum number called spin. For bosons, this quantum number is an integer. For fermions, it is a half integer. The main difference between those two classes, consequence of the spin statistics, is the Pauli principle. The Pauli principle states that two fermions cannot be in the same quantum state (have the same quantum numbers). This principle is only valid for fermions and leads to an additional quantum pressure in the fermionic systems. Bosons can be in the same quantum state. This leads to Bose-Einstein condensation for bosons and two examples of this phenomenon are the superfluidity and the superconductivity.

Note that it is also possible to have bosons from the combination of fermions giving particles with integer spins like the Helium atom.

Matter

It is divided in two classes: the leptons and the quarks [12].

u	c	t
d	s	b
e	μ	τ
ν_e	ν_μ	ν_τ

Table 2.1: Fundamental constituents of matter: The quarks are the first two lines and the leptons the last two ones. The neutrino family, part of the leptons, is the last line.

There are six flavours of leptons see Tab. 2.1 that can be separated in two subclasses: the uncharged neutrinos and the charged other leptons. There are three types for each called: electron, muon, tau and electronic neutrino, muonic neutrino and tauic neutrino. There are also six flavours of quarks. They are also subdivided in two subclasses, see Tab.2.1, up, down and strange for the light quarks and charm, bottom and top for the heavy quarks. The particles up, charm and top have an electric charge of $\frac{2}{3}$ and have increasing mass. The same increase is seen for down, strange, bottom with an electric charge $-\frac{1}{3}$ and the electron, muon and tau of electric charge -1. The neutrinos are neutral and the value of their mass remains an open question, experiments having brought limits on their value and the certitude that only one could be zero at most. The first column of Table 2.1 corresponds to the lightest particle of each line and is called a generation. The mass hierarchy makes it possible that the particle of a higher generation decay into lower generation and implies that only particles of the first generation are constituents of the matter around us.

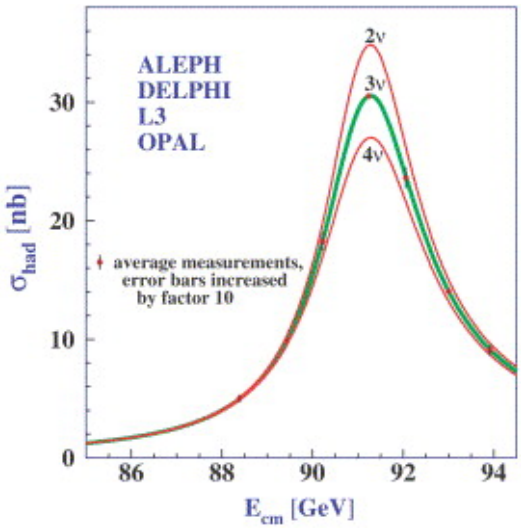

Fig. 2.1: Measurement of the resonance of the Z boson from different experiments in agreement with the theoretical models considering three generations of particles

The ALEPH, DELPHI, L3 and OPAL experiments have shown that there are only three generations see Fig.2.1 [13]. However, the limitations in energy of the collider do not exclude the existence of other generations with particles of even larger masses.

Interactions

They are mediated by a boson, exchanged between fermions. Four fundamental interactions are observed in nature: electromagnetic, weak, strong and gravitationnal interactions. The standard model describes only three of them: the electromagnetic, the weak and the strong interactions. The associated bosons are the photon, the W and Z bosons and the gluons.

Hadrons

The nature one meets in the "common" life. Quarks or gluons are not directly observable. No experiment has managed to observe free quarks or gluon up to now. This can be explained by the phenomenon of confinement. Experimentalists only observe combinations of quarks that are called hadrons. Two types of combinations are possible. Quark-antiquark pairs are called mesons, triplet of (anti)quarks are called (anti)baryons. Two famous examples of baryons are protons and neutrons and a famous meson is the pion.

More exotic hadrons have also been observed, like the tetraquark and the pentaquark [14] and even glueballs are predicted theoretically but not yet observed experimentally [15]. However, it is not yet known if a substructure exists and if it is actually a bound state of four quarks and an antiquark or a bound state of a meson and a baryon.

This work focus on the study of quarks and the strong interaction. The strong interaction is described by the theory of Quantum Chromo Dynamics (QCD), a Lagrangian density which is invariant under the local gauge transformation SU(3).

2.B QCD Lagrangian

The QCD Lagrangian is given by:

$$\mathscr{L}_{QCD} = i\delta_{ij}\bar{\psi}^i_k\gamma^\mu\partial_\mu\psi^j_k + g\bar{\psi}^i_k\gamma^\mu t^a_{ij}A^a_\mu\psi^j_k - m_k\bar{\psi}^i_k\psi^j_k - \frac{1}{4}G^a_{\mu\nu}G^{a\mu\nu} \tag{2.B.1}$$

There are three charges for the strong interaction: the colors red, blue and green. The gauge field A^a_μ has an index meaning that it is coloured unlike the photon in Quantum ElectroDynamics, the $t_a = \frac{1}{2}\lambda_a$ matrices comes from the symmetry SU(3) group and are eight, so do the gauge fields A^a_μ. In Eq. 2.B.1, the first term describes the propagation of the quark, the second term is the quark-gluon interaction, the third term is the mass term for the quarks and the last term describes the dynamics of the gluons and the gluon-gluon interactions, where:

$$G^a_{\mu\nu} = \partial_\mu A^a_\nu - \partial_\nu A^a_\mu + g f^{abc} A^b_\mu A^c_\nu. \tag{2.B.2}$$

The red characters in Eq. 2.B.1 are the free parameters of the theory. Their values are not given by QCD and will be parametrised in section 3.C to build the Nambu-Jona-Lasinio (NJL) effective model in order to reproduce experimental data.

The non abelian features can be seen in Eq.2.B.2 from the third term. It leads to a set of new possible vertices for Feynman diagrams, the three and four gluons vertices, see Fig. 2.2.

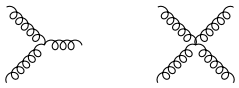

Fig. 2.2: 3 and 4-gluon vertices

The QCD Lagrangian also possesses a large set of symmetries. Not all of them are exact. In the next section, we give a summary of the particularly important ones for the physics of strong interaction.

2.C Symmetries

Exact symmetries:

- **Color symmetry**

This is the most important one. By requiring the Dirac Lagrangian to be invariant under the local SU(3) color symmetry, it gives birth to the Chromo Dynamics. The three fundamental color states of a quark are the colors blue, red or green which are the charges of the strong interaction. The generators of the symmetry are eight gluons made of combinations of colors and anticolors. The color symmetry also allows the renormalisation of the theory [16].

- **CPT**

The parity symmetry P is an important symmetry in the Standard Model and also in QCD and the NJL type models. It makes the difference between scalar and pseudoscalar particles, for example, and is closely related to the property of chiral restoration which is one of the signs of a phase transition in the phase diagram of QCD matter. The parity P reverse the $\vec{p}$ without flipping the spin and its operator is given by the γ_0 matrix in the Dirac representation. The following properties can be shown:

$$P\mathbb{1}P = \gamma_0\gamma_0 = \mathbb{1} \tag{2.C.1}$$

$$P\gamma_\mu P = \gamma_0\gamma_\mu\gamma_0 = (-1)^\mu\gamma_\mu \tag{2.C.2}$$

$$P\gamma_5 P = \gamma_0\gamma_5\gamma_0 = -\gamma_5 \tag{2.C.3}$$

$$P\gamma_\mu\gamma_5 P = \gamma_0\gamma_\mu\gamma_5\gamma_0 = -(-1)^\mu\gamma_\mu\gamma_5 \tag{2.C.4}$$

where $(-1)^\mu = 1$ for $\mu = 0$ and $(-1)^\mu = -1$ for $\mu = 1, 2, 3$. The matrix $\mathbb{1}$, γ_5, γ_μ and $\gamma_\mu\gamma_5$ being the different possible types of interactions: scalar, pseudoscalar, vector and axial.

The charge conjugation C changes a particle into its antiparticle. This operator will be of use to build the baryons from diquarks in the NJL model. It has the following form in the Dirac representation:

$$C = i\gamma_0\gamma_2 \tag{2.C.5}$$

The T symmetry operator reverses the time. It is not involved in the following study and is given here only for completeness in the Dirac representation [4]:

$$T = i\gamma_1\gamma_3 \tag{2.C.6}$$

The Dirac Lagrangian is invariant under C, P and T separately and the combination CPT. In the context of QCD, the strong CP problem and the value of the θ parameter of the strong interaction, finite or not and if finite the reason of a small value, remains an open question [17]. A finite value of θ would lead to a breaking of P, T and, via CPT theorem, CP symmetries and the nature of the breaking source is a current topic of beyond Standard Model studies [18].

- **Global phase redefinition of up/down field**

Associated to the symmetry $U(1)_V$. Lead to the conservation of the quark number.

Approximate symmetries:

- **Isospin symmetry**

Associated to the symmetry $SU(2)_V$. Valid in the limit $m_u = m_d$. The three pions and the nucleons can be built from the isospin symmetry.

- **Flavour symmetry**

$SU(3)_V$ global symmetry in the limit $m_s = m_u = m_d$. It predicts successfully the spectrum of light mesons and baryons that can be made from quarks: the octet of mesons, adjoint representation of the decomposition of the $q \otimes \bar{q}$ into its irreps in Eq. 1.D.10 and the octet and the decuplet of baryons irreps of the $q \otimes q \otimes q$ decomposition in Eq. 1.D.14. The quark model [19] is a first direct application of the decomposition of tensor product $q \otimes \bar{q}$ and $q \otimes q \otimes q$ into their respective irreps using the Young tableaux formalism that was developed in section 1.B. The octet of pseudoscalar mesons and the octet and decuplet of baryons are shown in Fig. 2.3.

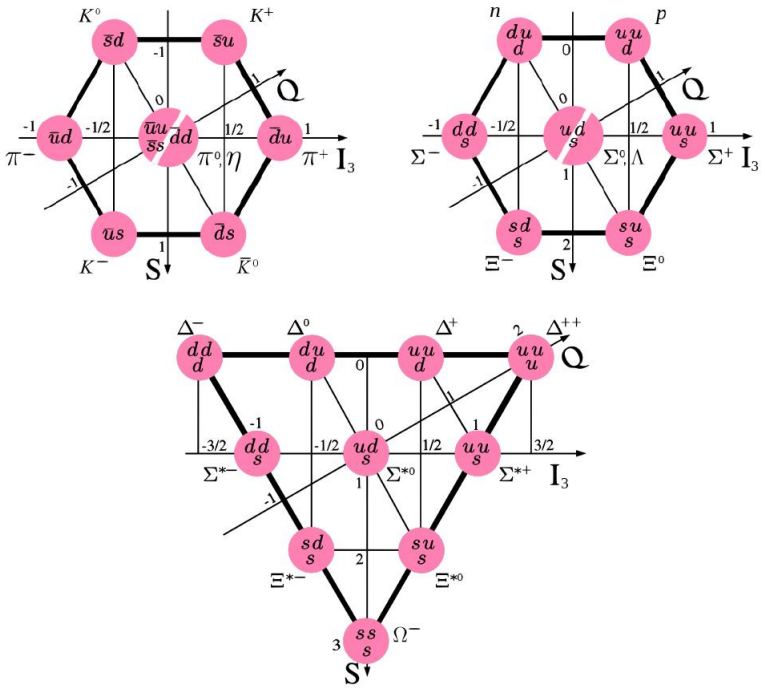

Fig. 2.3: (a) Octet of pseudoscalar mesons (b) Octet of baryons (c) Decuplet of baryons obtained from the quarks model based on the SU(3) flavour symmetry [20]

In addition, the singlet state needs to be taken into account as there are nine pseudoscalar mesons that are made from the quark-antiquark bound state. The breaking of the anomalous $U(1)_A$ symmetry by quantum fluctuations leads to a splitting of the η mesons into a mixed state of two mesons: η and η' [21]. The quark model remains phenomenological and not fully understood from first principle, like the puzzle of the pion being at the same time a quark-antiquark bound state and a Goldstone boson. This symmetry is less reliable than the isospin symmetry as the strange quark has a larger mass than the u and d quarks.

- **Chiral symmetry** $SU(2)$

Even larger symmetry corresponding to the $SU(2)_L \otimes SU(2)_R$ symmetry. This symmetry is exact in the limit $m_u = m_d = 0$ is taken.

- **Chiral symmetry** $SU(3)$

The $SU(3)_L \otimes SU(3)_R = SU(3)_V \otimes SU(3)_A$ symmetry includes the strange quark in the vanishing mass limit $m_u = m_d = m_s = 0$.

The chiral symmetry is closely related to the Dirac equation itself. One can find a representation of the γ matrices, known as the Weyl representation, in which the rotation transformation $S[\Lambda_{rot}]$ and the boost transformation $S[\Lambda_{boost}]$ which form the six matrices $S_{\mu\nu}$ are block diagonal [22]. The 4D spinors can be separated into two irreps (left and right) acting on two 2D spinors. The 2D spinors are called the Weyl spinors and transform

in the same way under rotations and oppositely under boosts. The Weyl representation of the γ matrices is also called the chiral representation. However, this is possible only in the Weyl representation of the γ matrices. To define chiral spinors for any representation of the γ matrices, it is required to introduce the γ^5 matrix:

$$\gamma^5 = -i\gamma^0\gamma^1\gamma^2\gamma^3 \tag{2.C.7}$$

which fulfills the properties [22]:

$$\{\gamma^5, \gamma^\mu\} = 0 \tag{2.C.8}$$
$$(\gamma^5)^2 = 1 \tag{2.C.9}$$
$$[S_{\mu\nu}, \gamma^5] = 0 \tag{2.C.10}$$

The second equation of 2.C.10 can be used to construct the chiral left and right projectors:

$$(\gamma^5)^2 = 1 \tag{2.C.11}$$
$$1 - (\gamma^5)^2 = 0 \tag{2.C.12}$$
$$(1 + \gamma^5)(1 - \gamma^5) = 0. \tag{2.C.13}$$

Normalised as:

$$P_L = \frac{1}{2}(1 - \gamma^5) \tag{2.C.14}$$
$$P_R = \frac{1}{2}(1 + \gamma^5) \tag{2.C.15}$$
$$\text{and} \quad P_L + P_R = 1 \tag{2.C.16}$$

which project into the two left and right irreps for any representation of the γ matrices.

The fact that the right and left spinors transform the same way under rotation and oppositely under boosts means that right and left spinors are related by parity transformation as the parity does not change rotation but changes the sign of the boost [23]. If the Lagrangian has a chiral symmetry, it means that it can be separated into two subLagrangians, left and right, and left and right spinors do never mix. The mass term $m\bar{\psi}\psi$ of the Lagrangian Eq. 2.B.1, however, explicitly mixes the left and right spinors and breaks the chiral symmetry. This chiral breaking behaviour can also be seen by considering the conservation of the vector and axial current:

$$j^\mu(x) = \bar{\psi}(x)\gamma^\mu\psi(x) \tag{2.C.17}$$
$$j^{\mu 5}(x) = \bar{\psi}(x)\gamma^\mu\gamma^5\psi(x) \tag{2.C.18}$$
$$\tag{2.C.19}$$

In the case of vanishing mass, $\partial_\mu j^\mu = \partial_\mu j^{\mu 5} = 0$ [4], but for non zero mass, $\partial_\mu j^{\mu 5} \neq 0$ and so the axial current is not conserved and the chiral symmetry is broken.

The chiral symmetry is hence explicitly broken by the bare mass of the quarks generated by the Higg's mechanism, but this mass is low enough to consider that the chiral symmetry is approximately conserved. However, experimental results do not show any measurement of chiral partners, particles which differs only by their parity like scalar and pseudoscalar mesons and have the same mass which settles that the strongly interacting matter is not chiral. As a consequence, the chiral symmetry must be dynamically broken, at least at low energy in the non perturbative part of QCD, by the generation of a non negligible mass term originating from interaction with QCD vacuum [24] while the QCD Lagrangian remains at first sight chiral invariant. The chiral symmetry $SU(3)_V \otimes SU(3)_A$ is said to be spontaneously broken into $SU(3)_V \otimes U(1)_V$, the flavour symmetry and the baryonic number. Pseudo-Goldstone bosons are produced as the breaking is done spontaneously, like the pseudoscalar mesons which have a very low mass (but non zero as the symmetry is not exact) compared to its chiral partner of scalar parity [25].

QCD is then directly responsible for most of the mass of the matter. This mechanism of mass generation is explained by a mass term dynamically generated in the medium known as the scalar chiral condensate $\langle\bar{\psi}\psi\rangle$ [24]. It is interesting to look at the eigenvalues of the discrete Euclidean Dirac operator $\not{D}^E_\mu$ in order to understand the different values that $\langle\bar{\psi}\psi\rangle$ takes at low and high energies. Here are some hints about it to give a general overview but more details can be found in [24][25][26]. Assuming, that the spectrum of the Dirac operator is discrete, it obeys the eigenvalues equation:

$$\not{D}^E u_k = \lambda_k u_k \tag{2.C.20}$$

where $\psi(x) = \sum_k c_k u_k(x)$, $\bar{\psi}(x) = \sum_k \bar{c}_k u_k^\dagger(x)$, $u_k(x)$ being a set of eigenfunctions of the Dirac operator and λ_k are the eigenvalues of the massless Dirac operator. One can see that the eigenvalues of the Euclidean Dirac operator $(\not{D}^E - \lambda_k)u_k = 0$ appears as a mass term by comparison with the Dirac equation 1.E.2. Using the fermion determinant defined in [25]

$$\mathrm{Det}(-i\not{D}^E + m) = \prod_k (-\lambda_k + m), \tag{2.C.21}$$

the quark condensate has the form:

$$\langle\bar{\psi}\psi\rangle = \langle\sum_k \frac{1}{m - i\lambda_k}\rangle \tag{2.C.22}$$

The discrete sum over the λ_k eigenvalues is related to the spectral function by [25]

$$\rho(\lambda) = \langle\frac{1}{V}\sum_k \delta(\lambda - \lambda_k)\rangle \tag{2.C.23}$$

The quark condensate is now described in terms of the spectral function by:

$$\langle\bar{\psi}\psi\rangle = \langle\sum_k \frac{1}{m - i\lambda_k}\rangle = \int_{-\infty}^{+\infty} \frac{\rho(\lambda)d\lambda}{m - i\lambda} = 2m\int_0^\infty \frac{\rho(\lambda)d\lambda}{m^2 + \lambda^2} \tag{2.C.24}$$

where the limit of integration are brought from $]-\infty,+\infty[$ to $2\times[0,\infty[$ using the fact that $u_k(-\lambda)=\gamma_5 u_k(\lambda)$ and $\gamma_5 \not{D}=0$. The integral is then pair in λ.

In the perturbative domain, the spectral function for free fermion is given in [25] to be $\rho(\lambda)\propto\lambda^3$ for λ greater than the hadron scale limit μ_{hadr}. The chiral condensate is then:

$$\langle\bar{\psi}\psi\rangle \propto m\Lambda_{UV}^2 \sim 0 \tag{2.C.25}$$

in the chiral limit. The large λ contribution to the chiral condensate is 0. In the non perturbative region, there is a contribution from the $\lambda=0$ mode of the Dirac operator which makes the value of the chiral condensate non vanishing:

$$\langle\bar{\psi}\psi\rangle = -\pi\rho(0) \tag{2.C.26}$$

Eq. 2.C.26 is known as the Banks-Casher relation [24]. This contribution from the zero mode of the Dirac operator is a dynamically generated mass term breaking spontaneously the chiral symmetry. The chiral condensate is known as the order parameter of the chiral symmetry breaking. The small non zero λ modes also contributes to the spectral density and to the breaking of the chiral symmetry [26].

- **Confinement** $Z(3)$

The phenomenon of confinement is not fully understood yet. It is the ability of an interaction to give bound states instead of free particles, with the strong fact that in addition, an isolated coloured object can never be observed. This phenomenon can be interpreted differently. Some people see it through the large value in the running of the coupling constant and the Landau pole, consequence of the non-perturbative gluon interaction at large distance [27]. Others do not connect it to the value of the coupling constant of the interaction but comes more from the lightness of the confined quarks compared to Λ_{QCD} [28]. In other words, if the value of α_s was small, the strong interaction would still be a confining theory at low energy but the hadrons size would be much larger with the consequence that quarks could be seen here and there though still not as asymptotic states. The confinement is supposed to disappear at high temperature/chemical potential in favour of a plasma state. Lattice calculations show that a non zero expectation value of the temporal component of that gauge field A_0 in Polyakov gauge, known as the Polyakov loop, breaks the confinement symmetry Z_3 in the case of pure Yang Mills, where only gluons are presents. The Polyakov loop is the order parameter of the confinement symmetry breaking in pure Yang Mills matter, but it is not in the physical case of QCD where both quarks and gluons are presents. The finite mass of the quarks breaks explicitly the symmetry Z_3 and one cannot rigorously talk of a phase transition. However, the Polyakov loop remains a good indicator of the confinement/deconfinement of the strongly interacting matter [29].

- **Columbia plot**

Chiral symmetry and center symmetry are two important symmetries of QCD, the breaking of the first one gives most of the mass of the matter. The second one is supposed

to explain why quarks are not observable. It is not settled how much they are related even though the 't Hooft anomaly matching condition gives an algebraic argument in favour of the fact that the confinement implies the breaking of the chiral symmetry [30]. The lattice results has however different critical temperatures for chiral symmetry breaking and confinement-deconfinement phase transition [31] giving a different argument. Results to be taken under all the necessary caution as based on the Polyakov loop as order parameter of the confinement-deconfinement phase transition. Those symmetries are both approximately fulfilled in QCD and have their phase transition expected to be in the same range of temperature and chemical potential. They are however theoretically radically different as chiral symmetry is assumed to be exact for a vanishing mass of the quarks and the center symmetry is assumed to be perfect for an infinite mass of the quarks. The Columbia plot [32] was made to gather both symmetries on the same graph in a general framework. The chiral and confinement symmetries are studied for different values of the quarks masses. Ordinate is the mass of the strange quark and abscissa is the mass of the u or d quarks. In this configuration, the chiral symmetry is exact at the bottom left corner where the quarks mass is vanishing [33] and the center symmetry is exact at the top right corner where the quarks mass is infinite. The top right corner is also called pure gauge or pure Yang Mills region as only gluons are dynamically present.

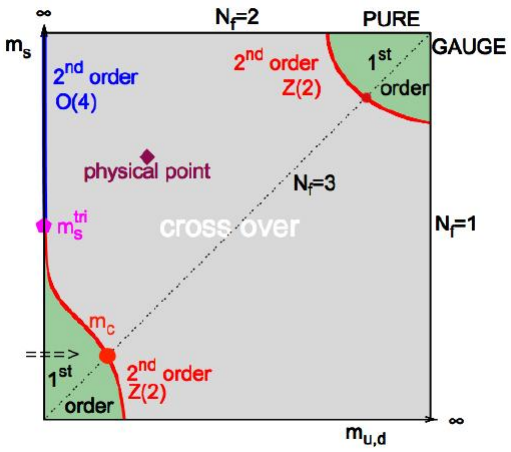

Fig. 2.4: Columbia plot [32]

Each symmetry can be studied separately in its own domain of validity before going to the real case of QCD where the fact that both symmetry are approximate makes everything much more difficult to understand.

Having discussed the Lagrangian and the symmetries of QCD, we present now the two main tools that exist to study QCD, the perturbative QCD (pQCD) approach and the Lattice QCD (lQCD) calculations.

2.D Studying QCD: the perturbative QCD

This section on perturbative QCD has three purposes: to present the concept of renormalisation and the consequence on the NJL model, to explain the asymptotic freedom and the Λ parameter from the renormalisation formalism to show the limitation of the perturbative approach and confirm the utility of effective non perturbative models like (P)NJL and to introduce finite temperature and chemical potential effects that contribute to the NJL approximation.

Perturbative QCD is at the moment the only analytical tool to study QCD. It consists as in QED, in calculating cross sections as an expansion in powers of α_s, the strong coupling constant.

$$\sigma = \sigma_0 + \alpha_s\sigma_1 + \alpha_s^2\sigma_2 + ... \tag{2.D.1}$$

In QED, $\alpha_E = \frac{1}{137}$ when the value of the running is taken at low virtuality, ie low energy and remains low on the whole spectrum of energies experimentally accessible. This facilitates the convergence of the perturbative expansion even though a logarithmic form factor can appear [34]. In QCD, $\alpha_s \sim \mathcal{O}(1)$ at low energy. The coupling is strong and a perturbative expansion does not converge.

Renormalisation and asymptotic freedom

In QFT, calculations including internal loops can be divergent which leads to consider that field theories are only effective models valid up to a certain limit in energy and momentum. The first idea of renormalisation was to consider that there are different parameters in the theory taken as constants, like the masses of the particles or the electric charge of the electron for example. However, they are not the same than their corresponding observables measured experimentally because they are defined at a given scale. Their value should depend on the scale and consequently should not be constant. The running of the constants parameters depends on a scale called the renormalisation scale. At first sight, diagrams are divergent if the numerator has a higher power of momentum than the denominator [4]. From this consideration the superficial degree of divergence D can be defined and diagrams with $D = 0$ are logarithmically divergent, $D > 0$ are Λ^D divergent, $D < 0$ are not divergent for 4 space-time dimensions. This consideration is a little crude as symmetries can reduce or cancel those divergences, but gives already a good insight. The degree of divergence can also be obtained by performing a dimensional analysis from the Lagrangian. Considering that the Lagrangian has the dimension $(mass)^{-d}$, d being the spacetime dimension, the dimensions of the fields and the coupling constant can be determined from dimensional analysis. The superficial degree of divergence D obeys:

$$D = d - N\frac{d-2}{2} - V(d - n\frac{d-2}{2}) \tag{2.D.2}$$

where V is the number of vertices, N the number of external lines and d the space-time dimension.

Three cases appear:

- super-Renormalisable theory: the coupling constant has positive mass dimension

- Renormalisable theory: the coupling constant is dimensionless
- Non-Renormalisable theory: the coupling constant has negative mass dimension

However the cancellation of the divergences must be mathematically clarified as it is the subtraction of two infinities integrals. This can be done by using a regulator cut-off or a dimensional regularisation [4]. A large choice of regulation scheme exists but at the end, the results must be independent of the regulator and the schemes. After the renormalisation procedure, divergences remains but in a way that it can be handled (logarithmic divergence for example) and there are a finite number of them. If this is not the case, the theory is non renormalisable. It sometimes considered as a weak point of the (P)NJL model that it is not renormalisable. The model being valid only up to a given scale because of the approximations made, it is however not of high importance. A ultraviolet cutoff will be added to the parameters of the model in order to prevent any divergences.

The importance of renormalisation in QCD is that among the constant parameters that becomes non constant figures the coupling of the strong interaction α. It obeys the renormalisation group equation [4] for a dimensionless quantity R and vanishing quark mass:

$$\left[Q^2\frac{\partial}{\partial Q^2} - \beta(\alpha(\mu))\frac{\partial}{\partial\alpha(\mu)}\right] R\left(\frac{Q^2}{\mu^2}, \alpha(\mu)\right) = 0 \tag{2.D.3}$$

with:

$$\beta(\alpha_\mu) = \mu^2\frac{\partial\alpha_\mu}{\partial\mu^2} \tag{2.D.4}$$

In QCD:

$$\beta(\alpha) = -b\alpha^2 \tag{2.D.5}$$

with:

$$b = \frac{11N_C - 2N_f}{12\pi} \tag{2.D.6}$$

The influence of the change in renormalisation scale on the results is measured with the β function. A positive β function means that the theory is divergent at large energies and has a Landau pole in the UV. Many theories have a Landau pole in the UV like QED and ϕ^4 theories, even though the small value of the coupling constant of QED naturally suppresses divergences in the energy range of experimental particle physics and even beyond. The Landau pole appears at such large energies that it does not trouble the accuracy of the predictions that are made with QED. On the other hand, QCD has a negative β function which gives birth to the phenomenon of asymptotic freedom. To solve the renormalization group equation, the running of the coupling constant is introduced $\alpha(Q^2) = \alpha\left(\frac{Q^2}{\mu^2}, \alpha_\mu\right)$. In order that $\alpha(Q^2)$ satisfies the renormalisation group equation, it must have the form:

$$\alpha(Q^2) = \frac{1}{b\left[\ln\left(\frac{Q^2}{\mu^2}\right) + \frac{1}{b}\left(\frac{1}{\alpha_\mu} - \frac{1}{\alpha_0}\right)\right] + \frac{1}{\alpha_0}} \tag{2.D.7}$$

In the limit $Q^2 \to \infty$:

$$\alpha(Q^2) \to \frac{1}{\ln\left(\frac{Q^2}{\mu^2}\right)}, \tag{2.D.8}$$

meaning that the coupling vanishes at high energy. One has to notice that the sign of the β function and consequently the possibility of having asymptotic freedom depends on the number of colors and flavours of the theory, see Eq.2.D.6. For QED, the running of the coupling is interpreted as a large value of the charge screened by the photon polarisation of the vaccum at large distance which leads to a small coupling constant. At short distance, there is no more screening and coupling becomes larger and larger. For QCD, this is the other way around. The value of the charge is low, but enhanced by the gluons polarisation to give a large coupling at large distance [27].

The Λ_{QCD} parameter

pQCD determine how the coupling constant changes with respect to the renormalisation scale, but does not give the value of the coupling constant. The value is given by experiments and is usually determined from the mass of the Z boson which belong to the perturbative domain and define the reference scale m_Z. In general, the m_Z dependance in α_{m_Z} is traded to a Λ_{QCD} parameter. There is only one parameter left, against two before and the coupling constant becomes at leading order:

$$\alpha(Q^2) = \frac{1}{b\ln\left(\frac{Q^2}{\Lambda^2_{QCD}}\right)} \tag{2.D.9}$$

Λ_{QCD} is the Landau pole, i.e. the value of Q at which Eq. 2.D.9 is singular. Then when Q^2 is of the order Λ_{QCD} ($\sim 200MeV$), we enter the non perturbative region. The definition and the use of the Λ_{QCD} parameter is not so easy mainly for three reasons:

- Λ_{QCD} depends on the number of flavour through the β function. It is then important to decide the number of flavour taken into consideration, especially the light ones for which the mass is negligeable as much below the energy scale [16].
- Λ_{QCD} depends on the renormalisation scheme. The two first coefficient of the β function b and b' are independent of the scheme, but this is not the case of the higher coefficients for next to next to leading order [16]. In any case, the value of the coupling constant obtained from the scheme in which Λ_{QCD} is calculated must be the same than the experimental value measured to decide the scale [16].

Finite temperature and chemical potential pQCD

A plasma of massless particles (Higg's mass is often neglected for light quarks) is characterized by a temperature T, a chemical potential μ, and a coupling constant g. Generally speaking, elementary particles are modified when they propagate in a medium. They are said to be "dressed" by their interactions and acquire a self energy and an effective mass. They become quasiparticles or collective modes. Quasiparticles are characterised by a dispersion law E(p) and a decay rate [35]. The collective modes appear generally as poles of the propagator with well defined quantum numbers. The real part is the dispersion law while the imaginary part is the decay rate. The standard pQCD is suitable to describe zero temperature system, but at finite T the convergence of the perturbative series are very poor and requires incredibly low value of the coupling constant. To overpass this problem and go to finite temperature, the Hard Thermal Loop (HTL) perturbation theory is used. In Eq. 1.G.9, the propagator must be modified by the self energy calculation to include the effect of the medium. The loop corrections to the self energy are proportional to $\frac{g^2T^2}{p^2}\tau$, τ being the amplitude without loop corrections (tree amplitude) [36]. One can separate the momenta p into two categories: the hard momenta $p \sim T$ and the correction are of order g times the tree amplitude, the soft momenta $p \sim gT$ and the correction are of order 1. For hard momenta, the perturbative series is as convergent as in the case of standard pQCD calculations. For soft momenta, the loop corrections are as important as the tree amplitude and the series are badly convergent, they are called the Hard Thermal Loop. The idea of the HTL consists in taking the high temperature limit of the self energy calculation where the mass term is vanishing and resuming all the Hard Thermal Loop into effective vertex and propagators. The leading order is in T^2 for the HTL contribution. The soft momenta contributions go as gT. Among the effects of those corrections induced by the medium, there are:

- The color screening or Debye screening. This phenomenon appears for space-like process like a gluon exchange in t-channel. The exchanged gluon is modified by the medium and its propagator becomes:

$$\frac{1}{p^2} \to \frac{1}{p^2 - \Pi(p_0, \vec{p})} \tag{2.D.10}$$

  Where Π is the HTL correction to the propagator. This correction is of order $\mathcal{O}(gT)^2$. The fourier transform of this new propagator has the shape of a potential:

$$\frac{\exp(-m_D + ...)}{r} \tag{2.D.11}$$

  which is coulombian at low r and exponential decay at large r. The exponential suppresion of the QCD potential is known as the color screening and m_D is the Debye mass of the particle. The HTL correction also apply to the quark propagator with the same $(gT)^2$ correction, but the coefficient in front is different for gluons and quarks, depending on the color structure. The particle being spacelike $p^2 < 0$, there is no pole in the propagator. The Debye mass is consequently not a real effective mass.

- The thermal mass are the HTL corrections for timelike particles. The order of corrections is the same $(gT)^2$ but the coefficient is different than for the Debye

screening. Another big difference is that p^2 is now positive which means that a pole can appear in the propagator. The correction turns out to be an effective mass dynamically generated by the medium. For a gluon exchange in s channel for example, the propagator of the gluon is modified:

$$\frac{1}{p^2} \to \frac{1}{p^2 - \Pi(p_0, \vec{p})} \tag{2.D.12}$$

and the dressed gluon acquires an effective mass called the thermal mass. We will see that this gluon mass dynamically generated by the medium accounts for the NJL approximation of replacing the gluon mediator of the interaction by a contact interaction in chapter section 3.B.1.

- The renormalisation equation becomes temperature dependent and so does the running of the coupling constant which behaves like [37]:

$$\alpha_s \to \frac{1}{\ln\left(\frac{T^2}{\Lambda^2_{QCD}}\right)} \tag{2.D.13}$$

  The asymptotic freedom now occurs at large temperature.

- Medium corrections also appear at finite chemical potentials with the Hard Dense Loop theory. The running of the coupling behaves similarly [38]

$$\alpha_s \to \frac{1}{\ln\left(\frac{\mu^2}{\Lambda^2_{QCD}}\right)} \tag{2.D.14}$$

The pQCD at finite T and μ is then limited to large temperatures and chemical potentials. At low energy, temperature or chemical potential, QCD must be treated non perturbatively.

2.E Studying QCD: non perturbative QCD

One has understood from section 2.D that below Λ_{QCD}, the standard perturbative formalism does not apply as series do not converge. One need non perturbative methods to understand the physics of the strong interacting matter at low energy. The main non perturbative theory from QCD first principles is the numerical lattice QCD theory, but analytical studies like the Dyson-Schwinger [39] or the Functional Renormalisation Group (FRG) [40] theories also exist and will be shortly presented in this section.

Discretisation and finite μ problem

One of the non perturbative approach to study QCD is the lattice approach. The space time is discretised in a 4D box of size L with lattice spacing a.

$$\int d^4x f(x) \to \sum_x f_x \tag{2.E.1}$$

The size of the box is fixed as $V = L^4$ where $L = N \cdot a$. The continuum limit is reached when $a \to 0$ and $\to \infty$. The lattice spinors gauge transform as $\psi'_x = \Omega\psi_x$, with Ω an arbitrary element of SU(3), and the derivative is $\partial_\mu\psi_x = \frac{\psi_{x+a\vec{\mu}}-\psi_x}{a}$. However, in practice, higher order derivatives are required to include more neighbours. The lattice action is invariant under gauge transformation if:

$$\bar{\psi}'_x\psi'_x \to \bar{\psi}_x\Omega^\dagger_x\Omega_x\psi_x = \bar{\psi}_x\psi_x \tag{2.E.2}$$

and:

$$\bar{\psi}'_x\psi'_{x+a\vec{\mu}} \to \bar{\psi}_x\Omega^\dagger_x\Omega_{x+a\vec{\mu}}\psi_{x+a\vec{\mu}} \neq \bar{\psi}_x\psi_x. \tag{2.E.3}$$

The derivatives are not gauge invariant and the gauge field: $\bar{\psi}_x U_{\mu x}\psi_x$ must be added in order to restore gauge invariance, transforming as : $U'_{\mu x} \to \Omega_x U_{\mu x}\Omega_{x+a\vec{\mu}}$. The gauge field is then a gauge link between the nodes of the lattice. The partition function of QCD in the grand canonical ensemble is [41]

$$Z = \int \mathscr{D}_U \mathscr{D}_{\bar{\psi}} \mathscr{D}_\psi \exp(-S) \tag{2.E.4}$$

with the action :

$$S = \int_0^{\frac{1}{T}} d^4x \left(\frac{1}{4}G_{\mu\nu}G^{\mu\nu} - \bar{\psi}M\psi\right) \tag{2.E.5}$$

The first term is the Yang Mills action describes the propagation of the gluons. The second term is the fermion matrix term $M = D[U] + m + \mu\gamma_4$ which depends on the gauge link U and the chemical potential. The Grassman integral over the fermion fields can be performed using $\int d\eta d\eta^\dagger \exp(-\eta A\eta^\dagger) = \exp[Tr\ln(A)]$ and the relation $Tr\ln = \ln\mathrm{Det}$[42] and:

$$Z = \int \mathscr{D}_U \exp(-S_{YM})\mathrm{Det}(M) \tag{2.E.6}$$

where $\mathrm{Det}(M)$ is the well known fermion determinant responsible of the large time consuming of the computational calculations on the lattice. The substitution of this term to a constant reduces this cost and is known as the quenched approximation, allowing lQCD to have a high performance in the description of the pure gluon matter. In addition, the fermion determinant turns out to be complex when the chemical potential μ is not zero. This is the sign problem and it prevents any lattice calculations at finite μ apart of a Taylor expansion.

The lattice calculations are done using the Monte Carlo integration statistical method, carrying both statistical and systematics error caused by the finite lattice spacing. The systematics error are highly reduced by considering several lattice spacing and the extrapolation to vanishing spacing corresponding to the continuum limit [43]. Solving the sign problem remains an active domain of research with approaches like deformation of

the integration contour into the complex plan, complex Langevin dynamics, Lefschetz thimbles [44, 45]...

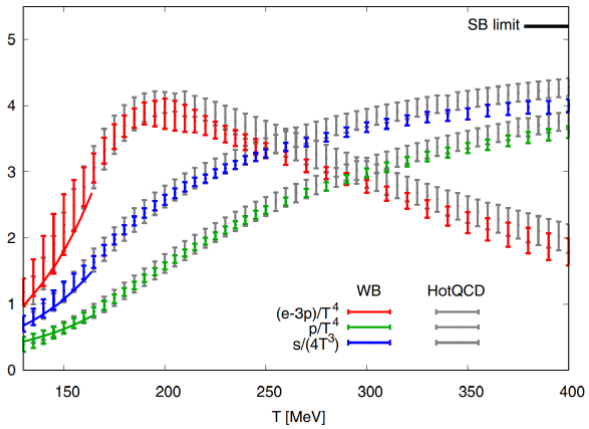

Fig. 2.5: 2+1 flavour continuum extrapolated lattice equation of state from the HotQCD collaboration [46] and the WB collaboration [31].

One of the success of the lattice calculation is the calculation of the QCD equation of state see Fig. 2.5, which is the reference in the community at the moment. The Hot QCD Collaboration [46] and the Wuppertal-Budapest WB collaboration [47] present two QCD equations of state for 2+1 flavours continuum extrapolated (including u,d and s quarks with $m_s \neq m_u, m_d$, both in agreement within the error bars. They predict a cross over transition at vanishing μ with $Tc \sim 155MeV$, a smooth transition in which all the derivatives of the order parameter are continuous.

2.F Phase diagram of QCD and experimental approach of the QGP

The aim of this research is to explore the phase diagram of the strongly interacting matter as a function of the temperature and the chemical potential. If this diagram is known, one could predict how strongly interacting matter behaves if it is in thermal equilibrium at a given T and μ. The main challenge of the QCD phase diagram is the transition between hadronic matter and the Quark Gluon Plasma (QGP).

Hadronic matter

Hadronic matter might seem to be a well known area of the phase diagram as it is experimentally observable. However, theories of nuclear physics are only effective theories of QCD and cannot explain why hadrons exist. The strong interaction is then described only from empiric interaction potential of interaction. Moreover, extreme conditions make it complicated to collect accurate data from interesting regions of the phase diagram as the neutron star for example.

QGP

To study experimentally QGP is harder than the hadronic matter. The temperature or density required and its lifetime and size are too extreme to get instruments able to measure it directly. On the other hand, many theoretical tools have been developed with success and experiments still manage to measure probes surviving or created in the QGP, see Fig. 2.6. The QGP region of high temperature and low chemical potential is expected to be the conditions that exists in the early universe few micro seconds after the Big Bang [48][49]. The large chemical potential and small temperature region is expected to be representative of the matter inside neutron stars. Whether the neutron star core is made of dense hadronic matter, dense QGP matter or hybrid matter, or even whether all those possibilities exist is still under discussion. At even larger chemical potential, pQCD calculations have predicted a color superconducting matter known as the Colour-Flavour Locking [50].

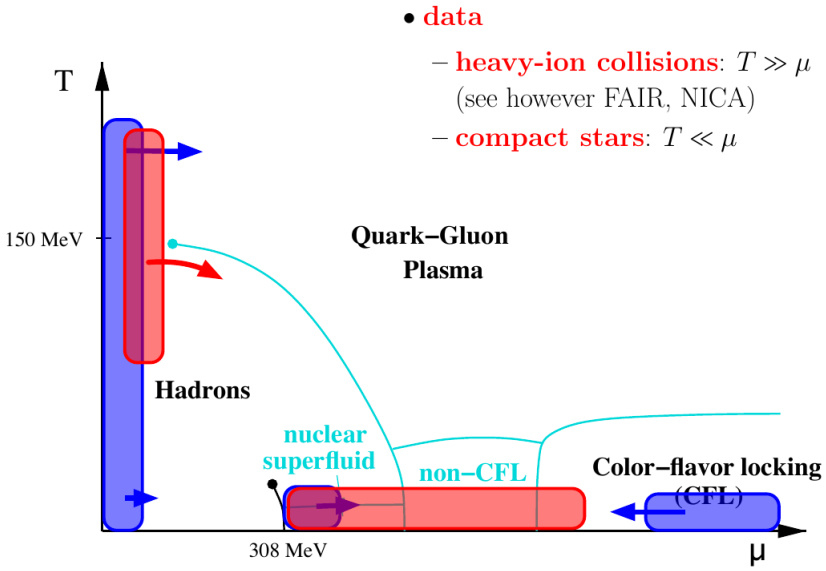

Fig. 2.6: Experimental data in red and theoretical predictions in blue of the phase diagram of strongly interacting matter [51]

For completeness, another important quantity of the phase diagram could be the magnetic field as the neutron stars generate a large magnetic field and also do the colliders when accelerating the bunch of particles [52]. This could affect the coordinates and nature of the transition. The challenge for QCD is the prediction of a state which is not directly experimentally observable because of the phenomenon of confinement. Experimentalist have to understand QGP matter from a matter which is not made of free quarks and gluons but of hadrons. To do so, they study observables which are considered as probes of QGP. The phase diagram of QCD covers a large area in T and μ, different colliders have been built, each of them having special characteristics, to study a special area of the QCD phase diagram. Here is a listing of the historical probes of the QGP in the low density region of the phase diagram. The probes are generally classified according to the energy required to produce them: soft probes for low energy and hard probes for high

energy. Hard particles tend to be produced at the origin of the QGP during hard parton scattering when soft particles appear more at the end of the QGP when it expands and start to cool down.

Soft probes

Strangeness enhancement comes from the fact that the channel $gg \rightarrow \bar{s}s$ is expected to be higher in the QGP phase and leads to a higher production of strange quarks and antiquarks in the medium [53]. The relative lightness of the strange quarks allows the assumption that strange quarks are thermalised like u and d quarks. An increase of the number of strange hadrons is then expected to be observed in the detectors.

Anisotropic flow The anisotropic flow shows that the distribution of the particles in momentum space in the final state is not isotropic. This anisotropy has as origin the geometry of the collision, which for non central collisions has an almond shape. This spatial deformation in the initial state induces an anisotropic momentum distribution in the final state enhanced by the multiple interactions in the medium. The anisotropic flow can be measured. It is a collective effect in the medium and a probe of the thermalisation of the medium which makes it a probe of the QGP [54]. 13 TeV collisions in proton-proton have shown a non zero elliptic flow [55] which has led to a reconsideration of either the anisotropic flow as probe of the QGP or the proton-proton collision as reference collision with no collective effects.

Photons are classified in many types. The direct photons are composed of thermal photons and prompt photons [56]. Thermal photons come from physical phenomenon taking place in hot medium as parton collisions, radiation of the medium... They are a large contributions to the low p_T spectrum. They are expected to come from thermal radiation of the QGP and are therefore a thermometer giving the temperature during the QGP formation: 300 MeV at LHC against 220 MeV at RHIC [57][58]. Prompt photons are produced in hard processes at the beginning of the collision. Direct photons are very useful to test the pQCD predictions. They represent roughly 50% of the photon production in QGP, leading to the conclusion that photon production is mostly done in the early stages of heavy ion collision in the center of the QGP.

Hard probes

Quarkonia are heavy flavour mesons as $c\bar{c}$ charmonium or $b\bar{b}$ bottomonium. Charmonium are mainly produced by fusion of gluons $gg \rightarrow c\bar{c}$ in the early stages of the heavy ion collision during or even before the QGP formation as their formation time is short. They are a thermometer of the QGP as they require a large energy to be produced. The large mass of the quarkonia makes them hard to thermalise and messaging many information about the QGP [59][60].

Jet quenching Jets are a flux of collimated particles coming from a high energetic parton traversing the QGP. The high energetic partons evolving in the QGP interact with

the medium which leads to energy loss via bremsstrahlung or parton-parton collisions. This is called the jet quenching. This energy loss provides useful information on the transport properties and the thermodynamics of the medium. The jets can be measured as they are mostly ejected from the QGP back to back.

Two main directions of the QGP study can be pointed out:

- The high energy colliders which study the matter at high temperature and small density, dedicated to the study of the early universe just after the big bang like the LHC or RHIC.
- The lower energy colliders (NICA, FAIR, SPS...)designed to study the matter at larger densities and smaller temperatures. They are dedicated to chiral phase transition studies and to the location of the Critical End Point: the second order phase transition point that ends the first order phase transition critical line.

The colliders of interest to study the QGP are now presented, with a particular emphasis of those devoted to low beam energy, for the search of the Critical End Point (CEP) and the first order phase transition of the phase diagram of strongly interacting matter.

CERN

The LHC is the most famous collider at CERN, being the highest beam energy collider in the world. Its main focus was the discovery of the Higgs boson. This goal was fulfilled in 2012 [61] but many questions remain like the search for supersymmetric particles, the study of the QGP, the CP violation for instance and four experiments are settled on the LHC ring. However, older and smaller colliders are used to accelerate particles before injection into the LHC and for lower energy experiments. Among them, the Super Proton Synchrotron (SPS) hosts the SHINE experiment to study the phase diagram of QCD at large μ.

SHINE The NA61/SHINE experiments at the CERN Super Proton Synchrotron (SPS) is a fixed target experiment devoted to the study of the first order phase transition and the search for the CEP [62]. The goal of SHINE is to study systematically the same reactions at different collision energies and repeat the procedure for different system size. SHINE is searching for fluctuations of conserved charges: electric, strangeness, baryon number..., considered as a manifestation of the presence of a CEP [63]. The measurement of SHINE should also constrain more the transport coefficients of the QGP [64].

RHIC

The Relativistic Heavy Ion Collider, in Brookhaven (USA) is the other presently working large ion collider. The ring is smaller than for the LHC with 3.83 kilometres of circumference but is also older as it has been delivering data for almost 20 years [54]. RHIC has also a low energy project called the Beam Energy Scan program (BES) [65], in order to study the finite density part of the phase diagram. The aim is to gather data for variable collision energies in order to scan a large number of combinations of

$T - \mu$ couples. The study of the probes of the QGP reveals if a QGP was or was not created during the collision. This could allow for constraining the range of a possible first order phase transition. The BES program uses statistical-thermal models to determine the temperature and the chemical potential at the freeze-out. Results have shown that at $\sqrt{s_{NN}} = 7.7$ GeV, QGP signatures seem to disappear, particularly the elliptic flow signature. The BES program has concluded that they expect the phase transition occurs between between $\sqrt{s_{NN}} = 11.5$ GeV and $\sqrt{s_{NN}} = 39$ [66]. This result has led to the BES II [67].

The BES program is also searching for signs of critical fluctuations, as expected to happen around the CEP. However, those critical fluctuations could be erased by many other effects like the finite size of the system for example [66].

GSI and FAIR

FAIR, the Facility for Antiproton and Ion Research in Darmstadt (Germany), is a project of a ring accelerator of 1.1 km of circumference called SIS100 using the already existing GSI colliders as first acceleration step [68]. The consequences are a higher intensity and quality beam and a high diversity of accelerated ions and antiprotons. The project relies on innovative technology like a ultra high vacuum (10^{15} less than atmospheric pressure), superconducting magnets and strong magnetic field that can be quickly change and still guide the ions with a high precision, cryogenic technology for superconductivity (Helium liquid at -269 C), high control system and parallel operation and big data center to process and store data [68].

CBM the Compact Baryonic matter experiment explores the QCD phase diagram in the region of high baryonic densities [69]. CBM targets to a better constrain of the equation of state of the neutron star core and to the study of a possible first order chiral phase transition looking for a CEP and chiral restoration. The detector is designed to study collective behaviour of hadrons like anisotropic flow and exotic particles as strange, charmed particles and vector mesons production [70].

NICA

In Dubna (Russia), the Nuclotron-based Ion Collider fAcility (NICA) is under construction in order to study the dense matter for $\sqrt{s}_{NN} = 8 - 11\ GeV$. The main ring of circumference 503.04 m is supplied by a network of linear accelerators, booster and nuclotron. The pre-accelerators have another exit that can also direct the bench of particles toward an area of fixed target experiments [71] Three detectors will be operational on NICA: the Baryonic Matter at Nuclotron (BM@N) detector for fixed target experiment, the Spin Physics Detector (SPD) and the MultiPurpose Detector (MPD) in the collider experiments, BM@N and MPD being the one especially devoted to work at maximum baryonic density in the search of chiral phase transition and the CEP. Also the possibilities of making both fixed target and colliding experiments allow for high precision measurements and a large phase space covering. NICA's main purpose is to reach the highest net baryon density to record a maximum in K+/p+ ratio, a transition from a

Baryon dominated system to a Meson dominated one in order to see a sign of first order phase transition,a mixed phase creation or a CEP. The BM@N detector is specialised in the measurement of the strange hadrons. The MPD will study fluctuations and correlations with a large covering in rapidity and p_T especially for low p_T considered as very important [72].

With BM@N and MPD at NICA, CBM at FAIR/GSI, NA61/SHINE at CERN and BES at RHIC, many experiments are now devoted to the study of the high baryonic matter in order to determine the localisation of the first order chiral phase transition and the CEP. All those experiments are at the same time complementary in energies in order to maximise the research area but also share a range of energy to double check possible results. However, the first principles theories are not yet operational on this part of the phase diagram. In this situation, approximations must be made and effective models come into business to make predictions. In this respect, the (P)NJL model is interesting as based on a Lagrangian and sharing almost the same symmetries than the QCD Lagrangian, with quarks degrees freedom. Its ability to work at low energy and finite chemical potential makes it an important tool for qualitative predictions of the localisation of the first order phase transition and the CEP and to the study of the dynamical and thermodynamical properties of the QGP at low temperature.

Chapter 3

The NJL model

Using the ingredients presented in the two first chapters, one can now build the NJL model in order to study the phase diagram of strongly interacting matter at finite T and μ. It consists in making approximations on the QCD Lagrangian to construct a effective Lagrangian and make sure that they share the same symmetries. Afterwards, the gap equations will be derived to describe the dynamical mass of the quarks in the medium and the mesons will be built as a bound state of the quarks and antiquarks degrees of freedom.

3.A What are effective models of QCD?

The fact that the pertubative theory breaks off at low energy and that the non perturbative calculations based on the QCD Lagrangian are hard to work out and are even limited (sign problem) means that in order to better understand the theory and the problem we face, more constraints are needed. Those constraints can only come from experiments, which can be helped by effective models. Both need to work together even though it is not so easy. What is observable is often hard to calculate and what is easy to calculate is often hard to measure.

Effective models are simplified models of a more rigorous theory, which have a limited range of validity but make calculations easier or possible to be carried out. In the case of QCD, approximations are made to simplify the Lagrangian in order to get predictions at low energy and finite chemical potential, the area that is not not reachable with pQCD or lQCD. In most of the cases, effective models are parametrised by fit with more trustful theories or experimental data. Many effective model of QCD exists apart of the NJL model like the Sigma model [73], the DQPM model [74]...

The effective models are the bridge between QCD and the experiments. There parameters are fixed with pQCD and/or lQCD in their range of validity, and/or experimental observables and in return, they make hopefully more predictions out of the range of validity of pQCD, lQCD. Most of the time, the effective models carry errors coming from the approximations, the fits... which only make them able to restrict the area of interest for the experiments. The measurement adds new constraints on QCD but also on the effective theories which can be discarded, improved or validated to reach a better understanding of QCD.

3.B The NJL model

3.B.1 From QCD to NJL

In nature, coloured objects are not observed. However, quarks do not only carry color as quantum number but also flavour. The color dynamics should then become a flavour dynamics with quark interactions leading to a color blind effective theory at low energy. The color blind approximation of QCD can be found by simplifying is equation of motion [75]. The Yang-Mills Euler Lagrange equation of motion for any field are:

$$\frac{\partial \mathscr{L}}{\partial \phi} - \partial_\mu \left[\frac{\partial \mathscr{L}}{\partial(\partial_\mu \phi)} \right] = 0 \tag{3.B.1}$$

for any ϕ. For quarks fields, $\phi = \bar{\psi}$, the equation of motion is:

$$(i\gamma^\mu \partial_\mu - m)\psi = -g\gamma^\mu t^a A^a_\mu \psi. \tag{3.B.2}$$

For gluons fields, $\phi = A^a_\nu$. The first part of the equation of motion is:

$$\frac{\partial \mathscr{L}}{\partial A^a_\nu} = g\bar{\psi}\gamma_\nu t^a \psi + \Pi_g, \tag{3.B.3}$$

where:

$$\Pi_g = \frac{\partial}{\partial A^a_\nu} \left[-\frac{1}{4} G^a_{\mu\nu} G^{a\mu\nu} \right] \tag{3.B.4}$$

and the second part is:

$$\frac{\partial \mathscr{L}}{\partial(\partial^\mu A^a_\nu)} = \partial^\mu A^a_\nu. \tag{3.B.5}$$

Together, we find:

$$\partial_\mu \partial^\mu A^a_\nu = g\bar{\psi}\gamma_\nu t^a \psi + \Pi_g \tag{3.B.6}$$

Using the approximation $\Pi_g \sim m_g^2 A_\mu$ to describe a dynamically generated gluon mass term, generated by the self interaction of the gluons predicted by Dyson-Schwinger [76] and lQCD [77] results,it gives:

$$(\partial_\mu \partial^\mu - m_g^2) A^a_\nu = g\bar{\psi}\gamma_\nu t^a \psi \tag{3.B.7}$$

The solution to Eq. 3.B.7 is:

$$A^a_\nu(x) = \int d^4y G(x-y) g\bar{\psi}(y)\gamma_\nu t^a \psi(y) \tag{3.B.8}$$

with the Green function:

$$G(x-y) = \int \frac{d^4p}{(2\pi)^4} \frac{\exp(ip(x-y))}{p^2 - m_g^2} \tag{3.B.9}$$

At low momentum transfer, equivalent in the NJL formalism to the limitation of the model to an integration from 0 to a cutoff Λ, $p^2 << m_g^2$. This traduces that the mass of the gluon is large compared to the scale of NJL. Eq. 3.B.9 becomes:

$$G(x-y) = \frac{1}{m_g^2}\int \frac{d^4x}{(2\pi)^4}\exp(ip(x-y)) = \frac{\delta^4(x-y)}{m_g^2}. \tag{3.B.10}$$

where the δ function is a manifestation of the local/contact interaction. The full equation of motion is now:

$$(i\gamma^\mu\partial_\mu - m)\psi + G_{eff}\gamma^\mu t^a\bar{\psi}\gamma_\mu t^a\psi = 0 \tag{3.B.11}$$

where $G_{eff} = \frac{g^2}{m_g^2}$. The simplest Lagrangian fulfilling this equation of motion is:

$$\mathscr{L}_{NJL} = \sum_{k=u,d,s}\overline{\psi}_k(i\gamma^\mu\partial_\mu - m)\psi_k + G_{eff}\sum_{a=1}^{8}(\bar{\psi_k}\gamma^\mu t^a\psi_k)^2 \tag{3.B.12}$$

NJL can also be obtained as a low energy color blind effective theory of QCD using the generating functional method. The functional of QCD is:

$$Z_{QCD} = \int \mathscr{D}_\psi\bar{\psi}\mathscr{D}^a_{A_\mu}\exp(\int d^4x\mathscr{L}_{QCD}) \tag{3.B.13}$$

The coloured part, here the gauge field, needs to disappear as one wishes to head to a color blind effective theory. In this aim, the functional integral is rewritten as [78]:

$$Z_{QCD} = \int \mathscr{D}_\psi\mathscr{D}_{\bar{\psi}}\exp(\int d^4x\bar{\psi}(i\gamma^\mu\partial_\mu - m^0)\psi + \Gamma[j]) \tag{3.B.14}$$

where $\Gamma[j]$ is the generating functional:

$$\Gamma[j] = \ln(\int \mathscr{D}^a_{A_\mu}\exp(-\frac{1}{4}\int F^2 + g\int A^a_\mu j^\mu_a)). \tag{3.B.15}$$

The evaluation of $\Gamma[j]$ is complicated and requires approximation to rewrite it in a Gaussian form. It is generally done by expanding this effective action is terms of the quark current j^a_μ. Then comes the following approximations. The 0^{th} order is a constant. The first order is the expectation value of the gauge field $\langle A^a_\mu\rangle$, the second order is the gluon correlation function and higher orders are negligible. For large momenta, $\Gamma^{(2)}(x,y)^{ab}_{\mu\nu}$ is the perturbative gluon propagator. For low momenta:

$$\Gamma^{(2)}(x,y)^{ab}_{\mu\nu} = \kappa\delta^{xy}\delta^{ab}g_{\mu\nu} \tag{3.B.16}$$

which again shows the NJL approximation. The NJL model is a low energy toy model of QCD with a simplified interaction term of the Lagrangian in the low energy limit 3.B.10. It is especially dedicated to the description of a QGP at low temperature and finite chemical potential. At low energy, the propagator of the gluon becomes :

$$S(p) = \frac{1}{p^2 - m^2} \quad \underset{p<<m}{\Longrightarrow} \quad -\frac{1}{m^2} = cste \tag{3.B.17}$$

and the momentum of the gluons is sufficiently low compared to their dynamical mass to be able to consider the gluons as frozen. There is no term of propagation anymore for the gluons and the gauge field in the interaction term becomes simply a constant. There is no color flux anymore and the SU(3) local color symmetry breaks down to a SU(3) global color symmetry. This type of interaction is called a four-point interaction or contact interaction like the Fermi interaction in the framework of the weak interaction. This approximation is expected to be realistic at low temperature where the gluons can be considered to be static. At higher temperature, transverse gluons starts to contribute significantly, the momenta of the gluons in the propagator cannot be considered as low anymore and the NJL model is no longer valid. The dynamical mass generation mechanism of the gluons has been studied from lattice QCD and Dyson-Schwinger calculations [76]. In addition, at finite temperature or density, the effective thermal mass coming from the Hard Thermal/Densed Loop also generates a dynamical mass enforcing the freezing of the gluons and the quarks, as discussed in section 2.D. This contribution is however very low compare to the QCD vacuum contribution and the gT correction to the quark mass is not taken into account in the NJL model presented here.

3.B.2 The $U(1)_A$ anomaly

As it was discussed in section 2.C, the QCD Lagrangian has the symmetries $SU(N_f)_L \otimes SU(N_f)_R \otimes SU(N_c)_V \otimes U(1)_V \otimes \mathscr{F}$ [79], $\mathscr{F}$ being the set of discrete symmetries C, P and T and $N_f = N_C = 3$. The NJL Lagrangian shares the same symmetry by construction, even though the $SU(N_c)_V$ symmetry is global instead of being local as the gluons are frozen. However, the three flavour NJL Lagrangian shows one more symmetry, the $U(1)_A$ symmetry, which is not present neither in nature nor in QCD. Something must be done in order to remove this symmetry from the NJL Lagrangian. The breaking of the $U(1)_A$ anomalous symmetry requires to add an extra term in the NJL Lagrangian with the constraint that the others symmetries must remain unbroken. The only term that does not break the previous symmetries but breaks the $U(1)_A$ is:

$$\begin{aligned}\mathscr{L} &= 2K\left[\mathrm{Det}(\bar{\psi}_R\psi_L) + \mathrm{Det}(\bar{\psi}_L\psi_R)\right] \\ &= K(\mathrm{Det}\left[(\bar{\psi}(1+\gamma_5)\psi\right] + \mathrm{Det}\left[\bar{\psi}(1-\gamma_5)\psi\right])\end{aligned} \tag{3.B.18}$$

This Lagrangian is known as the 't Hooft Lagrangian [80], [81]. In addition to the removed of the unwanted $U(1)_A$ symmetry, this new term splits the η meson into a $\eta - \eta'$ mixing which solves the problem of the measurement of nine mesons instead of eight, with a large mass of the η' preventing it to be a Goldstone boson [82]. The simplest three flavours NJL Lagrangian is then:

$$\mathscr{L}_{NJL} = \sum_{k=u,d,s} \overline{\psi}_k(i\gamma^\mu\partial_\mu - m)\psi_k + G_{eff}\sum_{a=1}^{8}(\bar{\psi}_k\gamma^\mu t^a\psi_k)^2 + K(\mathrm{Det}\left[(\bar{\psi}_k(1+\gamma_5)\psi_k\right] + \mathrm{Det}\left[\bar{\psi}_k(1-\gamma_5)\psi_k\right]) \tag{3.B.19}$$

3.B.3 Fierz Transformations

The four fermion interaction part of the NJL Lagrangian 3.B.19 is traditionally Fierz transformed. The Fierz transformation is a decomposition of a tensor product of vector space over its irreducible representations. The NJL Lagrangian can be Fierz transformed with respect to the color space, the flavour space and the Dirac space. The Fierz transformation of SU(3) color or flavour space for a quark-antiquark interaction in the s channel was already discussed in section 1.A, using the birdtracks formalism to be:

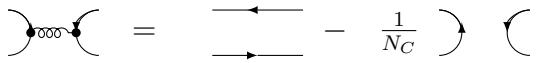

(3.B.20)

Rotating of 90° the s channel, Eq. 3.B.20, gives the t channel Fierz transformation:

(3.B.21)

Substituting 3.B.20,into 3.B.21:

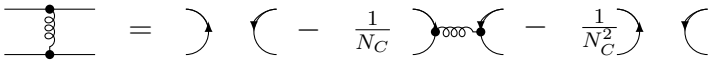

(3.B.22)

The Fierz identity for the t channel is:

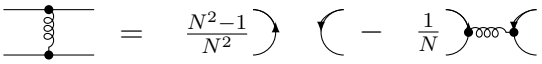

(3.B.23)

Using the traditional normalisation convention of the NJL literature:

$$\sum_{a=0} \lambda^a \lambda^a = 2\delta^a_b \delta^a_b \tag{3.B.24}$$

which introduces an additional factor 2. Eq. 3.B.23 and 3.B.20 give again the matrix form of the Fierz transformation of ref.[83]:

$$\begin{pmatrix} \delta_{ij}\delta_{kl} \\ \lambda^a_{ij}\lambda^a_{kl} \end{pmatrix} = \begin{pmatrix} \frac{1}{N} & \frac{1}{2} \\ 2\frac{N^2-1}{N^2} & -\frac{1}{N} \end{pmatrix} \begin{pmatrix} \delta_{il}\delta_{kj} \\ \lambda^a_{il}\lambda^a_{kj} \end{pmatrix} \tag{3.B.25}$$

According to Eq. 3.B.25, the $\lambda^a\lambda^a$ color interaction of QCD is Fierz transformed into a singlet representation and an octet representation, the Clebsch-Gordon coefficients indicating whether they are repulsive or attractive. Only the singlet is kept as there is no color flux in the NJL model. The interaction constant is then $G = G_{eff}\frac{N^2-1}{N^2} = \frac{8}{9}G_{eff}$. For the flavour, the $\delta_{ij}\delta_{kl}$ interaction of QCD is a also transformed into a singlet and a octet. The flavour octet term is kept only in order to have a flavour dynamics allowing the flavour to change when building interactions through meson exchange. A practical example will be shown in Chapter 5 to calculate the elastic cross sections. For the Dirac space, the irreps are $\mathbb{1}$, γ_5, γ_μ, $\gamma_\mu\gamma_5$, and $\sigma_{\mu\nu}$ and the $\gamma_\mu\gamma_\mu$ vector interaction in the s channel can be written as a linear combination of the irreducible representations:

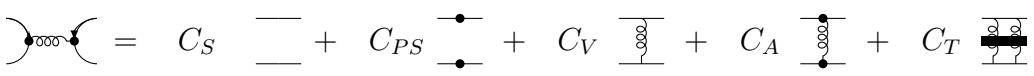

(3.B.26)

where $C_S = C_{PS} = -\frac{C_V}{2} = -\frac{C_A}{2} = 1$ and $C_T = 0$ see section 1.E. The dot accounts for γ_5 couplings and springs for γ_μ couplings. The Fierz transformation in Dirac space transforms the vector interaction into the sum of a scalar, pseudoscalar, vector and axial interactions. In addition, the index permutation gives the two possible Feynman diagrams of the Wick theorem corresponding to the mean field approximation Hartree and Fock terms. The Fierz transformation of the NJL Lagrangian is then:

$$\mathscr{L}_{NJL} = \sum_{k=u,d,s} \overline{\psi}_k(i\gamma^\mu\partial_\mu - m)\psi_k + G(\bar{\psi}_k\psi_k)^2 + G(\bar{\psi}_k\gamma_5\psi_k)^2 - \frac{G}{2}(\bar{\psi}_k\gamma^\mu\psi_k)^2$$
$$- \frac{G}{2}\sum_{a=1}^{8}(\bar{\psi}_k\gamma^\mu\gamma_5\psi_k)^2 + K(det\left[(\bar{\psi}_k(1+\gamma_5)\psi_k\right] + det\left[\bar{\psi}_k(1-\gamma_5)\psi_k\right]) \quad (3.B.27)$$

In this work, only the scalar and the pseudoscalar part of the NJL model will be studied. The vector and axial part are left for future studies.

3.C Parameters of the model

The QCD Lagrangian has, taking only light quarks into consideration, four free parameters: the QCD coupling constant g and the bare mass of the u, d and s quarks. Those parameters are not given by the theory itself, but are restricted either experimentally or from other theories like the Yukawa coupling to the Higg's mechanism for the bare mass of the quarks. In NJL, it is generally assumed that the SU(2) isospin symmetry is exact and the mass of the quarks u and d are the same. To those are added the four and six fermion coupling constants G and K. The last parameter is the regularisation cutoff Λ, as a quick dimensional analysis shows that the four fermion interaction is not renormalisable as discussed in section 2.D. In total, five parameters are required to describe the physics with the NJL model.

Those parameters are chosen by fit to experimental vacuum data like the mass of the pion (m_u), the mass of the kaon (m_s),the η-η' splitting (K) and the decay constant of the pion and the quark condensate (G and Λ)[84].

$m_u[GeV]$	$m_s[GeV]$	G	K	$\Lambda[GeV]$
0.005	0.134	$\frac{2.3}{\Lambda^2}$	$\frac{11}{\Lambda^5}$	0.569

Table 3.1: Table of the parameters of the NJL model used in this work

Different sets of parameters exist for the NJL model. Most of them lead to the same kind of physical phenomena although the numerical values predicted can be different.

3.D Mass of the quarks: the gap equations

In the NJL model, the dressed mass of the quarks is obtained by solving the gap equations. The gap equations connect the mass present in the NJL Lagrangian known as the bare mass, to the dressed mass which in addition includes the dynamical generation of mass by the QCD vacuum.

The chiral condensate is the order parameter of the chiral symmetry breaking and the thermal equilibrium is given by the differentiation of the grand potential with respect to the mass, see Eq. 1.F.3:

$$\begin{aligned}\frac{\partial\Omega}{\partial m_q} &= 0\\ \frac{\partial\Omega}{\partial m_s} &= 0\end{aligned} \tag{3.D.1}$$

One is now interested in calculating explicitly this differentiation. To do so, let's determine the form of the NJL grand potential. The partition function is defined as:

$$Z[\bar{\psi},\psi] = \int \mathscr{D}_{\bar{\psi}}\mathscr{D}_{\psi} \exp\left\{ i\int d^4x \mathscr{L}_{NJL}\right\} \tag{3.D.2}$$

For simplification, I will sketch the steps of the calculation only for the scalar four fermion interaction term. Using the Hubbard-Stratonovitch transformation, the NJL Lagrangian [85] becomes:

$$\mathscr{L}' = \mathscr{L}_{NJL} - \frac{1}{G}(\frac{\sigma}{2} + G\bar{\psi}\psi)^2 \tag{3.D.3}$$

$\mathscr{L}'$ is the bosonised NJL Lagrangian [86][87]

$$\mathscr{L}' = \overline{\psi}(i\gamma^\mu\partial_\mu - m)\psi + G(\bar{\psi}\psi)^2 - \frac{1}{4G}\sigma^2 - \sigma\bar{\psi}\psi - G(\bar{\psi}\psi)^2 = \overline{\psi}(i\gamma^\mu\partial_\mu - m)\psi - \frac{1}{4G}\sigma^2 - \sigma\bar{\psi}\psi \tag{3.D.4}$$

where σ is a bosonic field. The functional now depends on both fermionic and bosonic fields:

$$Z = \int \mathscr{D}_{\psi}\mathscr{D}_{\bar{\psi}}\mathscr{D}_{\sigma} \exp i\left(\int d^4x (i\bar{\psi}\partial\!\!\!/\psi - \frac{\sigma^2}{4G} - \sigma\bar{\psi}\psi - m\bar{\psi}\psi)\right). \tag{3.D.5}$$

The Grassman integration over the quark and antiquark fields can be performed using the Gaussian Grassman integration relation $\int d\eta d\eta^\dagger \exp(-\eta A\eta^\dagger) = \exp[Tr\ln(A)]$[88], the NJL functional becomes:

$$Z = \int \mathscr{D}_{\sigma} \exp i\left(\int d^4x\Big(- \frac{\sigma^2}{4G} - iTr(ln(i\partial\!\!\!/ - m - \sigma))\Big)\right). \tag{3.D.6}$$

The relation between the grand potential and the partition function is given by:

$$\Omega = -T\ln(Z) \tag{3.D.7}$$

which gives the following grand potential:

$$\Omega = \int d^4x i(-i\ln Tr[(i\partial\!\!\!/ - m - \sigma)] - \frac{\sigma^2}{4G}). \tag{3.D.8}$$

One can define an effective mass M:

$$M = m + \sigma \tag{3.D.9}$$

and differentiate Eq. 3.D.8 with respect to the mass:

$$\frac{\partial \Omega}{\partial m} = \frac{M-m}{2G} - \frac{2i}{Tr(i\partial\!\!\!/ - m - \sigma)} = 0. \tag{3.D.10}$$

The bosonic field σ is then given by:

$$\sigma = M - m = -\frac{4iG}{Tr(i\partial\!\!\!/ - M)} = -4G\langle\bar{\psi}\psi\rangle. \tag{3.D.11}$$

We define the scalar chiral condensate $\langle\bar{\psi}\psi\rangle$, which can be written in terms of the one fermion loop function A given in [89]

$$< \bar{\psi}_k\psi_k >= \frac{M_k}{4\pi^2} A(M_k, \mu_k, T) \tag{3.D.12}$$

where:

$$A(m_k, \mu_k, T) = -4\int_0^\Lambda \frac{p^2 dp}{\sqrt{p^2+m^2}} \left(f\left(\frac{E-\mu}{T}\right) - f\left(\frac{-E-\mu}{T}\right)\right) \tag{3.D.13}$$

The grand potential becomes:

$$\Omega = \ln Tr[\exp(\int d^4x(i\partial\!\!\!/ - M))] + 2G\sum_k < \bar{\psi}_k\psi_k >^2 \tag{3.D.14}$$

The mean field interaction $2G\sum_k < \bar{\psi}_k\psi_k >^2$ is in its final form, but not the free quark term $\ln Tr[\exp(\int d^4x(i\partial\!\!\!/ - M))]$. First, one performs a Fourier transform to the momentum space and then uses the Matsubara formalism to discretise the energy:

$$\ln Tr[\exp(\int d^4x(i\partial\!\!\!/ - M))] = \ln Tr[\exp(\int d^4p(\not{p} - M))] = -T\ln Tr[\exp(\sum_n \int d^3p(\gamma_0 i\omega_n - \gamma_i\vec{p} - M))] \tag{3.D.15}$$

The Trace over flavour, colour and spin can be performed using $Tr\ln = \ln Det$. Considering the fact that $\gamma_0 i\omega_n - \gamma_i\vec{p} - M$ is just the inverse fermion propagator $S(p)^{-1}$, one needs to bring it to a matrix form in order to calculate the determinant. The technical details of this calculation are given in ref [90] and the free fermion grand potential is brought to the form:

$$-T\ln Tr[\exp(\sum_n \int d^3p(\gamma_0 i\omega_n - \gamma_i\vec{p} - M))] = -T\sum_n \int \frac{d^3p}{(2\pi)^3} \sum_k \sum_n \ln\left(\frac{\omega_n^2 + E_k^2)}{T^2}\right) \tag{3.D.16}$$

Evaluating the Matsubara sum as seen in section 1.G and adding the 't Hooft term of Eq. 3.B.18 for which the bosonisation procedure has also been done ref. [91], the full grand potential has the final form:

$$\Omega = -2N_C(\int_0^\Lambda \frac{d^3p}{(2\pi)^3}E_p + T\int_0^\infty (\ln[1+\exp(-\beta(E_p-\mu))] + \ln[1+\exp(-\beta(E_p+\mu))]) + 2G\sum_k <\bar{\psi}_k\psi_k>^2 -4K\prod_k <\bar{\psi}_k\psi_k>) \quad (3.D.17)$$

and the full gap equations are:

$$M_k = m_k - 4G<\overline{\psi}_k\psi_k> +2K<\overline{\psi}_{k'}\psi_{k'}><\overline{\psi}_{k''}\psi_{k''}> \quad (3.D.18)$$

where k, k' and k" represents the three flavour of the quarks.

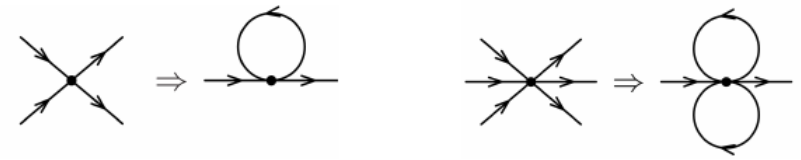

Fig. 3.1: Mean field approximation for the 4-fermion and 6-fermion interactions [20].

The gap equation 3.D.18 gives the "dressed" mass of the quarks and two possible cases appear:

- M = m. This is the QGP phase where the quarks are free. The value of the chiral condensate Eq. 3.D.12 vanishes leaving the bare mass coming from the Higgs mechanism as only contribution. The chiral symmetry is approximately restored and the bare mass is very low.
- $M \neq m$, this is the hadronic phase where the mass of the quarks is large. The value of the chiral condensate is non zero and the chiral symmetry is spontaneously broken.

The chiral condensate is considered to be the order parameter of the chiral phase transition. When its value becomes non zero, the dressed mass mixes left and right spinors and breaks spontaneously the chiral symmetry.

To summarise, the construction of the NJL Lagrangian has been done based on the static approximation made on the gluon propagator which simplifies the QCD Lagrangian 3.B.1 and by symmetry agreement with QCD and nature 3.B.2. From the Lagrangian, the grand potential is determined and from it the gap equations giving the dynamical mass of the quarks in section 3.D. From the grand potential and the mass of the quarks, all the thermodynamics can be determined and the next section presents the result obtained for the phase diagram of the NJL model.

3.E Phase diagram from the standard NJL model

In this section, the coordinates in temperature and quark chemical potential of the transition lines and their nature are calculated from the mass given by the gap equations Eq. 3.D.18 and the pressure Eq. 3.D.17.

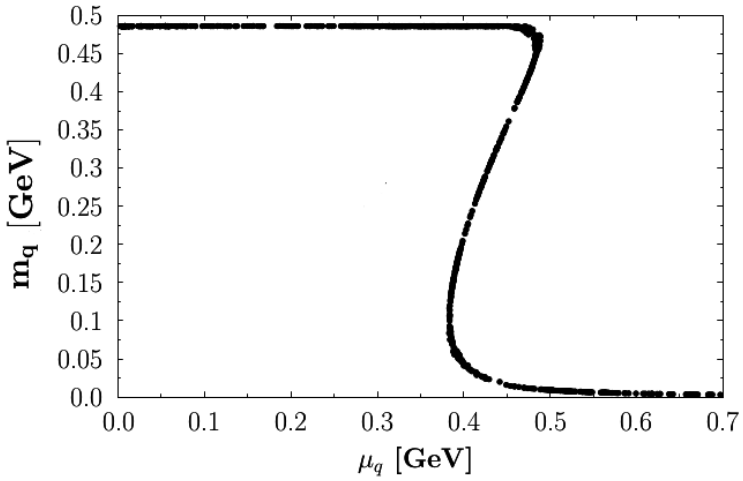

Fig. 3.2: Mass of the u quark around the quark chemical potential for which a first order chiral phase transition occurs for a temperature of $T = 0.001\ GeV$.

One can see in Fig.3.2 that at low chemical potential, for the range $\mu_q = 0-0.37\ GeV$, a single solution to the gap equations, Eq. 3.D.18, exists: the dressed mass solution with non zero chiral condensate $\langle\bar{\psi}\psi\rangle$. For large chemical potentials, for $\mu_q > 0.5\ GeV$, also a single solution to the gap equations Eq. 3.D.18 exists: the bare mass solution where the mass is the Higgs mass only. The region in between has three solutions. This is the typical feature of a first order phase transition [11]. If the upper and lower solution are physical, their lifetime beyond the critical chemical potential is very short. On the other hand, the third solution is unphysical.

The critical chemical potential of the transition can be determined using the Maxwell construction. The Maxwell construction consists in dividing the region where several solutions are possible by a vertical line such that the area on the left and on the right of this line are equal. The critical chemical potential is the chemical potential associated to this line. However, calculating the line in between the dress mass solution and the bare mass solution is not a simple exercise. It is easier and more accurate to calculate the critical chemical potential using the pressure. The pressure is a smooth observable that does not jump during the transition. The pressures related to the dressed mass solution and the one related to the bare masses cross at a point at which the state which minimises the energy changes see Fig. 3.3. This crossing point is at the critical chemical potential.

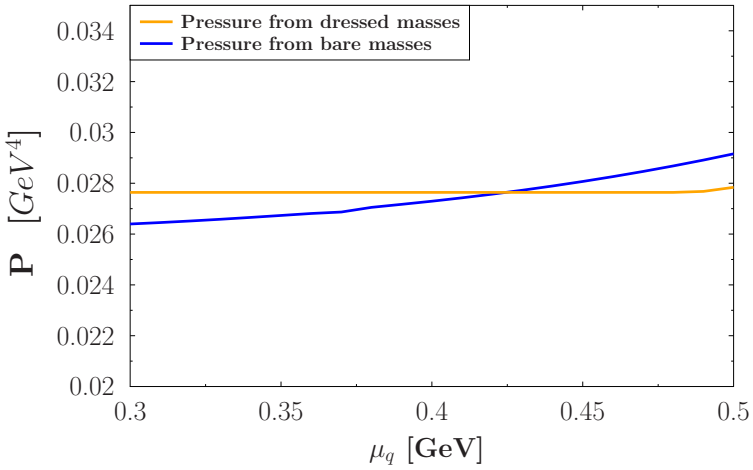

Fig. 3.3: Pressure of the two phases around the quark chemical potential for which the first order chiral phase transition occurs for a temperature of $T = 0.001\ GeV$.

For very low temperatures, the phase diagram is then characterised by a first order phase transition at a critical quark chemical potential of μ_c =0.425 GeV. The order parameter of this phase transition is the chiral condensate. The evolution of the mass of the quark u as a function of the chemical potential is displayed in Fig. 3.4.(b) (for a temperature of $T = 0.001 GeV$).

The critical chemical potential μ_c decreases as a function of the temperature and finally the phase transition becomes a cross over. The cross over region and the first order phase transition region are separated by the critical end point (CEP). The gap equations provide a convenient way to calculate it. The CEP is reached when the first and second derivative of the mass with respect to the chemical potential become infinite giving the critical temperature and chemical potential. For this couple of coordinates, the mass of the u and s quarks are given by the gap equations. In total, the CEP is determined by a set of four equations with four unknowns [90]:

$$\begin{aligned} g_u(\mu, T, mq, ms) &= 0 \\ g_s(\mu, T, mq, ms) &= 0 \\ \frac{\frac{\partial g_u(\mu,T,mq,ms)}{\partial mq}}{\frac{\partial g_u(\mu,T,mq,ms)}{\partial \mu}} &= 0 \\ \frac{\frac{\partial^2 g_u(\mu,T,mq,ms)}{\partial mq^2}}{\frac{\partial g_u(\mu,T,mq,ms)}{\partial \mu}} &= 0 \end{aligned} \tag{3.E.1}$$

g_k being the gap equation established in Eq. 3.D.18 for the flavour k. The solution of this system is $T_{CEP} = 0.113\ GeV$ and $\mu_q^{CEP} = 0.342\ GeV$.

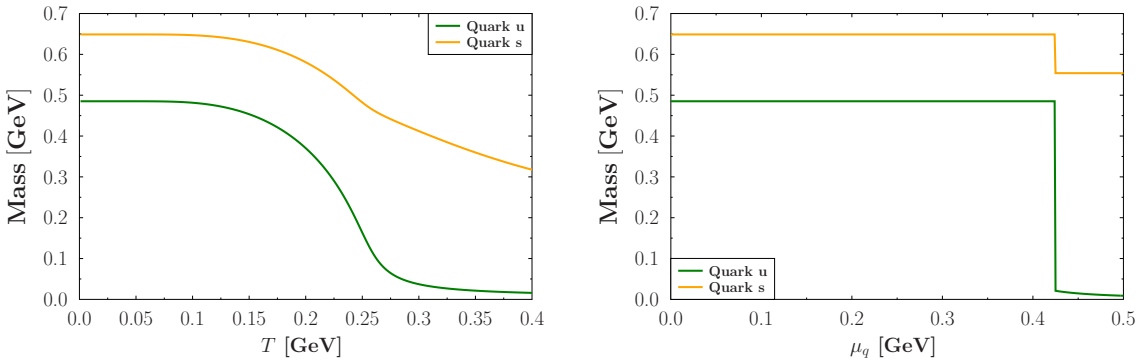

Fig. 3.4: Mass of u and s quarks (a) at $\mu_q = 0$ (b) at $T = 0.001GeV$

A first order phase transition is then predicted by the NJL model for a fixed low temperature and an increasing quark chemical potential as the mass drops sharply to its bare value in Fig. 3.4.(b). For a fixed quark chemical potential and increasing temperature, a cross over transition is predicted as the mass goes smoothly from its dynamical to its bare value in Fig. 3.4.(a). The cross over transition is chosen here as that at the inflexion point of the mass of the u quark. The whole phase diagram is shown in Fig.3.5.

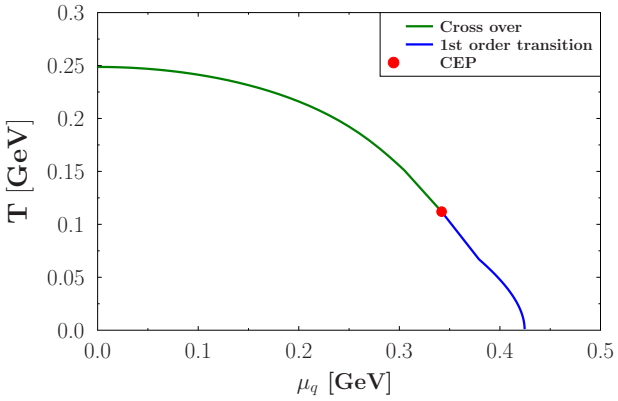

Fig. 3.5: Phase diagram of the NJL model

Fig. 3.5 shows the evolution of the inflexion point of the mass of the u quark with respect to the chemical potential, giving the critical line of the cross over phase transition, the first order line obtained from the pressure using the method presented in Fig. 3.3 and the CEP determined from Eq. 3.E.1. If the exact localisation of the CEP and the first order phase transition is not settled yet, the localisation of the inflexion point of the chiral condensate at vanishing chemical potential is trustfully predicted by the lattice calculation to occur at $T \sim 0.150GeV$. The value presented here is much higher and indicates that the NJL model can still be improved in order to described a realistic phase diagram of the strongly interacting matter.

3.F Correction to the cutoff for the calculation of the one fermion loop

One of the problem of having a cutoff in the theory is that momentum contributions beyond Λ become important for high T. A partial solution is to rewrite the Fermi-Dirac distribution in the one fermion loop function A in Eq. 3.D.12 using the relation:

$$f\left(\frac{E-\mu}{T}\right) - f\left(\frac{-E-\mu}{T}\right) = 1 - f\left(\frac{E-\mu}{T}\right) - f\left(\frac{E+\mu}{T}\right) \tag{3.F.1}$$

This leads to a separation of the integral into a thermal part (red) with Fermi-Dirac functions and a vacuum part (blue) which does not explicitly depend on temperature.

$$A = -4\left(\int \frac{p^2 dp}{\sqrt{p^2+m^2}} - \int\left(\frac{p^2}{\sqrt{p^2+m^2}} f\left(\frac{E-\mu}{T}\right) + \frac{p^2}{\sqrt{p^2+m^2}} f\left(\frac{E+\mu}{T}\right) dp\right)\right) \tag{3.F.2}$$

The thermal part is not divergent and can be integrated up to infinity. The advantage and disadvantage of this approach is discussed in [92].

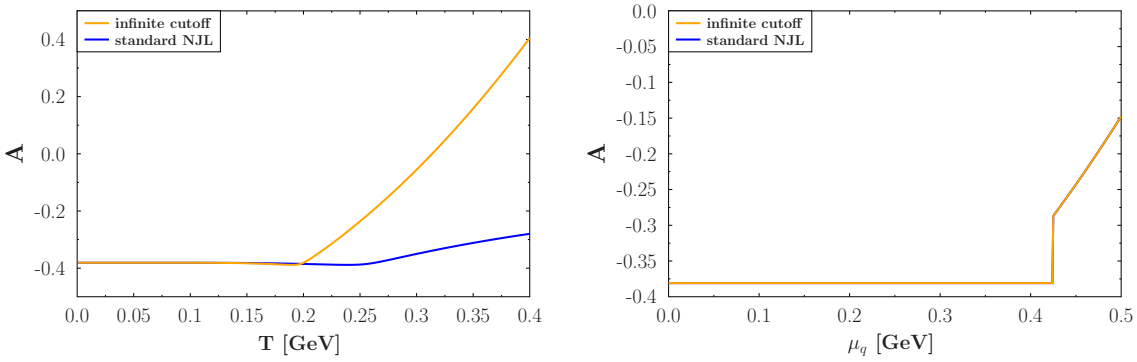

Fig. 3.6: The one fermion loop A with cutoff and with cutoff taken to infinity for the thermal part (a) as function of T at $\mu_q = 0$ (b) as function of μ_q at $T = 0$.

The Fig. 3.6 (a) shows that from T = 0.2 GeV on, the contributions of f that were taken off by the cutoff cannot be neglected anymore. This contribution was not taken into account in the previous study section 3.E. It is a first improvement of the NJL model. The Fig. 3.6 (b) shows that this correction does not make any difference at low temperatures and finite chemical potentials where high momenta do not contribute to the integral and both line are exactly the same.

With this correction to the one fermion loop, the new CEP has the coordinates: $T_{CEP} = 0.115\ GeV$, $\mu_q = 0.310\ GeV$ and the masses are modified as shown in Fig. 3.7.

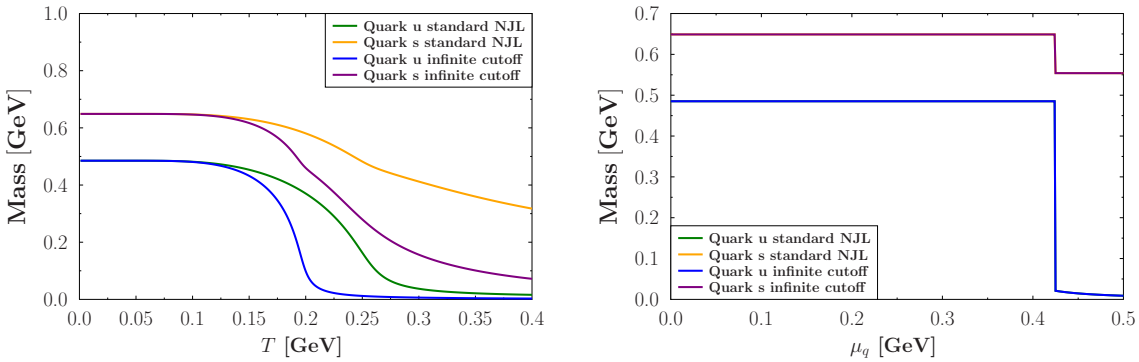

Fig. 3.7: Comparison of the mass of u and s quarks in the standard A function [89] and with the A function partially integrated to infinity Eq. 3.F.2 as a function of T (a) for $\mu_q = 0$, as a function of μ (b) for $T = 0.001 GeV$

This correction makes the cross over transition sharper and decreases the value of the inflexion point down to T = 0.190 GeV. It becomes therefore closer to the prediction of lQCD: $T_{cr} \sim 150 MeV$. The mass of the s quark becomes lower at large temperature which enforces the flavour symmetry and the chiral symmetry restoration in the QGP phase. The new phase diagram of the NJL model, considering this correction to the one fermion loop, is shown in Fig. 3.8, where it is compared with the previous phase diagram of Fig. 3.5.

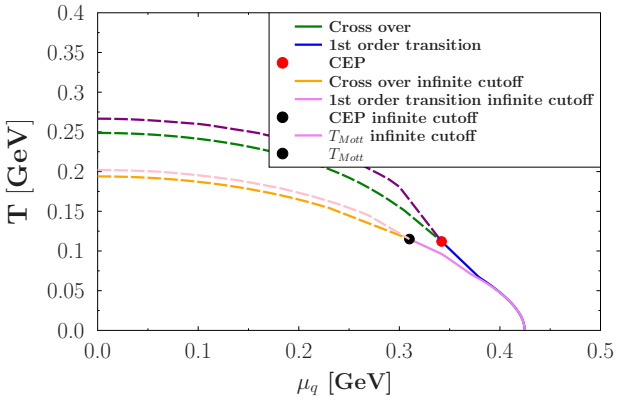

Fig. 3.8: Comparison of the NJL phase diagram with and without cutoff in the integrals over the Fermi distribution

Even if the inflexion point of the u mass is lower than in Fig. 3.5, it is still 40 MeV higher than what is predicted by the lattice results. The CEP occurs now at a lower chemical potential than before but for the same temperature. The first order transition is not much influenced by the cutoff in the vicinity of the CEP.

3.G Mesons

The NJL model describes the matter assuming that quarks are the fundamental constituents. Mesons are consequently no degrees of freedom of the model. They have to be built as quark-antiquark bound states and give the octet of mesons predicted by the quark model of $SU(3)$ flavour mentioned in section 2.C and confirmed experimentally with the addition of a ninth meson coming from the splitting of the η into the η-η' mixed state. The mesons and all the machinery developed in this section will be used to calculate the elastic quark-quark and quark-antiquark cross sections in section 5.A, first step of the calculation of the transport coefficients. The building of the mesons starts with the construction of the quark-antiquark bound state equation called the Bethe-Salpeter equation.

3.G.1 The Bethe-Salpeter equation

In NJL, to build a quark-antiquark bound state, the four fermion interaction is expanded in power of the coupling constant at the lowest order of the large N_C expansion $O(\frac{1}{N_C}$:

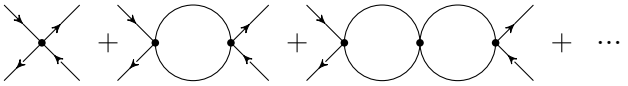

The perturbative expansion has the form of a geometric series which simplifies to:

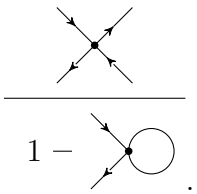

Algebraically, the associated amplitude is:

$$iU(k^2) = \Gamma(g_m + g_m\Pi(k^2)g_m + g_m\Pi(k^2)g_m\Pi(k^2)g_m + ...)\Gamma \tag{3.G.1}$$

And :

$$iU(k^2) = \Gamma\frac{2ig_m^2}{1 - 2g_m^2\Pi(k^2)}\Gamma \tag{3.G.2}$$

where g_m is the coupling constant and Π is the quark-antiquark polarisation function. One can compare this amplitude with the one of a quark-antiquark scattering occurring via a meson exchange, see Fig. 3.9, which takes the form:

$$[\bar{\psi}\Gamma\lambda_i\psi] = \frac{-ig_{m-q\bar{q}}^2}{k^2 - m^2}[\bar{\psi}i\Gamma\lambda_j\psi] \tag{3.G.3}$$

where Γ can be scalar, pseudoscalar, vector or axial depending on the spin and polarisation of the exchanged meson and the λ matrices select the flavour channel.

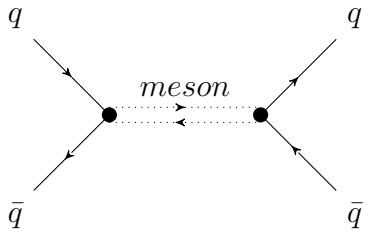

Fig. 3.9: Quark-antiquark scattering occurring via a meson exchange

The mass of the meson exchanged is given by the pole of the propagator. From Eq**??** and assuming that $\vec{k} = 0$ in $k = (k_0, \vec{k})$, the mass of the meson in the NJL bound state of Eq. 3.G.3 is the value of k_0 that verifies the equation:

$$1 - 2g_m^2 \Pi(k_0^2 = m^2) = 0 \tag{3.G.4}$$

In the bound state community, this equation is known as the Bethe-Salpeter equation. To solve the Bethe-Salpeter equation, one need to know the expression of the quark-meson coupling constant g_m and the polarisation function Π.

3.G.2 Mixing of the coupling constant

In the mean field approximation, the six fermion vertex of the t'Hooft term can be reduced to a four-point interaction by tracing over one propagator as shown in Fig. 3.10.

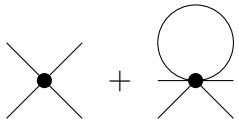

Fig. 3.10: Combination of the four-fermion and the six-fermion interaction for the calculation of the mesons

It is then possible to use the Gell-Mann matrices in flavour space to rewrite the G and the K coupling constant into a single K_{aa} constant using the meson table 3.2.

quark antiquark	$\bar{u}$	$\bar{d}$	$\bar{s}$
u	$\pi^0\ \eta\ \eta'$	π^+	K^+
d	π^-	$\pi^0\ \eta\ \eta'$	K^0
s	K^-	$\bar{K}^0$	$\eta\ \eta'$

Table 3.2: Mesons matrix in the quark model

One can see for example that $\lambda_3 = \begin{pmatrix} 1 & 0 & 0 \\ 0 & 1 & 0 \\ 0 & 0 & 0 \end{pmatrix}$ is the channel for π_0 by identification with the Table 3.2. The other channels are summarised in Table 3.3.

λ_3	π^0
$\frac{1}{\sqrt{2}}(\lambda_1 \pm i\lambda_2)$	$\pi^\pm$
$\frac{1}{\sqrt{2}}(\lambda_6 \pm i\lambda_7)$	$K^0\ \bar{K}^0$
$\frac{1}{\sqrt{2}}(\lambda_4 \pm i\lambda_5)$	$K^\pm$
λ_8	η
λ_0	η'

Table 3.3: λ representation of the light mesons

The NJL Lagrangian becomes [84]

$$\begin{aligned}
\mathscr{L} =& \bar{\psi}_k(i\partial\!\!\!/ - m_k)\psi_k \\
&+ \sum_{a=0}^{8}[K^-_{aa}(\bar{\psi}_k\lambda^a\psi_k)^2 + K^+_{aa}(\bar{\psi}_k i\gamma_5\lambda^a\psi_k)^2] \\
&+ K^-_{30}(\bar{\psi}_k\lambda^3\psi_k)(\bar{\psi}_k\lambda^0\psi) + K^+_{30}(\bar{\psi}_k i\gamma_5\lambda^3\psi_k)(\bar{\psi}_k i\gamma_5\lambda^0\psi) \\
&+ K^-_{03}(\bar{\psi}_k\lambda^0\psi_k)(\bar{\psi}_k\lambda^3\psi) + K^+_{03}(\bar{\psi}_k i\gamma_5\lambda^0\psi_k)(\bar{\psi}_k i\gamma_5\lambda^3\psi) \\
&+ K^-_{80}(\bar{\psi}_k\lambda^8\psi_k)(\bar{\psi}_k\lambda^0\psi) + K^+_{80}(\bar{\psi}_k i\gamma_5\lambda^8\psi_k)(\bar{\psi}_k i\gamma_5\lambda^0\psi) \\
&+ K^-_{08}(\bar{\psi}_k\lambda^0\psi_k)(\bar{\psi}_k\lambda^8\psi) + K^+_{08}(\bar{\psi}_k i\gamma_5\lambda^0\psi_k)(\bar{\psi}_k i\gamma_5\lambda^8\psi) \qquad (3.G.5) \\
&+ K^-_{83}(\bar{\psi}_k\lambda^8\psi_k)(\bar{\psi}_k\lambda^3\psi) + K^+_{83}(\bar{\psi}_k i\gamma_5\lambda^8\psi_k)(\bar{\psi}_k i\gamma_5\lambda^3\psi) \\
&+ K^-_{38}(\bar{\psi}_k\lambda^3\psi_k)(\bar{\psi}_k\lambda^8\psi) + K^+_{38}(\bar{\psi}_k i\gamma_5\lambda^3\psi_k)(\bar{\psi}_k i\gamma_5\lambda^8\psi) \\
&- G_V[(\bar{\psi}_k\gamma_\mu\lambda^a\psi)^2 + (\bar{\psi}_k\gamma_\mu i\gamma_5\lambda^a\psi)^2] \qquad (3.G.6)
\end{aligned}$$

with the constants:

$$\begin{aligned}
K^\pm_{00} &= G_S \mp \frac{1}{3}N_C K[iTr(S^u) + iTr(S^d) + iTr(S^s)] \\
K^\pm_{11} &= K^\pm_{22} = K^\pm_{33} = G_S \pm \frac{1}{2}N_C K[iTr(S^s)] \\
K^\pm_{44} &= K^\pm_{55} = G_S \pm \frac{1}{2}N_C K[iTr(S^d)] \qquad (3.G.7) \\
K^\pm_{66} &= K^\pm_{77} = G_S \pm \frac{1}{2}N_C K[iTr(S^u)] \\
K^\pm_{88} &= G_S \pm \frac{1}{6}N_C K[2iTr(S^u) + 2iTr(S^d) - iTr(S^s)].
\end{aligned}$$

with S^k being the propagator of the quark k. The state corresponding to the isospin I=0 and the strangeness S=0 is degenerated into three mesons: π^0, η and η'. The product $\lambda_0 \otimes \lambda_8$, $\lambda_3 \otimes \lambda_8$ and $\lambda_0 \otimes \lambda_3$ are non zero which means that unlike the others mesons, the flavour matrix is not diagonal and therefore mixing terms like K_{03}... appear [84].

$$
\begin{aligned}
K^{\pm}_{03} = K^{\pm}_{30} &= \mp\frac{1}{\sqrt{6}} N_C K[iTr(S^u) - iTr(S^d)] \\
K^{\pm}_{08} = K^{\pm}_{80} &= \pm\frac{\sqrt{2}}{12} N_C K[iTr(S^u) + iTr(S^d) - 2iTr(S^s)] \\
K^{\pm}_{38} = K^{\pm}_{83} &= \pm\frac{1}{2\sqrt{3}} N_C K[iTr(S^u) - iTr(S^d)]
\end{aligned}
\tag{3.G.8}
$$

This recombination of terms is only for the scalar and pseudoscalar part of the Lagrangian as the term of 't Hooft has the purpose to break the $U_A(1)$ symmetry and does not appear in the vector and axial domains. Now that the quark-meson coupling constant is known, one can now look for an expression for the polarisation function Π.

3.G.3 Polarisation function

The polarisation function Π, see Fig. 3.11, as the form:

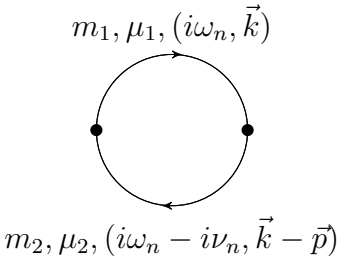

Fig. 3.11: Polarisation loop

$$
\Pi(k) = i \int \frac{d^4p}{(2\pi)^4} Tr(\bar{\Omega} S(k) \Omega S(k-p)) \tag{3.G.9}
$$

where

$$
S(k) = \frac{\not{k} + m_1}{k^2 - m_1^2} \tag{3.G.10}
$$

is the quark or antiquark propagator and $\Omega = (\text{color} \otimes \text{flavour} \otimes \text{spin})$. The factor associated for colour and flavour were given in section 3.B.3. The color space is simply $\mathbb{1}$ for the meson sector and tracing over brings a factor N_C. The flavour space is given by the Gell-Mann matrices λ^a and tracing over brings a factor $\frac{1}{2}$. The Dirac space is $\mathbb{1}, i\gamma_5, \gamma_\mu, i\gamma_5\gamma_\mu$, depending on the type of the meson. The dependence of the polarisation function in temperature is introduced with the help of the Matsubara formalism, developed in section 1.G:

$$
\int \frac{d^4p}{(2\pi)^4} \to iT \sum_n \int \frac{d^3\vec{p}}{(2\pi)^3} \tag{3.G.11}
$$

and :

$$\Pi(k) = -T\sum_n \int \frac{d^3\vec{p}}{(2\pi)^3} Tr(\bar{\Omega}S(k)\Omega S(k-p)) \tag{3.G.12}$$

Pseudoscalar mesons

For pseudoscalar mesons, the Γ matrix is $i\gamma_5$. The polarisation function becomes :

$$\Pi(k) = -\frac{TN_C}{2}\sum_n \int \frac{d^3\vec{p}}{(2\pi)^3} Tr(i\gamma_5 S(k) i\gamma_5 S(k-p)). \tag{3.G.13}$$

Using the relations $\gamma_5\gamma_\mu = -\gamma_\mu\gamma_5$ et $\gamma_5^2 = \mathbb{1}$, the trace calculation relations $tr[\gamma_\mu\gamma^\mu] = 4$ and the fact that an odd product of γ matrices gives no contribution:

$$\Pi^{ps}(k) = 2TN_C\sum_n \int \frac{d^3\vec{p}}{(2\pi)^3} \frac{k(k-p) - m_1 m_2}{(k^2 - m_1^2)((k-p)^2 - m_2^2)}. \tag{3.G.14}$$

Using the identity

$$k(k-p) - m_1 m_2 = \frac{1}{2}(k^2 - m_1^2 + (k-p)^2 - m_2^2 + (m_1 - m_2)^2 - (k - (k-p))^2), \tag{3.G.15}$$

we obtain the polarisation function expressed in terms of the one-fermion loop A, already met in the calculation of the chiral condensate in Eq. 3.D.12 and the two-fermion loop B_0 given in [89].

$$\begin{aligned}\Pi^{Ps}_{ff'}(k_0, \vec{k}) = &-\frac{N_C}{4\pi^2}[A(m,\mu,T) + A(m',\mu',T) \\ &+ [(m_f - m_{f'})^2 - (k_0 + \mu_f - \mu_{f'})^2 + \vec{k}^2]B_0(\vec{k}, m, \mu, m', \mu', k_0)].\end{aligned} \tag{3.G.16}$$

Using the Bethe-Salpeter equation Eq. 3.G.4 with the polarisation function Eq. 3.G.16 gives the mass for the pion and the kaon.

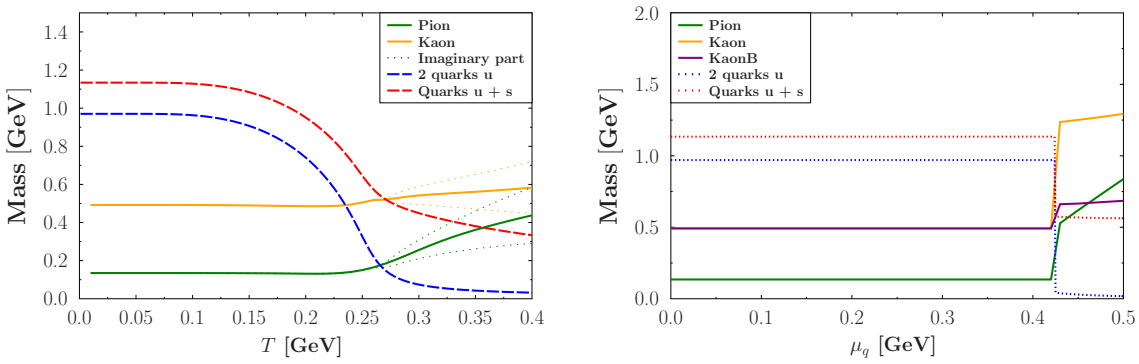

Fig. 3.12: Mass of the pion and kaon compared with the masses of the constituent quarks (dashed lines) (a) at $\mu_q = 0$ (b) at $T = 0.001\ GeV$. The decay width of the mesons is represented in dotted lines

The temperature for which the mass of the constituents becomes lower than the mass of the meson is the Mott temperature. The stable particle is the one which requires the lowest energy to exist. The particle which does not minimise the energy must obey either to confinement or decay into stable particles. When the meson mass becomes larger than the mass of the constituent quarks, the mass of the meson becomes complex and the imaginary part represents the decay width of the meson into a quark and an antiquark. The larger the temperature the larger the decay rate. Fig. 3.12 shows (left) the evolution of the masses with respect to temperature for vanishing chemical potential and (right) with to respect to the chemical potential at $T = 0.001\ GeV$. On the right figure, a jump of the mass of the meson occurs at the critical chemical potential while the mass grows smoothly in the left figure.

Scalar mesons

For scalar mesons, the Γ matrix is $\mathbb{1}$ instead of $i\gamma_5$. Repeating the same steps than in the previous section, the polarisation function becomes:

$$\Pi^S_{ff'}(k_0, \vec{k}) = -\frac{N_c}{4\pi^2}[A(m,\mu,T) + A(m',\mu',T) + [(m_f + m_{f'})^2 - (k_0 + \mu_f - \mu_{f'})^2 + \vec{k}^2]B_0(\vec{k}, m, \mu, m', \mu', k_0)] \quad (3.G.17)$$

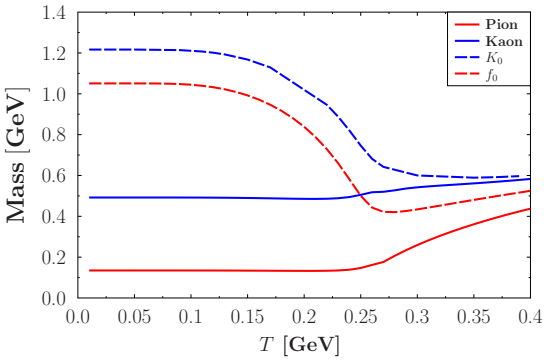

Fig. 3.13: Mass of the scalar and pseudoscalar mesons at $\mu_q = 0$ showing the chiral restoration.

Fig. 3.13 shows the mass difference between the scalar and pseudoscalar partners. At low temperature, the mass of the pion and the kaon are very low as compared to the other hadrons what allows to consider them as the Goldstone bosons of the spontaneous breaking of the chiral symmetry discussed in section 2.C. Their scalar partner is much heavier. The masses of u and s quarks become low at large temperatures. The chiral symmetry, broken by the quark condensates at low temperature, is approximately restored in the QGP phase. This phenomenon is known as the chiral restoration and can be seen by the fact that the mass of the scalar mesons decreases first before increasing when the

mass of their pseudoscalar partner increases. Asymptotically, the masses of scalar and pseudoscalar become identical.

3.G.4 Mesons with the cutoff correction

Correcting the one fermion loop as we have done for the quark mass in section 3.F changes the mass of the mesons at large temperatures. This difference is presented in Fig. 3.14.

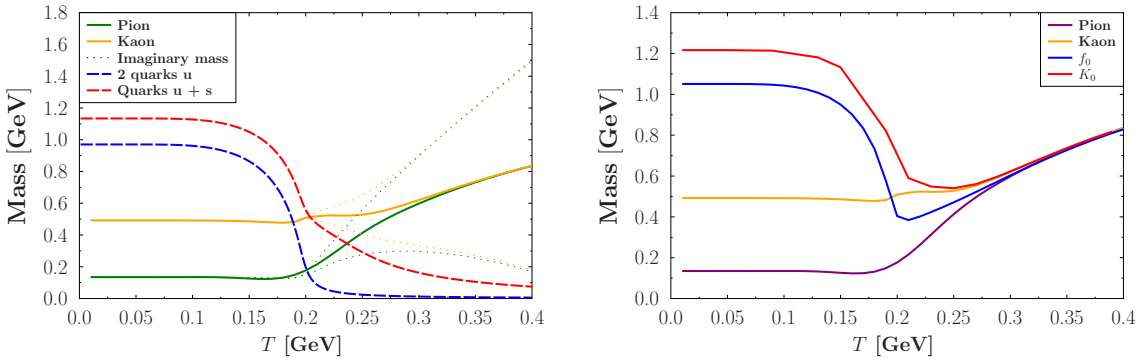

Fig. 3.14: Left: Mass of the pseudoscalar mesons compared with the mass of the quark constituents(dashed lines) showing the Mott temperature $\mu_q = 0$ with the inclusion of the cutoff correction Eq. 3.F.2. Right: Mass of the pseudoscalar mesons compared to the scalar mesons showing the chiral restoration at $\mu_q = 0$.

The Mott temperature is slightly lower as compared to the standard NJL model, following the behaviour of the inflexion point of the mass of the u quark. In Fig. 3.14 right, one can see that the chiral symmetry is restored at large temperatures as the mass of the chiral partners becomes identical. One can see the improvement compared to Fig. 3.13 where the masses of the chiral partners were getting close but not identical though. The flavour symmetry also becomes more exact than before as the kaon and the pion also have identical masses at large temperature. The decay width of the pion and the kaon is now larger than in Fig. 3.12. The new phase diagram, taking into account this cutoff correction, is shown in Fig. 3.15. Below the CEP, we have a cross over and if the critical line is usually define from the chiral condensate inflexion point, here figures also the Mott temperature, critical line of other effective models unable to calculate the chiral condensate. The fact that they are not exactly the same at low temperature accounts for the fact that the transition occurring is a cross over, where a mixed state of hadrons and partons exists and where the concept of critical line is not well defined: it is a critical region.

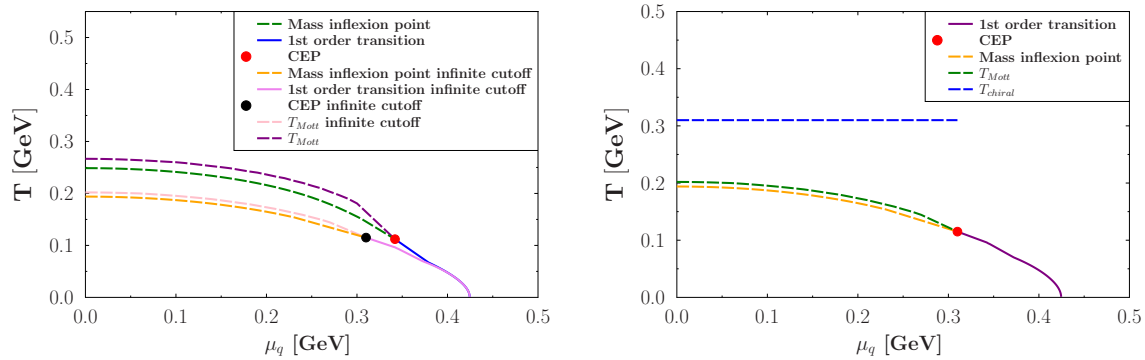

Fig. 3.15: Left: Comparison of the phase diagrams of the NJL model with and without correction to the cutoff. Right: Phase diagram of the NJL model including the chiral restoration critical line.

Unlike the Mott temperature, the temperature of the chiral restoration of the pion and the f_0 is $T_c = 310\ MeV$ and is much larger than the temperature of the inflexion point of the mass of the quark u. The value of the temperatures of chiral restoration is rather stable and does not decrease to meet with the CEP at large μ.

3.G.5 Case of η and η' mesons - mixed states

As already mentioned in section 3.G.2, for the η and η' mesons, mixing terms occurs between the Gell-Mann matrices λ_0 and λ_8. One needs to work a little bit more to obtain the mass of the η and η' meson by solving the eigenvalue problem of a matrix equation. K becomes a matrix of the 0 and 8 component[84]:

$$\mathbf{K} = \begin{pmatrix} K_{00} & K_{08} \\ K_{80} & K_{88} \end{pmatrix} \tag{3.G.18}$$

and so does Π[84]:

$$\mathbf{\Pi} = \begin{pmatrix} \Pi_{00} & \Pi_{08} \\ \Pi_{80} & \Pi_{88} \end{pmatrix} \tag{3.G.19}$$

with:

$$\Pi_{00} = \frac{2}{3}(2\Pi_{\bar{q}q} + \Pi_{\bar{s}s}) \tag{3.G.20}$$

$$\Pi_{08} = \frac{2\sqrt{2}}{3}(\Pi_{\bar{q}q} - \Pi_{\bar{s}s}) \tag{3.G.21}$$

$$\Pi_{88} = \frac{2}{3}(2\Pi_{\bar{s}s} + \Pi_{\bar{q}q}) \tag{3.G.22}$$

where q and $\bar{q}$ are the u or d quarks. The equation giving the mass is now[84]:

$$\mathbf{M} = \frac{2\mathbf{K}}{1 - 2\mathbf{\Pi K}} \tag{3.G.23}$$

The inverse is:

$$\mathbf{M}^{-1} = \frac{1}{2\mathrm{Det}\mathbf{K}} \begin{pmatrix} A & B \\ B & C \end{pmatrix} \tag{3.G.24}$$

Where:

$$C = K_{88} - 2\Pi_{00}\mathrm{Det}\mathbf{K} \tag{3.G.25}$$

$$B = -K_{08} - 2\Pi_{08}\mathrm{Det}\mathbf{K} \tag{3.G.26}$$

$$A = K_{00} - 2\Pi_{88}\mathrm{Det}\mathbf{K} \tag{3.G.27}$$

and Det **K** is:

$$\mathrm{Det}\mathbf{K} = K_{00}K_{88} - K_{08}^2 \tag{3.G.28}$$

To determine the mass of the η and η' mesons, one need to diagonalise the matrix M^{-1} in Eq. 3.G.24. This procedure [93] leads to a set of two equations:

$$A + C - \sqrt{(A-C)^2 + 4B^2} = 0 \tag{3.G.29}$$

for η and for η':

$$A + C + \sqrt{(A-C)^2 + 4B^2} = 0 \tag{3.G.30}$$

Both equations are valid for scalar or pseudoscalar η mesons. The nature of the polarisation function and the K constant, scalar or pseudoscalar gives the value of the mass for scalar η, η' and pseudoscalar η, η'.

The results, for the pseudoscalars η and η', are displayed in Fig. 3.16. The mass of the η' is much larger than the mass of the η, confirming that the η' is not a Goldstone boson produced during the dynamical breaking of the chiral symmetry. The axial anomalous symmetry $U(1)_A$ is restored at large temperature as both η and η' have identical mass. Although the restoration of the $U(1)_A$ symmetry in the QGP region is still debated [94], recent lattice results expect the restoration of the $U(1)_A$ to appear around 1.5 T_C. The NJL model shows a restoration of the $U(1)_A$ around $T \sim 0.3\ GeV \sim 1.5\ T_C^{NJL}$, in agreement with those lattice results [95].

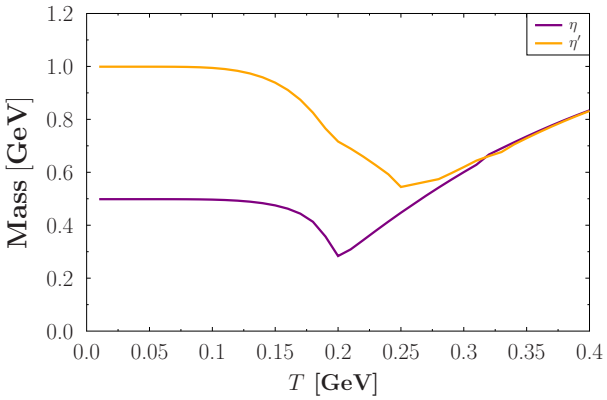

Fig. 3.16: Mass of the η and η' mesons at $\mu_q = 0$

Eventually, the NJL model allows for a description of a low energy strongly interacting matter, using a Lagrangian in with the degrees of freedom are the quarks and the antiquarks and building the mesons from a bound state of quark and antiquark. However, one of the weakness of the NJL is the absence of confinement. It means that quark are present in the medium at low temperature in the hadronic phase although they should not. A solution to this problem is the Polyakov-Nambu-Jona-Lasinio model which applies a statistical confinement which suppresses partially the quarks in the hadronic phase.

3.H Polyakov-Nambu-Jona-Lasino Model

The PNJL model is an extension of the NJL model including two new quantities: the Polyakov loop ϕ and its conjugate $\bar{\phi}$. To motivate this approach, we come back to a covariant derivative in the Lagrangian where only the time component of the gauge field is kept and we add an effective potentials $U(\phi, \bar{\phi}, T)$ that accounts for the presence of a static external color field. The Lagrangian becomes [96]:

$$\begin{aligned}\mathscr{L}_{PNJL} = &\overline{\psi}_k(i\gamma^\mu D_\mu - m)\psi_k + G_S^2\{(\overline{\psi}_k\lambda_i\psi_k)^2 + (\overline{\psi}_k i\gamma_5\lambda_i\psi_k)^2\} \\ &- K[det[\overline{\psi}_k(1+\gamma_5)\psi_k] + det[\overline{\psi}_k(1-\gamma_5)\psi_k]] - U(\phi, \bar{\phi}, T)\end{aligned} \tag{3.H.1}$$

with the covariant derivative $D_\mu = \partial_\mu - iA_\mu\delta_0^\mu$ in the Polyakov gauge and the effective potential $U(\phi, \bar{\phi}, T)$ which is a function of the temperature, the Polyakov loop and its conjugate [97]. The interaction remains a contact interaction as the spatial degrees of freedom of the gluons are still frozen, meaning that the domain of validity of the model does not change. The Polyakov loop is the trace in color space over the Polyakov line in the fundamental representation [98]

$$\phi(\vec{x}) = \frac{Tr_c << L(\vec{x}) >>}{N_c} \quad \bar{\phi}(\vec{x}) = \frac{Tr_c << L^\dagger(\vec{x}) >>}{N_c} \tag{3.H.2}$$

And the Polyakov line L is an imaginary time Wilson line:

$$L(\vec{x}) = \mathscr{P} \exp(-i \int_0^\beta d\tau A_4(\vec{x}, \tau)) \tag{3.H.3}$$

where P means path ordering and $A_4 = iA_0$ is the Euclidean gauge field. The gluons are then related to the imaginary time which is considered as a temperature in finite temperature field theory and are called thermal gluons. They are present as a mean field surrounding the quarks and adding a pressure contribution to the medium. The PNJL Lagrangian, Eq. 3.H.1, has an effective confinement at low temperature and chemical potential. This confinement comes from the effective potential mimicking the action of the thermal gluons which add a confining pressure to the quarks, see Fig. 3.17, and from the modification of the quark thermal distribution by the coupling of the quarks with A_4 in the covariant derivative, inducing a statistical confinement.

A_4 couples to the quarks with γ_0 like the chemical potential. Consequently, it modifies the Fermi distribution of the quark, which becomes [29]:

$$f_\phi^+(E_i - \mu_i) = \frac{(\phi + 2\bar{\phi}\exp(\frac{-E_i-\mu_i}{T}))\exp(-\frac{E_i-\mu_i}{T}) + \exp(-3\frac{E_i-\mu_i}{T})}{1 + 3(\phi + \bar{\phi}\exp(-\frac{E_i-\mu_i}{T}))\exp(-\frac{E_i-\mu_i}{T}) + \exp(-3\frac{E_i-\mu_i}{T})} \tag{3.H.4}$$

$$f_\phi^-(E_i + \mu_i) = \frac{(\bar{\phi} + 2\phi\exp(\frac{-E_i+\mu_i}{T}))\exp(-\frac{E_i+\mu_i}{T}) + \exp(-3\frac{E_i+\mu_i}{T})}{1 + 3(\bar{\phi} + \phi\exp(-\frac{E_i+\mu_i}{T}))\exp(-\frac{E_i+\mu_i}{T}) + \exp(-3\frac{E_i+\mu_i}{T})} \tag{3.H.5}$$

Two limits appear:

- For $\phi = \bar{\phi} = 1$, this is the NJL limit corresponding to deconfinement.
- For $\phi = \bar{\phi} = 0$, the one and two quarks terms become zero leaving only the three quarks term $E_N = 3E$, $\mu_N = 3\mu$. This is a "poor man's nucleon". The coupling to the Polyakov loop leads to a quarks and diquark suppression below T_c known as statistical confinement.

Regarding the effective potential, several parametrisations have been performed. In any case the parameters are chosen to fit the calculations of the pure Yang Mills pressure obtained from lattice QCD and mimic the $\frac{1}{4}F^a_{\mu\nu}F^{a\mu\nu}$ term in the QCD Lagrangian. In this work, the polynomial form of the potential will be used [90]:

$$\frac{U(\phi, \bar{\phi}, T)}{T^4} = -\frac{b_2(T)}{2}\bar{\phi}\phi - \frac{b_3}{6}(\bar{\phi}^3 + \phi^3) + \frac{b_4}{4}(\bar{\phi}\phi)^2 \tag{3.H.6}$$

with the parameters : $b_2(T) = a_0 + a_1(\frac{T_0}{T}) + a_2(\frac{T_0}{T})^2 + a_3(\frac{T_0}{T})^3$.

a_0	a_1	a_2	a_3	b_3	b_4	T_0
6.75	-1.95	2.625	-7.44	0.75	7.5	270 MeV

Table 3.4: Table of parameters for the polynomial parametrisation of the PNJL model.

The logarithmic parametrisation is also popular [99]:

$$\frac{U(\phi,\bar{\phi},T)}{T^4} = -\frac{a(T)}{2}\bar{\phi}\phi + b(T)\ln(1-6\bar{\phi}\phi+4(\bar{\phi}^3+\phi^3)-3(\bar{\phi}\phi)^2) \tag{3.H.7}$$

with the parameters : $a(T) = a_0 + a_1(\frac{T_0}{T}) + a_2(\frac{T_0}{T})^2$ and $b(T) = b_3(\frac{T_0}{T})^3$.

In both parametrisation, T_0 represents the critical temperature of the confinement-deconfinement phase transition.

a_0	a_1	a_2	b_3	T_0
3.51	-2.47	15.2	-1.7	270 MeV

Table 3.5: Table of parameters for the logarithmic parametrisation of the PNJL model.

The spontaneous breaking of the confinement symmetry can be shown by plotting the effective potential for temperatures lower than T_0 and higher than T_0. The graph obtained is consistent with a singlet minimum for $T < T_0$ corresponding to the hadronic state and three minima for $T > T_0$ corresponding to the three fold degenerate state of the red, blue and green colors, characteristic of the breaking of the confinement symmetry.

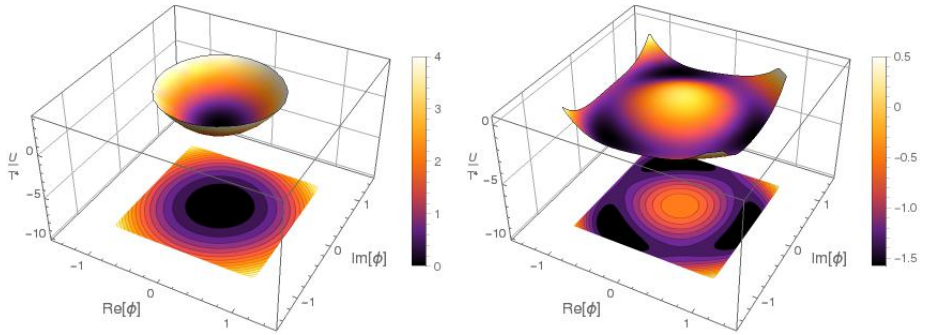

Fig. 3.17: Polyakov potential at left T = 0.15 GeV and right T = 1 GeV.

The Polyakov loop is the order parameter of the confinement symmetry breaking in pure gauge theory. It is not for QCD, but the Polyakov loop is however a measurement of the confinement. The thermal equilibrium in PNJL is then given by the minimisation of the grand potential with respect to ϕ and $\bar{\phi}$ in addition to the minimisation with respect to the mass:

$$\begin{cases} \dfrac{\partial\Omega_{PNJL}}{\partial\phi} = 0 \\ \dfrac{\partial\Omega_{PNJL}}{\partial\bar{\phi}} = 0 \\ \dfrac{\partial\Omega_{PNJL}}{\partial m_q} = 0 \\ \dfrac{\partial\Omega_{PNJL}}{\partial m_s} = 0 \end{cases} \tag{3.H.8}$$

where the PNJL grand potential has the form:

$$\begin{aligned}\Omega_{PNJL} = &-2N_C \int_0^{\Lambda} \frac{d^3p}{(2\pi)^3} E_p \\ &- 2T \int_0^{\infty} \frac{d^3p}{(2\pi)^3} (\ln[1 + 3(\bar{\phi} + \phi \exp(-\frac{E_i + \mu_i}{T}) \exp(-\frac{E_i + \mu_i}{T}) + \exp(-3\frac{E_i + \mu_i}{T})] \\ &+ \ln[1 + 3(\phi + \bar{\phi} \exp(-\frac{E_i - \mu_i}{T})) \exp(-\frac{E_i - \mu_i}{T}) + \exp(-3\frac{E_i - \mu_i}{T})]) \\ &+ U(\phi, \bar{\phi}, T) + 2G \sum_k <\bar{\psi}_k \psi_k>^2 - 4K \prod_k <\bar{\psi}_k \psi_k> \end{aligned} \tag{3.H.9}$$

The expectation values ϕ, $\bar{\phi}$, obtained from Eq. 3.H.8, are shown in Fig. 3.18 as function of the temperature and the quark chemical potential. They are real in the mean field unlike in the Yang-Mills case [100].

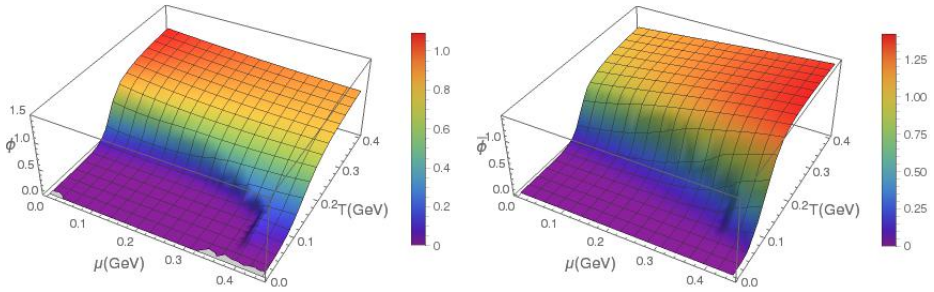

Fig. 3.18: Polyakov loop left ϕ, right $\bar{\phi}$ as function of the temperature and the chemical potential.

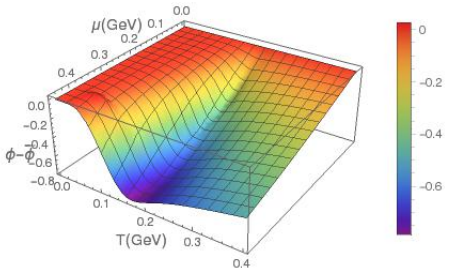

Fig. 3.19: Difference between the Polyakov loop ϕ and its conjugate $\bar{\phi}$ as function of the temperature and the chemical potential.

Fig. 3.19 shows that ϕ and $\bar{\phi}$ are equal only at $\mu = 0$ but not at μ except at in the low temperature region. Fig 3.18 shows that ϕ and $\bar{\phi}$ are 0 at low temperature and low chemical potential, when the system is in the hadronic phase. They become non zero when the temperature increases and the system enters the QGP phase. They reach one at large temperature. At finite μ, the value of $\bar{\phi}$ exceed one whereas ϕ slightly decreases.

Part II

Determination of a PNJL equation of state matching the results of the lattice calculations and application to a thermodynamic and dynamic study of the QGP

Chapter 4

Equation of state of the QCD-like matter

We have shown in chapter 3 some results of the NJL model: the mass of the quarks, of the mesons and the phase diagram which shows a Critical End Point and a first order phase transition.We are now interested in calculating the PNJL equation of state, using the grand potential Eq. 3.H.9, in order to compare with the lattice results regarding the following observables: Pressure, Entropy, Energy density and Interaction measure. We start out by comparing the PNJL and NJL results to the lattice results [46] in Fig.4.1.

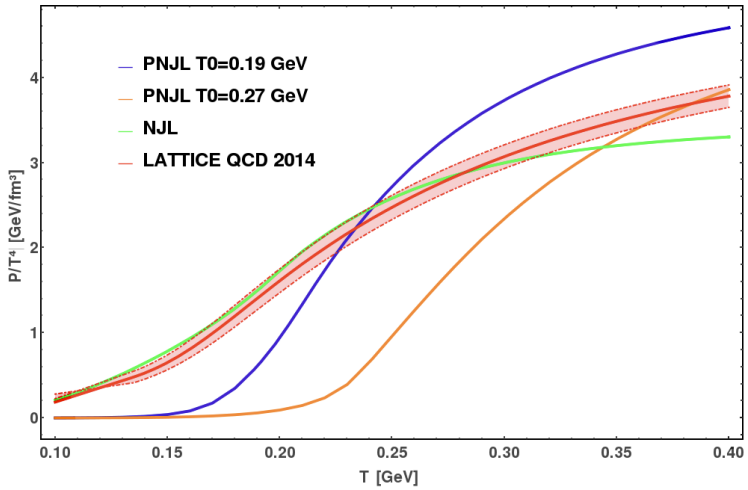

Fig. 4.1: Comparison of the pressure from lQCD [46], NJL and PNJL calculations. In PNJL we use the two values of the T_0 parameter from Table 3.5: $T_0 = 270$ MeV (pure Yang Mills) and T_0 190 MeV to account for the interactions between gluons and quarks [101].

The NJL model seems to be close to the lattice results, especially at low temperature, but this is an artefact of the model. At low temperature quarks are confined and the pressure is created from hadrons. Therefore, the Hadron Resonance Gas theory matches very well with the lattice results [102]. The lack of confinement in the NJL model leads at low T to a non vanishing pressure of the quarks which wrongly mimics this feature. The PNJL model suppresses quark degrees of freedom at temperatures below the critical temperature more strongly. The pressure vanishes at low temperature as a consequence of the "confinement" induced by the coupling with the Polyakov loop and the action of the effective potential. At high temperature, NJL does not saturate at the same pressure as

the lattice calculations because of the lack of gluons whose contribution to the pressure is missed. The PNJL model with $T_0 = 270\ MeV$ does not match the lattice pressure either above the critical temperature as it is parametrised for pure gluonic matter, different of the quark-gluons interactions happening in the QCD medium. The PNJL calculation for $T_0 = 190\ MeV$ [101], which takes into consideration the presence of quarks in the medium in an approximate way, has the same features than the one for $T_0 = 270\ MeV$ but comes closer to the lattice results around the critical temperature. However, the cross over remains too sharp to match them. As a consequence, the reproduction of lattice results requires the addition of a mesonic pressure at low temperature vanishing naturally at high temperature [103] and a more evolved description of the quark-gluon interaction which we will obtain using a phenomenological parametrisation of the T_0 parameter of the PNJL model.

4.A Fixing the low temperature: mesonic corrections

The grand potential of Eq.3.D.17 has only two contributions: the quarks and the thermal gluons. However, at low temperature, mesons are stable. Their presence in the medium is highly expected meaning that they should also contribute to the pressure. To include mesons in the grand potential, one needs to go beyond the mean field approximation and has to include mesonic corrections. Diagrammatically speaking, the next term after the Hartree approximation in the large N_c expansion is a ring term corresponding to mesonic corrections.

4.A.1 $\frac{1}{N_c}$ expansion

In the $\frac{1}{N_c}$ expansion, one performs a 't Hooft scaling [104]:

$$\alpha_s \to \alpha_s N_c \frac{1}{N_c} \sim g^2 N_c \frac{1}{N_c} \tag{4.A.1}$$

where $g = \sqrt{4\pi\alpha_s}$ and α_s is the coupling constant of the strong interaction. We set:

$$\lambda = g^2 N_c = cst \tag{4.A.2}$$

This scaling is taken to be constant, g^2 tends to 0 and N_C tends to infinity. One is now interested in calculating the dressed propagator of the quark in the large N_C expansion. The diagrammatic series of the quark self energy in given in Fig.4.2. To calculate the order of correction of the diagrams in the series, one considers on one hand that a fermion loop contributes a factor N_c and on the other hand that a gluon line contribute a factor $g^2 = \frac{1}{N_c}$ as every interaction vertex is $g = \frac{const}{\sqrt{N_C}}$. It is summarised in the following relation for g^2 and N_C:

$$g^{2l} N_c^k = (g^2 N_c)^l {N_c}^{k-l} \tag{4.A.3}$$

where $(g^2 N_c)$ is constant, k is the number of fermion lines and l is the number of interaction lines.

Fig. 4.2: Diagrammatic $\frac{1}{N_c}$ expansion. The second and third terms are respectively the Hartree and Fock diagrams of the mean field approximation. For clarity, the contact interaction is indicated by a dashed line.

The equivalent algebraic series is given by Eq. 4.A.4, where the order in gN_C (red) and N_C (blue) are calculated by counting the number of quark and gluon lines.

$$iS_\Sigma(p) = iS(p)(\boxed{O(1)O(1)} + \boxed{O((g^2N_c))O(1)} + \boxed{O((g^2N_c))O(\frac{1}{N_c})} + \boxed{O((g^2N_c)^2)O(\frac{1}{N_c})} + ...) \tag{4.A.4}$$

The Hartree term is then of the order $O(1)$ and the Fock term is of the order $\mathrm{O}(\frac{1}{N_c})$. But the Fock term is not the only term of order $\mathrm{O}(\frac{1}{N_c})$, as the ring term is also of this order. Its correction is nevertheless lower as of $O((g^2N_c)^2)$ order in the gN_c expansion. Going beyond mean field means therefore adding the ring term to the grand potential to go to the $\mathrm{O}(\frac{1}{N_c})$ order. The Grand potential associated to this ring diagram (violet) is:

$$\Omega^{(0)}(T,\mu) = \int \frac{d^4p}{(2\pi)^4} Tr[S(p)\Sigma(p)]. \tag{4.A.5}$$

This calculation makes use of the coupling-constant integration method, which consists in rescaling the coupling constant K into λK, to evaluate the correction to the mean field included in the Σ^λ term [103]:

$$\Omega_M^{(0)}(T,\mu) = \frac{1}{2}\int \frac{d\lambda}{\lambda} \int \frac{d^3\vec{p}}{(2\pi)^3} T \sum_n Tr[S^\lambda(i\nu_n,\vec{p})\Sigma^\lambda(i\nu_n,\vec{p})] \tag{4.A.6}$$

where:

$$\Sigma^\lambda(i\nu_n - i\omega_m,\vec{p}) = T\sum_m \int \frac{d^3\vec{k}}{(2\pi)^3} \Omega S(i\omega_m,\vec{p}-\vec{k})\bar{\Omega}U_M^\lambda(i\nu_n - i\omega_m,\vec{k}) \tag{4.A.7}$$

and:

$$U^\lambda(i\nu_n - i\omega_m,\vec{k}) = \frac{2\lambda K}{1 - 2\lambda K\Pi(i\nu_n - i\omega_m,\vec{k})} \tag{4.A.8}$$

with Π being the quark-antiquark correlation function which we already met previously in Eq. 3.G.12. The corrections depends on $\frac{2\lambda K}{1-2\lambda K\Pi(i\nu_n - i\omega_m,\vec{k})}$ which turns out to be the same expression as in the bound state formula to generate mesons in Eq.3.G.4. The corrections to the mean field are then mesonic. Ω^0 is the sum of all the mesons contributing to the grand potential :

$$\Omega^{(0)}(T,\mu_i) = \sum_M \Omega_M^{(0)}(T,\mu_i) \tag{4.A.9}$$

where :

$$\Omega_M^{(0)} = \frac{g_M}{2}\int_0^1 d\lambda T\sum_n \int \frac{d^3\vec{k}}{(2\pi)^3} T\sum_m \int \frac{d^3\vec{p}}{(2\pi)^3} Tr[S(i\nu_n,\vec{k})\Omega S(i\nu_m - i\omega_m,\vec{p}-\vec{k})\bar{\Omega}\frac{2\lambda K}{1-2\lambda K\Pi(i\omega_m,\vec{k})}]. \tag{4.A.10}$$

Using $T\sum_m \int \frac{d^3\vec{p}}{(2\pi)^3} Tr[S(i\nu_n,p)\Omega S(i\nu_n - i\omega_m,\vec{p}-\vec{k})\bar{\Omega}] = -\Pi(i\omega_m,\vec{k})$ gives:

$$\Omega_M^{(0)} = -\frac{g_M}{2}\int_0^1 d\lambda T\sum_n \int \frac{d^3\vec{k}}{(2\pi)^3}\frac{2\lambda K\Pi(i\omega_m,\vec{k})}{1-2\lambda K\Pi(i\omega_m,\vec{k})}]. \tag{4.A.11}$$

Performing the integration over λ leads to [105]

$$\Omega_M^{(0)} = \frac{g_M T}{2}\sum_m \int \frac{d^3k}{(2\pi)^3}\ln[1-2K\Pi(i\omega_n,\vec{k})]. \tag{4.A.12}$$

The Matsubara sum is evaluated using a contour integral [103]
and using the variable shift $\omega \to \omega - \mu_M$, we get :

$$\begin{aligned} T\sum_m \ln[1-2K\Pi(i\omega_n,\vec{k})] = &\frac{1}{2\pi i}\int_0^{+\infty} d\omega \frac{1}{\exp(\beta(\omega-\mu_M))-1}\frac{\ln[1-2K\Pi(\omega-\mu_M+i\epsilon,\vec{k})]}{\ln[1-2K\Pi(\omega-\mu_M-i\epsilon,\vec{k})]} \\ &- \frac{1}{2\pi i}\int_0^{+\infty} d\omega \frac{1}{\exp(-\beta(\omega+\mu_M))-1}\frac{\ln[1-2K\Pi(\omega-\mu_M+i\epsilon,\vec{k})]}{\ln[1-2K\Pi(\omega-\mu_M-i\epsilon,\vec{k})]} \end{aligned} \tag{4.A.13}$$

Using $\frac{1}{\exp(-\beta(\omega+\mu_M))-1} = -1 - \frac{1}{\exp(\beta(\omega+\mu_M))-1}$, we obtain:

$$\begin{aligned} \Sigma_{Matsu} = &\frac{1}{2\pi i}\int_0^{+\infty} d\omega (1 + \frac{1}{\exp(\beta(\omega-\mu_M))-1} + \frac{1}{\exp(\beta(\omega+\mu_M))-1}) \\ &\frac{\ln[1-2K\Pi(\omega-\mu_M+i\epsilon,\vec{k})]}{\ln[1-2K\Pi(\omega-\mu_M-i\epsilon,\vec{k})]}. \end{aligned} \tag{4.A.14}$$

At the end of the day:

$$\begin{aligned} \Omega_M^{(0)} = &\frac{g_M}{2}\int \frac{d^3p}{(2\pi)^3}\int_0^{+\infty} d\omega \left(1 + \frac{1}{\exp(\beta(\omega-\mu_M))-1} + \frac{1}{\exp(\beta(\omega+\mu_M))-1}\right) \\ &\times \ln\left[\frac{1-2K\Pi(\omega-\mu_M+i\epsilon,\vec{k})}{1-2K\Pi(\omega-\mu_M-i\epsilon,\vec{k})}\right] \end{aligned} \tag{4.A.15}$$

The masses and the Polyakov loop are still calculated on the level of mean field and the minimisation does not include Ω_M.

4.A.2 Beth-Uhlenbeck approach

Beth and Uhlenbeck evaluate in [106] the second virial coefficient of the Kamerlingh-Onnes equation of state for non ideal gas in terms of the two body scattering phase shift. The same can be done here as the amplitude of the exchanged mesons appears in the expression of the S-Matrix for quark-antiquark scattering channel. In the Jost representation, the S-matrix reads:

$$S(p,E) = \exp(2i\delta(\vec{k},E)) = \frac{F_J(\vec{k},E^*)}{F_J(\vec{k},E)} \tag{4.A.16}$$

where F_J are the Jost functions. The zeros of the Jost function are the poles of the S-matrix:

$$S(p,\omega) = \frac{1-2K\Pi(\omega-\mu_M-i\epsilon,\vec{k})}{1-2K\Pi(\omega-\mu_M+i\epsilon,\vec{k})} \tag{4.A.17}$$

and :

$$\delta(\vec{p},\omega) = -\frac{1}{2i}\ln\left[\frac{1-2K\Pi(\omega-\mu_M-i\epsilon,\vec{k})}{1-2K\Pi(\omega-\mu_M+i\epsilon,\vec{k})}\right] \tag{4.A.18}$$

Replacing 4.A.18 in 4.A.15, one obtains:

$$\Omega_M^{(0)} = \frac{g_M}{2}\int\frac{d^3\vec{k}}{(2\pi)^3}\int_0^{+\infty}d\omega\left(1+\frac{1}{\exp(\beta(\omega-\mu_M))-1}+\frac{1}{\exp(\beta(\omega+\mu_M))-1}\right)\delta(\omega,\vec{k},T,\mu_M). \tag{4.A.19}$$

Eventually, the fact that the phase shift is approximately Lorentz invariant allows one to rewrite Eq.4.A.19 in term of the Mandelstam variable $s=\omega^2-\vec{k}^2$ and to obtain the final expression of the meson grand potential:

$$\Omega_M = -\frac{g_M}{8\pi^3}\int dpp^2\int\frac{ds}{\sqrt{s+\vec{k}^2}}\left[\frac{1}{\exp(\beta(\sqrt{s+\vec{k}^2}-\mu)-1)}+\frac{1}{\exp(\beta(\sqrt{s+\vec{k}^2}+\mu)-1)}\right] \times\delta(\sqrt{s},T,\mu_M). \tag{4.A.20}$$

Using 4.A.17, one can see that:

$$Arg\left[\frac{1-2K\Pi(\omega-\mu_M-i\epsilon,\vec{k})}{1-2K\Pi(\omega-\mu_M+i\epsilon,\vec{k})}\right] = 2\delta(\sqrt{s},T,\mu_M) \tag{4.A.21}$$

As:

$$\begin{aligned}\mathrm{Arg}\left[\frac{1-2K\Pi(\omega-\mu_M-i\epsilon,\vec{k})}{1-2K\Pi(\omega-\mu_M+i\epsilon,\vec{k})}\right] &= \mathrm{Arg}\left[\frac{(1-2K\Pi(\omega-\mu_M+i\epsilon,\vec{k}))^*}{1-2K\Pi(\omega-\mu_M+i\epsilon,\vec{k})}\right]\\ &= -2\mathrm{Arg}(1-2K\Pi(\omega-\mu_M+i\epsilon,\vec{k}))\end{aligned} \tag{4.A.22}$$

using $\mathrm{Arg}(\frac{z_1}{z_2} = \mathrm{Arg}(z_1) - \mathrm{Arg}(z_2)$ and $\mathrm{Arg}(z^*) = -\mathrm{Arg}(z)$. The phase shift is then:

$$\delta(\sqrt{s}, T, \mu_M) = -\mathrm{Arg}[1 - 2K\Pi(\omega - \mu_M + i\epsilon, \vec{k})] \tag{4.A.23}$$

where Π_M is the polarisation function of the meson.

4.B Fixing the high temperature: from pure Yang-Mills to a quark and gluon medium

The interaction of quarks and gluons, represented by the Polyakov loop potential, modifies not only the quark properties but the gluon field itself. This back reaction has been studied in ref.[101] by comparing the pure Yang Mills potential U_{YM} with U_{glue} obtained, when allowing for quark-antiquark excitation in the gluon propagator. The authors found that quark-antiquark loops change U_{YM} considerably. U_{glue} is related to U_{YM} by:

$$\frac{\mathcal{U}_{glue}}{T^4}(t_{glue}, \Phi, \bar{\Phi}) = \frac{\mathcal{U}_{YM}}{T^4}(t_{YM}(t_{glue}), \Phi, \bar{\Phi}) \ , \tag{4.B.1}$$

where the t's are the reduced temperature: t_{YM} and t_{glue}

$$t_{YM} = \frac{T - T^{cr}_{YM}}{T^{cr}_{YM}} = 0.57 \ \frac{T - T^{cr}_{glue}}{T^{cr}_{glue}} = 0.57 t_{glue} \ . \tag{4.B.2}$$

T^{cr}_{YM} is the deconfinement temperature in the pure YM case (and fixed to $T^{cr}_{YM} = 270$ MeV), whereas T^{cr}_{glue} is the transition temperature in the unquenched case. The numerical coefficient 0.57 is the outcome from the comparison of the two effective potentials. This procedure rescales the critical temperature from $T^{cr}_{YM} = 270$ MeV to $T^{cr}_{glue} = 190$ MeV. In this work, we use a purely phenomenological approach and go beyond a pure rescaling of the temperature due to the presence of the quarks. Instead, we modify the parameters of the U_{glue} to:

$$\frac{U(\phi, \bar{\phi},)}{T^4} = -\frac{b_2(T)}{2}\bar{\phi}\phi - \frac{b_3}{6}(\bar{\phi}^3 + \phi^3) + \frac{b_4}{4}(\bar{\phi}\phi)^2, \tag{4.B.3}$$

with the parameters : $b_2(T) = a_0 + \frac{a_1}{1+\tau} + \frac{a_2}{(1+\tau)^2} + \frac{a_3}{(1+\tau)^3}$ where:

$$t_{phen} = 0.57 \frac{T - T_{phen}(T)}{T_{phen}(T)}. \tag{4.B.4}$$

One assumes a phenomenological temperature dependence of T_{phen} of the form

$$T_{phen}(T) = a + bT + cT^2 + dT^3 + e\frac{1}{T}, \tag{4.B.5}$$

and determine the coefficients a,..,e, see table II, by comparison with lattice gauge calculations.

This new parametrisation leaves the asymptotic limit of the gluon pressure unchanged, see Fig.4.6. The rescaling is now a function of the temperature assuming that the quark-antiquark excitation depend on the temperature of the medium. The parametrisation is

a_0	a_1	a_2	a_3	b_3	b_4	a	b	c	d	e
6.75	-1.95	2.625	-7.44	0.75	7.5	0.082	0.36	0.72	-1.6	-0.0002

Table 4.1: Table of all parameters for the PNJL model

taken to be polynomial. The term in T^{-1} does not depend on the quark-gluon interaction. It increases the pressure at low temperature and compensates partially for the fact that only four types of mesons (π, K, σ, a_0) are taken into consideration at the moment. In Fig. 4.3 the different reduced temperatures for pure Yang-Mills, from [101] Eq. 4.B.2 and from our approach, Eq. 4.B.4, are compared. The reduced temperature t_{phen} is higher at low temperature (where hadrons are the relevant degrees of freedom) but comes close to the effective temperature of [101] around the phase transition temperature. It tends to the pure Yang Mills reduced temperature for high temperatures.

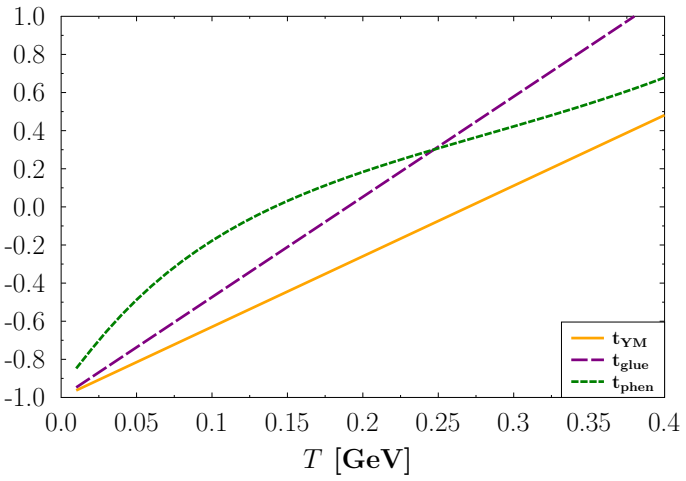

Fig. 4.3: t_{YM}, t_{glue} [101] and t_{phen}, Eq. 4.B.4, as function of the temperature.

4.C Equation of state of the improved PNJL

4.C.1 Equation of state at zero chemical potential and comparison with the lattice results

As was shown in Fig. 4.1, the PNJL approach with a constant T_0 in Table 3.5 does not match the lattice equation of state at $\mu = 0$.

Using the temperature dependent interaction between quarks and gluons with the parametrisation given above and taking into consideration the pseudoscalar pions and kaons and the scalar mesons σ and a_0 in the next to leading order in N_C terms of the partition sum, one can reproduce the pressure as function of the temperature obtained by lattice gauge calculations [46], Fig. 4.4. On the hadronic side of the phase diagram, it is expected that also higher mass hadrons contribute to the pressure even if they are

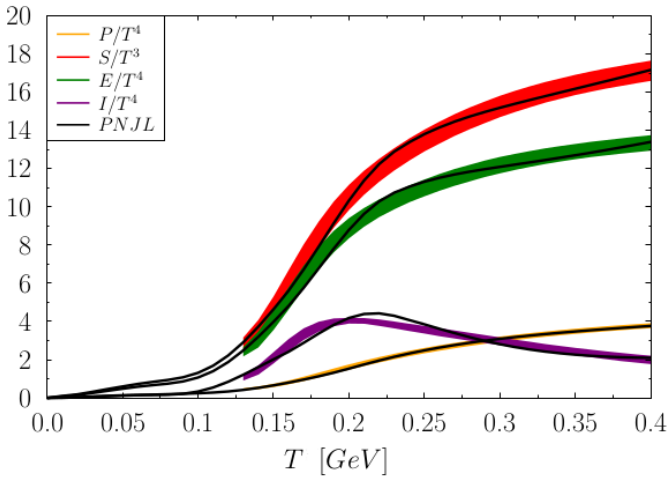

Fig. 4.4: Pressure, entropy density, energy density and interaction measure calculated with PNJL, using eq. 4.B.5, for $\mu = 0$. Results (lines) are compared with the lattice results (colored bands) [46]

suppressed by their large mass. Also the derivatives of the pressure as entropy, energy density and interaction measure, defined in section 1.F, reproduce well the results of the lattice gauge calculations.

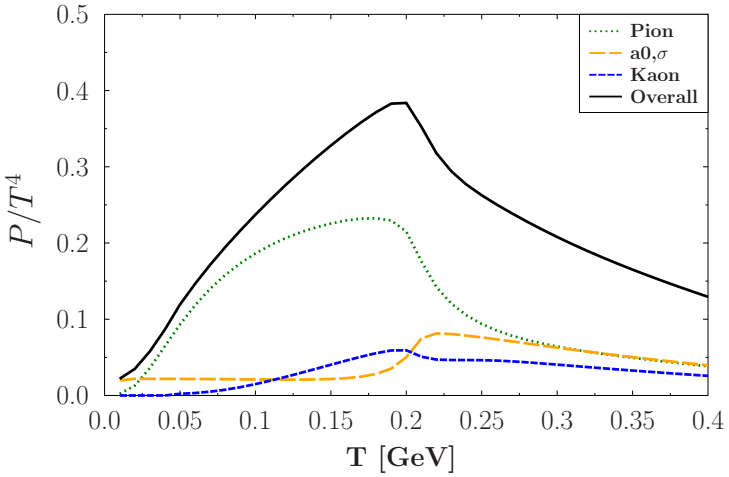

Fig. 4.5: Different mesonic contributions to the pressure at $\mu = 0$.

Fig. 4.5 shows the contribution to the pressure of the different mesons included in our calculation. In leading order in N_c neither in NJL nor in PNJL such a contribution exists. Being the lightest meson, the pseudoscalar pion has the highest contribution to the pressure. Although unstable, the mesons contribute to the pressure also above the phase transition but naturally this contribution tends to vanish at large temperatures.

The pressure of the scalar mesons exhibits two different contributions. Due to its large width the scalar σ contributes to the pressure already at very low temperatures. At higher temperatures, one can observe a chiral restoration for the scalar and pseudoscalar mesons which have there the same finite mass and consequently the same contribution to the pressure. At large temperature, the width of the meson becomes large but remains finite such that in our model the contribution does not completely vanish. The results are in agreement with the calculations from [105].

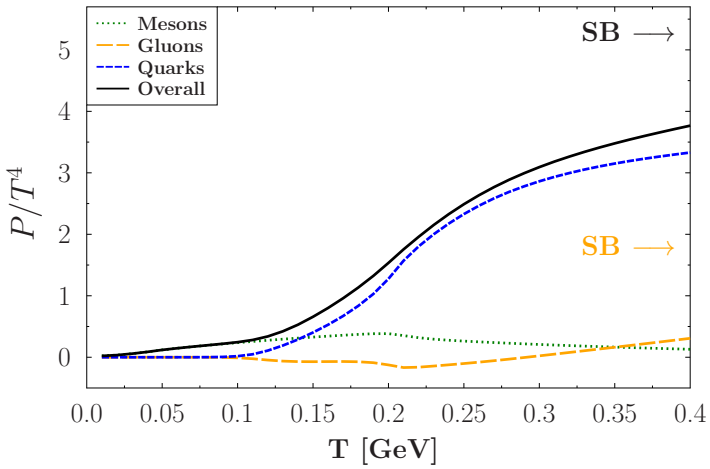

Fig. 4.6: The different contributions to the total pressure at $\mu = 0$ as a function of the temperature.

Fig. 4.6 shows the pressure contribution and the Stefan-Boltzmann limits [107]of gluons from the PNJL effective potential, quarks and mesons as a function of the temperature. At high temperatures, the pressure is dominated by the quark contribution. Mesons dominate at low temperature and present a non negligible contribution around T_c indicating that at $\mu = 0$ a cross over occurs with a mixed phase and not a sharp transition between the phases. The gluon pressure from the effective Polyakov potential is negative at low temperature what can be interpreted as an attractive interaction. It becomes positive at higher temperature and reaches asymptotically the YM pressure.

Another quantity which signals the phase transition between hadronic matter and the QGP is the speed of sound. When the temperature of hadronic matter approaches the phase transition, additional energy goes into the population of high lying resonances and not into momentum (and hence to pressure). Consequently, the speed of sound decreases. Also partons, when approaching the phase transition temperature from above, increase their quasi-particle mass which decreases as well the speed of sound. Consequently, we expect that the transition between hadronic and partonic matter is characterized by a minimum of the speed of sound. Lattice calculations have found that the softest point of the equation of state, the minimum of the speed of sound, is slightly below the cross over temperature [47]. In our PNJL calculations, we observe two minima which are related to the deconfinement and chiral phase transition.

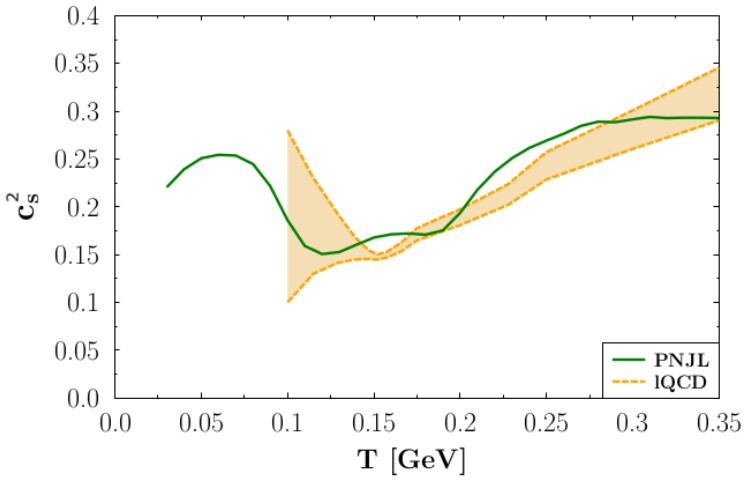

Fig. 4.7: Speed of sound at $\mu = 0$. We compare lattice calculations [47] with our approach.

The parametrisation of the quark-gluon interaction, which reproduces the lattice pressure, compensates in our approach the limitation of the hadronic spectrum to scalar and pseudoscalar mesons. For the speed of sound it shifts the minimum of the confinement phase transition to a lower temperature and that of the chiral phase transition to a higher temperature than the one determined in the lattice approach. This is not visible in the pressure or the entropy but only in quantities which are sensitive to the their derivatives. The inclusion of more hadrons and the calculation of the gap equations beyond mean field should hopefully bring the two phase transitions close together.

4.C.2 Taylor expansion around $\mu = 0$

In the (P)NJL approach the extension to a finite chemical potential is straight forward. One has only to add a chemical potential in the distribution function of the quarks. One can therefore, without introducing any new parameter, calculate the thermodynamical quantities in the whole μ, T plane and with the assumption that the effective Polyakov potential U(ϕ, $\bar{\phi}$,T) does not depends on μ. To make contact with the lattice gauge calculations one can, however, also apply the same procedure by which in lattice gauge calculations the thermodynamical quantities are calculated for small but finite μ. For this, a Taylor expansion of the critical temperature around zero baryonic potential is performed.

$$\frac{T_c(\mu_B)}{T_c(0)} = 1 - \kappa \left(\frac{\mu_B}{T_c(\mu_B)} \right)^2 + \ldots \tag{4.C.1}$$

The κ coefficient is [108]:

$$\kappa = -T_c(0) \left. \frac{\partial T_c(\mu_B)}{\partial (\mu_B)^2} \right|_{\mu_B = 0} \tag{4.C.2}$$

At $\mu_B = 0$, the critical temperature is determined from the quark mass inflexion point, which is in our approach:

$$T_c = 204 \quad MeV. \tag{4.C.3}$$

The corresponding κ coefficient is :

$$\kappa = 0.00989 \tag{4.C.4}$$

In Fig. 4.8 this coefficient is compared with the result of lattice calculations and is found to be in good agreement. Consequently, our PNJL approach agrees with lattice data also for finite but small chemical potentials.

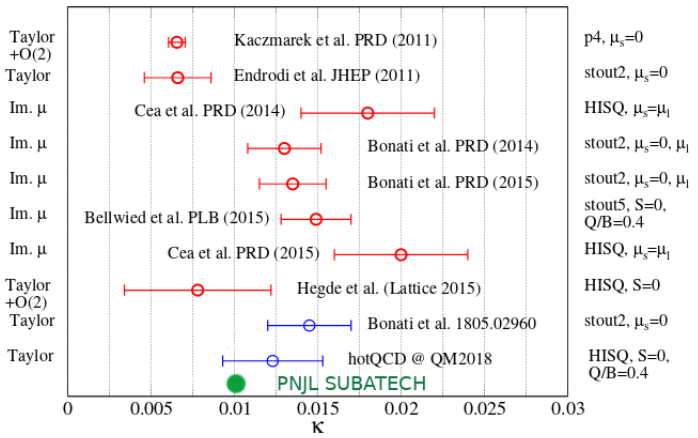

Fig. 4.8: The expansion coefficient of the first order Taylor expansion Eq. 4.C.2 for finite μ in different approaches.

4.C.3 Calculation at finite μ

After having verified that our approach agrees with lattice calculation at $\mu = 0$, we investigate the large μ limit of our approach and proceed to a finite μ_q expansion, as μ_s is considered to be zero, and compares the results with perturbative QCD calculations in the hard dense loop formalism ref.[109], where:

$$P_{SB} = \frac{3}{4\pi^2}(\mu_B/3)^4 \tag{4.C.5}$$

As seen in Fig.4.9 the results agrees within the errors bars also with the pQCD calculations. The verification that our PNJL approach gives the right value of the pressure for a vanishing and for large chemical potentials is a solid basis to study the phase diagram in between the two extremes. The result of our calculation is presented in Fig. 4.10. We see that the cross over between hadronic and quark phase continues for finite values of μ, as predicted by the lattice results. With increasing chemical potential the cross over

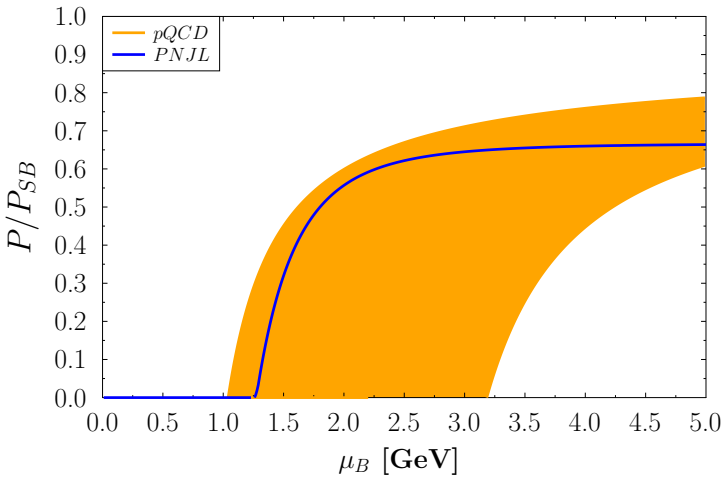

Fig. 4.9: The quark pressure compared to the Stefan-Boltzmann limit as a function of μ for a temperature of T= 0.001 GeV. We compare pQCD calculations [109], [110] (orange area) with the result of our PNJL approach (blue line).

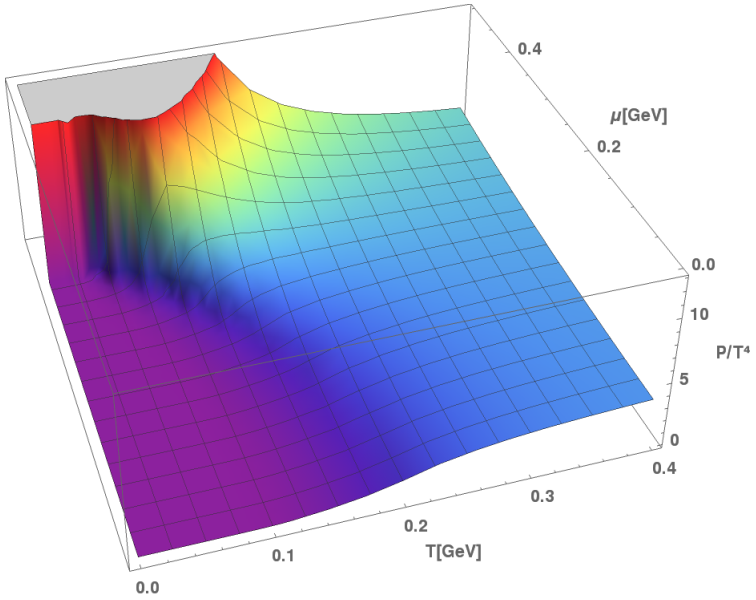

Fig. 4.10: PNJL pressure as a function of T and μ

becomes steeper and steeper and finally ends up in a first order phase transition. The increase of the pressure at high μ is dominated by the $\frac{1}{T^4}$ factor in $\frac{P}{T^4}$.

4.C.4 Phase Transition

The structure of the phase transition looks like the one we have calculated with our previous NJL or PNJL models, however, the localisation of the transition lines and the coordinates of the CEP are slightly shifted. For very low temperatures, the critical quark

chemical potential is still μ_c =0.425 GeV, see Fig. 4.11 which confirms again the accuracy of NJL at low temperature.

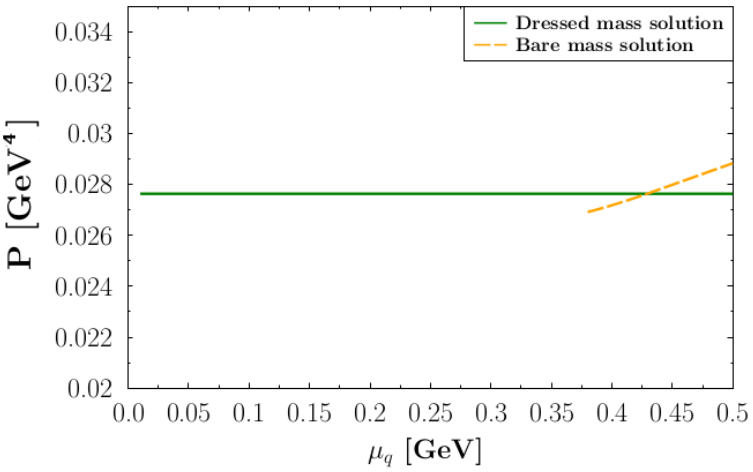

Fig. 4.11: Pressure obtained from the dressed mass (green line) and the bare mass (orange line) in the improved PNJL model.

Fig. 4.12 shows the pion mass and the sum of up and down quark masses as a function of μ_q. The mass of the pion, being a Goldstone boson, remains constant up to $\mu_q \approx 0.425\ GeV$ and increases moderately for larger μ_q. At the phase transition the pion mass becomes larger than the sum of the quark masses and quarks become the relevant degrees of freedom.

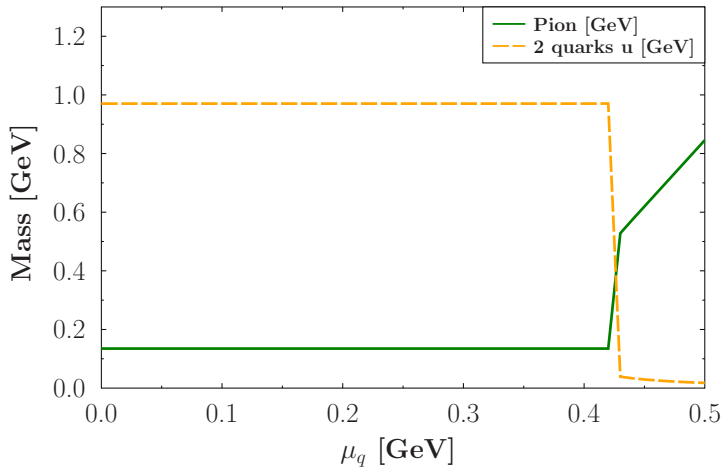

Fig. 4.12: Meson and quark masses at vanishing temperature in the PNJL model.

The CEP is now given by a system of six equations with six unknowns: the masses of the u and s quarks, the Polyakov loop ϕ and its complex conjugate $\bar{\phi}$, the temperature and the chemical potential ref.[90]:

$$\begin{aligned} g_u(\mu, T, mq, ms, \phi, \bar{\phi}) &= 0 \\ \frac{\partial \Omega_{PNJL}(\mu, T, mq, ms, \phi, \bar{\phi})}{\partial \phi} &= 0 \\ \frac{\partial \Omega_{PNJL}(\mu, T, mq, ms, \phi, \bar{\phi})}{\partial \bar{\phi}} &= 0 \\ g_s(\mu, T, mq, ms, \phi, \bar{\phi}) &= 0 \\ \frac{\frac{\partial g_u(\mu,T,mq,ms,\phi,\bar{\phi})}{\partial mq}}{\frac{\partial g_u(\mu,T,mq,ms,\phi,\bar{\phi})}{\partial \mu}} &= 0 \\ \frac{\frac{\partial^2 g_u(\mu,T,mq,ms,\phi,\bar{\phi})}{\partial mq^2}}{\frac{\partial g_u(\mu,T,mq,ms,\phi,\bar{\phi})}{\partial \mu}} &= 0 \end{aligned} \tag{4.C.6}$$

They are the same four equations than in Eq. 3.E.1 depending now on the Polyakov loop and its conjugate and two additional equation to determine the value of ϕ and $\bar{\phi}$ at the CEP. The coordinates of the PNJL CEP are $T_{CEP} = 0.11\ GeV$ and $\mu_{CEP} = 0.32\ GeV$. Fig. 4.13 displays the relevant critical temperatures of our calculations as a function of the chemical potential: the Mott temperature of pions, the chiral phase transition given by the temperature of the inflexion point of the quark mass, the CEP point coordinates and the transition in the pressure for the first order phase transition.

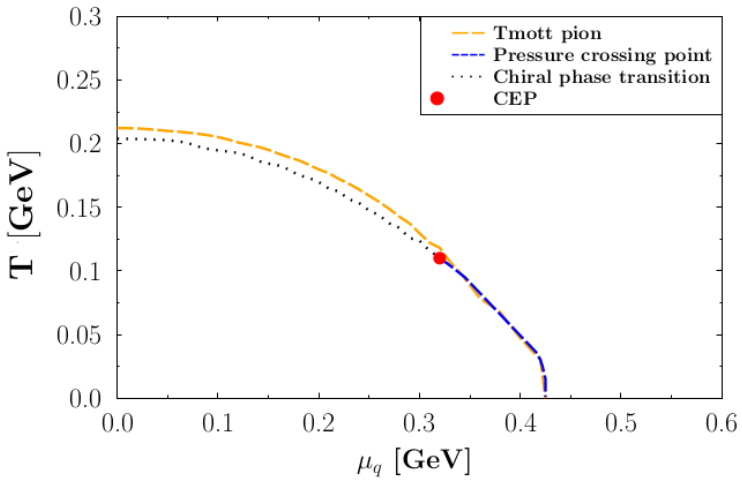

Fig. 4.13: Phase diagram of strongly interacting matter described by our PNJL approach.

Can this chiral phase transition be studied by heavy ion experiments? To discuss this question one compares in Fig. 4.14 in the T, μ plane the line of the chiral first order phase transition with the freeze out curve, calculated by Cleymans and al. [111], which is determined by fitting the observed hadron multiplicities in the framework of a statistical model. In this approach it is assumed that after having passed the freeze-out line hadrons scatter only elastically. The point in the T, μ plane which is reached in heavy ion collisions before the system expands is not known and even whether the system comes to thermal equilibrium before the freeze-out is debated. To be consistent it has to be above the freeze-out curve. Our PNJL approach fulfils this condition. Therefore to study this first order chiral phase transition may be in reach in heavy-ion experiments.

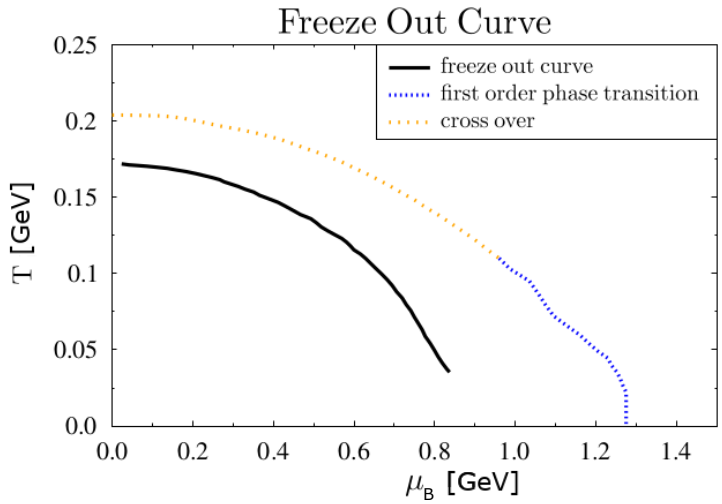

Fig. 4.14: Comparison of the Freeze-out curve to the PNJL phase diagram in the $T - \mu_B$ plan from statistical model calculations [111].

Chapter 5

Tranport coefficients and caracterisation of the Quark Gluon Plasma

We now want to make predictions using the equation of state and the new PNJL model developed in the previous chapter. The transport coefficient of the QGP will be the first prediction. This work was done in collaboration with Olga Soloveva (Goethe-Universität Frankfurt). They are important because related to the energy loss of partons in the QGP. At zero chemical potential, transport coefficients can be compared with the lattice results. They are related to the elastic cross section of partons in the medium. Therefore, they control the scattering of partons in the QGP in non equilibrium transport approaches. Here, the transport coefficients will be calculated from the quark-quark and quark-antiquark elastic cross sections. More cross sections like quark-meson or quark-diquark can also be found in the literature [112] but are not treated here. The calculation of the cross sections will use the mass of the quarks as well as the scalar and pseudoscalar mesons exchanged between the quarks, determined from the new parametrised PNJL model. The new equation of state will be used, especially to determine the viscosity over entropy ratio η/S.

5.A Elastic cross sections

As there is no gauge gluons to propagate the interaction, the PNJL model needs the exchange of a meson exchange for the elastic cross section. The cross sections are restricted to low temperatures $T = 0-0.4\,GeV$ and $\sqrt{s}$. However, one can notice that free quarks do not exist at low temperature, in the hadronic phase. We can therefore limit the evaluation of the cross section to temperature slightly below the Mott temperature $T_{Mott}(\mu)$ as only hadronic cross sections are relevant for lower temperatures.

5.A.1 Quark-quark scattering

There are two possible Feynman diagrams for quark-quark scattering which are those for the t and u channels, see Fig. 5.1.

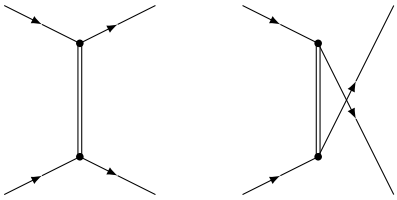

Fig. 5.1: t channel and u channel for quark-quark cross sections

The associated matrix elements are [113]:

$$\frac{1}{4}|M_{qq}|^2 = |M_u|^2 + |M_t|^2 - 2|M_{ut}| \tag{5.A.1}$$

with:

$$|M_u|^2 = |\mathscr{D}_u^S|^2 u_{14}^+ u_{23}^+ + |\mathscr{D}_u^P|^2 u_{14}^- u_{23}^- \tag{5.A.2}$$

$$\begin{aligned} |M_{tu}| = \frac{1}{4N_C}[&\mathscr{D}_t^S \mathscr{D}_u^{S*}(t_{13}^+ t_{24}^+ - s_{12}^+ s_{34}^+ + u_{14}^+ u_{23}^+) \\ &- \mathscr{D}_t^S \mathscr{D}_u^{P*}(t_{13}^+ t_{24}^+ - s_{12}^- s_{34}^- + u_{14}^- u_{23}^-) \\ &- \mathscr{D}_t^P \mathscr{D}_u^{S*}(t_{13}^- t_{24}^- - s_{12}^- s_{34}^- + u_{14}^+ u_{23}^+) \\ &+ \mathscr{D}_t^P \mathscr{D}_u^{P*}(t_{13}^- t_{24}^- - s_{12}^+ s_{34}^+ + u_{14}^- u_{23}^-)] \end{aligned} \tag{5.A.3}$$

$$|M_t|^2 = |\mathscr{D}_t^S|^2 t_{13}^+ t_{24}^+ + |\mathscr{D}_t^P|^2 t_{13}^- t_{24}^- \tag{5.A.4}$$

where :

$$s_{ij}^{\pm} = s - (m_i \pm m_j)^2 \tag{5.A.5}$$

$$t_{ij}^{\pm} = t - (m_i \pm m_j)^2 \tag{5.A.6}$$

$$u_{ij}^{\pm} = u - (m_i \pm m_j)^2. \tag{5.A.7}$$

and:

$$\mathscr{D}^i = \frac{2ig_m}{1 - 2g_m \Pi_{ff'}^{\pm}(k_0, \vec{k})} \tag{5.A.8}$$

is the amplitude of the exchanged meson, where i indicates if the meson is scalar or pseudoscalar. The different possible processes are given in Table 5.1.

Process	Exchanged mesons in u-channel	Exchanged mesons in t-channel
$ud \to ud$	π, σ_π	π, η, η', σ_π, σ, σ'
$uu \to uu$	π, η, η', σ_π, σ, σ'	π, η, η', σ_π, σ, σ'
$us \to us$	K, σ_K	η, η', σ, σ'
$ss \to ss$	η, η', σ, σ'	η, η', σ, σ'

Table 5.1: Independent quark-quark cross sections and list of the possible exchanged meson for each process. σ_π and σ_k respectively represents the scalar partner of the pion and the kaon. σ and σ' are the scalar partners of the η and η' mesons.

5.A.2 Quark-antiquark scattering

For quark-antiquark scattering, only the s and t channel contribute, see Fig. 5.2.

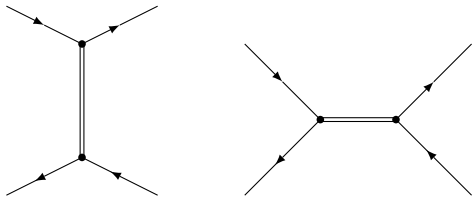

Fig. 5.2: t and s channel for the quark-antiquark cross section

The associated matrix elements are:

$$\frac{1}{4}|M_{q\bar{q}}|^2 = |M_t|^2 + |M_d|^2 - 2|M_{ts}| \tag{5.A.9}$$

with:

$$|M_s|^2 = |\mathscr{D}_s^S|^2 s_{12}^+ s_{34}^+ + |\mathscr{D}_s^P|^2 s_{12}^- s_{34}^- \tag{5.A.10}$$

$$\begin{aligned} |M_{st}| = \frac{1}{4N_C}[&\mathscr{D}_s^S \mathscr{D}_t^{S*}(s_{12}^+ s_{34}^+ - u_{14}^+ u_{23}^+ + t_{13}^+ t_{24}^+) \\ &- \mathscr{D}_s^S \mathscr{D}_t^{P*}(s_{12}^+ s_{34}^+ - u_{14}^- u_{24}^- + t_{13}^- t_{24}^-) \\ &- \mathscr{D}_s^P \mathscr{D}_t^{S*}(s_{12}^- s_{34}^- - u_{14}^- u_{23}^- + t_{13}^+ t_{24}^+) \\ &+ \mathscr{D}_s^P \mathscr{D}_t^{P*}(s_{12}^- s_{34}^- - u_{14}^+ u_{23}^+ + t_{13}^- t_{24}^-)] \end{aligned} \tag{5.A.11}$$

The different possible processes are given in Table 5.2.

Process	Exchanged mesons in s-channel	Exchanged mesons in t-channel
$u\bar{d} \to u\bar{d}$	π, σ_π	π, η, η', σ_π, σ, σ'
$u\bar{u} \to u\bar{u}$	π, η, η', σ_π, σ, σ'	π, η, η', σ_π, σ, σ'
$u\bar{u} \to d\bar{d}$	π, η, η', σ_π, σ, σ'	π, σ_π
$u\bar{s} \to u\bar{s}$	K, σ_K	η, η', σ, σ'
$u\bar{u} \to s\bar{s}$	η, η', σ, σ'	K, σ_K
$s\bar{s} \to u\bar{u}$	η, η', σ, σ'	K, σ_K
$s\bar{s} \to s\bar{s}$	η, η', σ, σ'	η, η', σ, σ'

Table 5.2: Independent quark-antiquark cross sections and list of the possible exchanged meson for each process. σ_π and σ_k respectively represents the scalar partner of the pion and the kaon. σ and σ' are the scalar partners of the η and η' mesons.

5.A.3 Limits of integration and total cross section

The differential cross section is given by:

$$\frac{d\sigma}{dt} = \frac{1}{16\pi s_{12}^{+} s_{12}^{-}} \frac{1}{4N_C^2} \sum_{s,c} |\mathscr{M}_{s/u} - \mathscr{M}_t|^2 \tag{5.A.12}$$

The total cross section is obtained by integration over t:

$$\sigma = \int_{t_-}^{t^+} dt \frac{d\sigma}{dt} [1 - f_F(\beta E_3)][1 - f_F(\beta E_4)] \tag{5.A.13}$$

Where f_F is the Fermi blocking factor given by the Fermi functions modified by the coupling with the Polyakov loop [29] and the limit of the integrations are [114]:

$$\begin{aligned} t_\pm = m_1^2 + m_3^2 - \frac{1}{2s}(s + m_1^2 - m_2^2)(s + m_3^2 - m_4^2) \\ \pm 2\sqrt{\frac{(s + m_1^2 - m_2^2)^2}{4s} - m_1^2}\sqrt{\frac{(s + m_3^2 - m_4^2)^2}{4s} - m_3^2} \end{aligned} \tag{5.A.14}$$

5.A.4 Results for elastic cross section

The general behaviour of the (P)NJL quark-quark and quark-antiquark cross sections are well known from the literature [112, 115]. The quark-quark cross sections are small and do not show any particular behaviour, see Fig. 5.3. This is a consequence of the fact that no cross sections with diquark exchange are considered in this work. They decrease when the temperature and the chemical potential increase as expected as the QGP tends to behave like a free gas at large temperature and chemical potential, as the mass of the exchanged meson and its decay width increase. One can see on Figs. 5.3 that at low μ and low T, the cross section takes finite values only for large $\sqrt{s}$. This is a consequence of the threshold given by the mass of the incoming or outcoming quarks : $\sqrt{s}_{thr} = Max(m_{in}^a + m_{in}^b, m_{out}^a + m_{out}^b)$. At low temperature and chemical potential, the mass of the quarks is large, but tend to vanish at large T and μ.

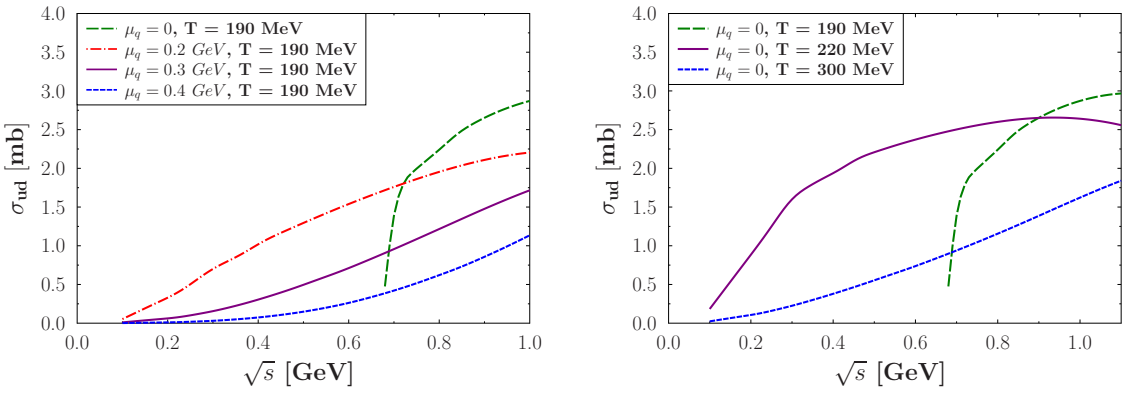

Fig. 5.3: ud cross section (let) at $T = 190\ MeV$ for $\mu = 0,\ 0.1\ GeV,\ 0.2\ GeV$ (right) at $\mu = 0$ for $T = 190\ MeV, 214\ MeV,\ 300\ MeV$

The more interesting processes are the quark-antiquark cross sections. In this case, the s channel allows for a resonance of the exchanged meson with the incoming quarks which leads to a large peak in the cross sections.

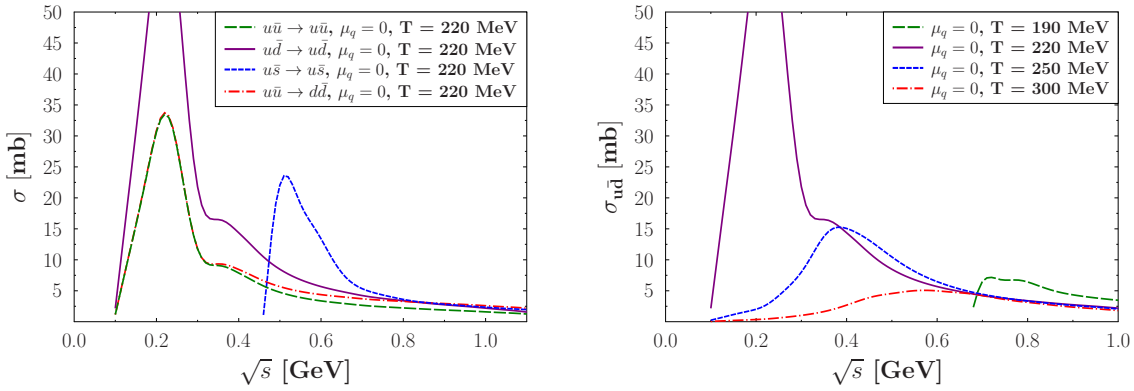

Fig. 5.4: Left: Resonance behaviour of the $u\bar{u} \to u\bar{u}$, $u\bar{d} \to u\bar{d}$, $u\bar{u} \to d\bar{d}$ and $u\bar{s} \to u\bar{s}$ cross sections at T = 220 GeV and $\mu = 0$. Right: Resonance behaviour of the $u\bar{d} \to u\bar{d}$ cross sections at $\mu = 0$ for $T = 190\ MeV$, $220\ MeV$, $250\ MeV$ and $300\ MeV$

Fig. 5.4 left displays different channel showing a resonance behaviour. The $u\bar{s} \to u\bar{s}$ resonance is lower than the others displayed, the strange quark being heavier than the u and d quarks at $\mu_q = 0$ and $T = 200\ MeV$. The other resonances differ only by their flavour factors [116]. $u\bar{d} \to u\bar{d}$ has the largest one reaching 73 mb at its maximum value, $u\bar{u} \to u\bar{u}$ has a lower flavour factor than $u\bar{u} \to d\bar{d}$ but allows the η meson exchange which is not the case of the $u\bar{u} \to d\bar{d}$.

The evolution of the $u\bar{d} \to u\bar{d}$ resonance for different temperatures is displayed in Fig. 5.4 right. One can see that the resonance is shifted to the left when the temperature increases. As the mass of the mesons increases with the temperature, the $\sqrt{s}$ required to be resonant with the pion in the s channel must be higher. The peak becomes lower and lower when the temperature increases to finally disappear at large temperature as the decay width of the pion becomes larger and larger with increasing temperature Fig.5.6.

The kinematic threshold forbids any resonance before the Mott temperature. This explains the flatness of the $u\bar{d} \to u\bar{d}$ at $T = 190\ MeV$.

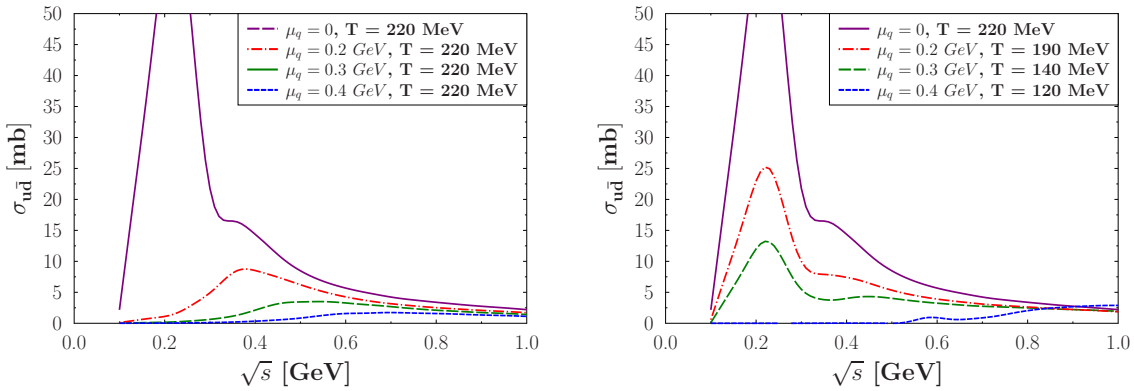

Fig. 5.5: Left: $u\bar{d}$ cross section at T=220 MeV as function of μ. Right: Evolution of the resonance as function of μ.

Fig.5.5 shows the evolution of the resonance peak with increasing chemical potential. For a given temperature, the mass of the pion becomes larger with increasing chemical potential and the peak is shifted to smaller values of temperature.

Beyond the critical end point $\mu_{CEP} = 0.32$, the cross section is flat and no resonance behaviour shows up anymore.

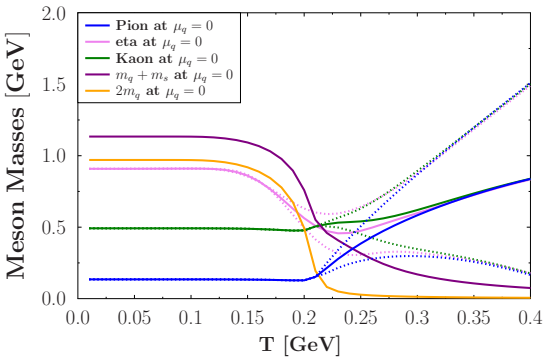

Fig. 5.6: Mesons mass at $\mu_q = 0$

The two processes $s\bar{s} \to u\bar{u}$ and $u\bar{u} \to s\bar{s}$ can be double checked as they obey the detailed balance [117].

$$\sigma_{c+d\to a+b}(s) = \frac{p_{ab}^2(s)}{p_{cd}^2(s)}\sigma_{a+b\to c+d}(s) \tag{5.A.15}$$

Fig. 5.7 shows that both calculations agrees.

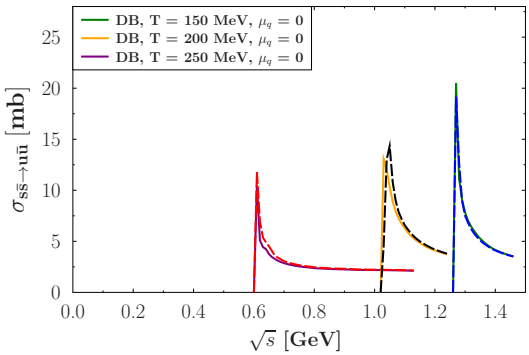

Fig. 5.7: Cross section calculated by detailed balance (DB) for T = 150, 200, 250 MeV at $\mu = 0$ (full line). Dashed lines represents the same cross section calculated directly.

5.B Transport coefficients in the relaxation time approximation

The interaction of a parton which traverses the QGP is usually described in form of cross sections with the QGP constituents. The cross sections which are employed are, however, not identical as the parameters which enter their calculation like coupling constants, parton masses or infrared cutoff, differ considerably from one model to the other. This makes it difficult to conclude from the cross sections on the energy loss a parton suffers during its passage through the QGP. Therefore, in order to compare different approaches, one uses transport coefficients which can be calculated in all approaches and reduces these differences to a number. The transport coefficients could be separated into two classes [118]:

- the transport coefficient associated to the description of the particles that make the medium, the light quarks (u, d and s) and the gluons. They are the interaction rate and what can be calculated from it, the viscosities (bulk and shear) and the conductivities (electric).

- The transport coefficients associated to the passage of a particle through that medium, energy loss, drag coefficient, diffusion coefficient [119]...

In this work, we are interested in the calculation of the ratio of shear viscosity to the entropy density (η/S) and the electric conductivity σ. The viscosity is inversely proportional to the cross section. Therefore, the smaller the viscosity the larger the interaction with the medium. For $\eta/S < 0.3$, hydrodynamics can be used to describe the medium, otherwise, one must use the kinetic theory [120]. If the η/S is low, close to the Kovtun-Son-Starinets (KSS) limit, calculated from strongly coupled $\mathcal{N} = 4 \quad SYM$ theory [121], this is a strongly coupled plasma. For a large η/S, the plasma is weakly coupled and tend to the pQCD limit.

The electric conductivity describes the response of the medium to an applied electric field and characterises the transport of the electric charge.

Viscosities and conductivities can be calculated exactly in the Kubo formalism [122]. For QCD, the complexity of the theory prevents an exact resolution yet and one needs to make approximations. For the calculation of the viscosity and the conductivity, one can use the Boltzmann equation in the Relaxation Time Approximation (RTA) which simplifies the calculations compared to the Kubo formalism [123]:

$$k_i^\mu \partial_\mu f_i + \frac{1}{2}\partial_\mu M_i^2 \partial_{(k_i,\mu)} f_i = \sum_{j=1}^{N_{species}} C_{ij}(x,k) \tag{5.B.1}$$

The Boltzmann equation gives the evolution of a system out of equilibrium [43] for the quasiparticles with dynamical masses $M_i(T,\mu)$. $C_{ij}(x,k)$ is the two-body collision term. The second term $\partial_\mu M_i^2$ is an external force attributed to the residual mean field interaction due to medium dependent effective masses $M_i(T,\mu)$. Assuming that the particles of type i are slightly out of equilibrium, we can write:

$$f_i = f_i^{eq} + \delta f_i. \tag{5.B.2}$$

In this configuration, the system goes back to the equilibrium with a characteristic time: the relaxation time. The collision term of the Boltzmann equation can then be written in terms of the non equilibrium part of the distribution function and the relaxation time the system takes to reach back the equilibrium [124].

$$C_i[f] = -E_i \frac{f^i}{\tau_i}. \tag{5.B.3}$$

In the dilute gas approximation, where the gas is dilute enough such that the mean free path is larger that the time between two collisions, the system has a relaxation time to reach back equilibrium given by [125]:

$$\tau_i^{-1}(T,\mu) = \sum_{j=q,\bar{q}} n_j(T,\mu)\sigma_{ij}(T,\mu), \tag{5.B.4}$$

where the n_q is the (anti)quark density, see Fig. 5.8, and the averaged cross sections are given by:

$$< \sigma_{iq}(T,\mu) >= \int_{th}^{s_{max}} \sigma_{iq}(T,\mu,s) P(T,\mu,s) ds \tag{5.B.5}$$

where $P(T,\mu,s)$ is a weight function [125]:

$$P(T,\mu,s) = C(T,\mu) p_{cm}^2 f_q(E_{p_q} - \mu) f_{\bar{q}}(E_{p_{\bar{q}}}(E_{p_{\bar{q}}} + \mu) \tag{5.B.6}$$

which is normalised as $\int_{th}^{s_{max}} ds P(T,\mu,s) = 1$ and all quantities are in the center of mass.

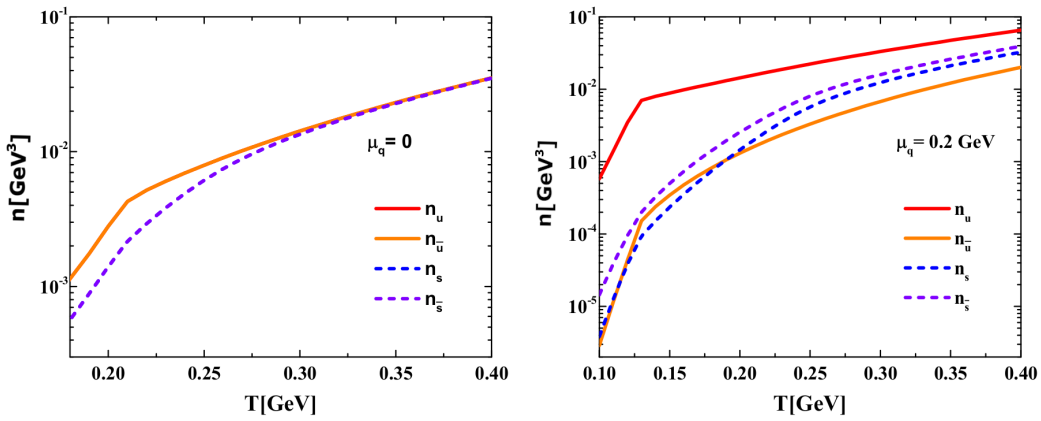

Fig. 5.8: (anti)quarks densities for $\mu_q = 0$(left) and $\mu_q = 0.2\ GeV$(right)

Eq. 5.B.4 shows that the relaxation time is inversely proportional to the cross section, ie to the interaction rate. This is in agreement with the Kubo formalism. One can see in Fig. 5.9 that the relaxation time becomes very small around the Mott temperature where the cross sections reach their highest value.

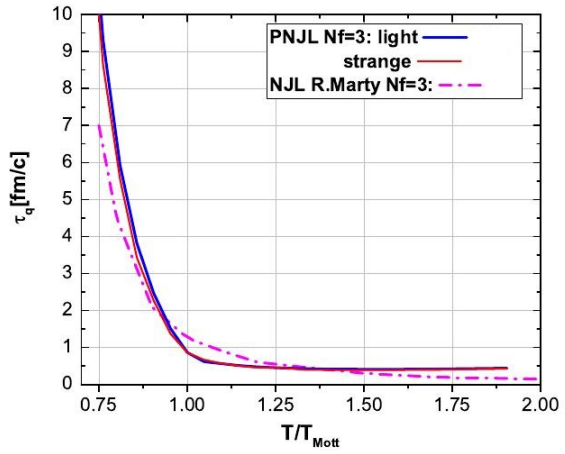

Fig. 5.9: PNJL relaxation time of the u, d and s quarks at zero chemical potential compared to the NJL results of [115]

The viscosities and conductivities are calculated directly from the relaxation time. The shear viscosity is [126]:

$$\eta^{\mathrm{RTA}}(T,\mu_B) = \frac{1}{15T}\sum_{i=q,\bar{q}}\int\frac{d^3p}{(2\pi)^3}\frac{\mathbf{p}^4}{E_i^2}\tau_i(T,\mu_B)d_i f_i, \tag{5.B.7}$$

where d_i is the degeneracy factor.

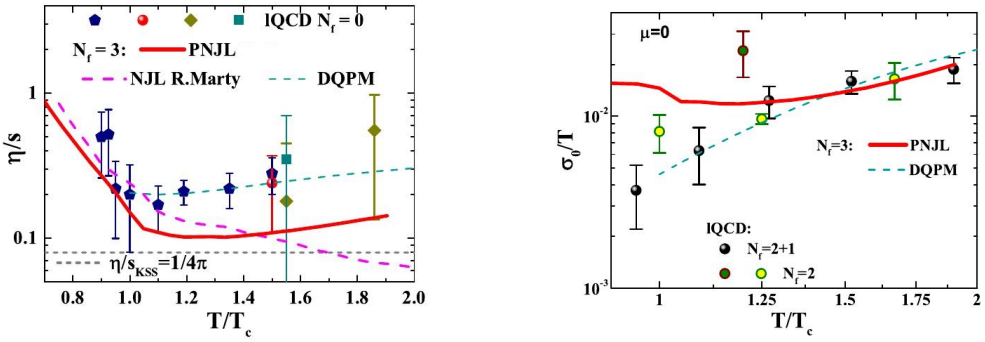

Fig. 5.10: Left: Shear viscosity to entropy density ratio at zero chemical potential. Right: Electric conductivity at zero chemical potential.

The shear viscosity, Fig. 5.10 left, shows a minimum close to the Mott temperature, considered as the critical temperature of the NJL type models. This minimum is the consequence of the increase of the cross sections due to the resonance with the exchanged mesons in the quark-antiquark s-channel. The shear viscosity looks similar to the NJL results of [115] with the considerable improvement that it does not go below the KSS limit [121] $(\eta/s)_{\rm KSS} = 1/(4\pi)$. This improvement comes from the entropy which is much closer to the lattice result and consequently lower than before at large temperatures. The correction on the integration of the one fermion loop, already discussed in section 3.F, also brings non negligible corrections. It leads to a larger mass and decay width of the exchanged meson at large temperatures what lowers the cross section. The shear viscosity is then higher than in the NJL model [115]. This comparison with the lattice results is qualitative for three reasons. The quark-hadron cross sections have not been taken into account which leads to an incomplete description of the viscosity near $T = T_C$. In addition, gluon contributions enter the calculation of the viscosity on the lattice. This contribution is not fully present in the PNJL model by construction and represents another limitation of the prediction. Eventually, the lattice results for the transport coefficients are calculated in the quenched approximation discussed in section 2.E. The quarks are considered as infinitely massive ($N_f = 0$) which makes another difference to our PNJL model. A more quantitative comparison can be made with the electric conductivity as the gluons are electrically neutral. Electric conductivity contains then only a quark contribution which corresponds exactly to the NJL approximation. The electric conductivity can also be calculated from the RTA results [127]:

$$\sigma_0^{\rm RTA}(T,\mu_B) = \frac{e^2}{3T}\sum_{i=q,\bar{q}} q_i^2 \int \frac{d^3p}{(2\pi)^3}\frac{\mathbf{p}^2}{E_i^2}\tau_i(T,\mu_B)d_i f_i, \tag{5.B.8}$$

where $e^2 = 4\pi\alpha_{em}$, $q_i = +2/3(u), -1/3(d), -1/3(s)$ are the quark charges, $d_q = 2N_c = 6$ are degeneracy factors for spin and color in case of quarks and anti-quarks.

Fig. 5.10 right shows the electric conductivity at $\mu_q = 0$. The lattice results for $N_f = 2 + 1$, three quarks u,d,s with $m_s \neq m_u = m_d$, are on the same level of description of the light quarks than our PNJL model. With no surprises, the low temperatures domain suffers from the lack of the quark-hadron cross sections and does not match the lattice

results. However, above T_c, our electric conductivity is in very good agreement with the lattice results.

Using the cross section calculations at finite μ_q, we can now determine the transport coefficients for large values of μ_q, near the CEP and in the first order phase transition region. Our results can be compared with the DQPM results at low μ_q [128].

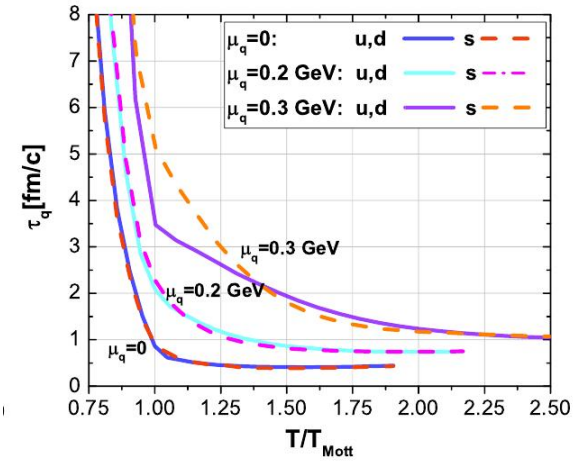

Fig. 5.11: Relaxation time of q and s quarks at finite chemical potential

The relaxation time of the u, d and s quarks is displayed in Fig. 5.11. The u, d and s quarks have a similar relaxation time at low μ. It differs more and more with increasing chemical potential as the mass of the u and d quark drops faster and to a lower value than the mass of the s quark at a finite chemical potential. One can see that the decrease in the relaxation time is sharper and sharper when approaching the CEP and the first order phase transition. The η/S and σ_0/T calculated from the relaxation time are shown in Fig. 5.13. Both shear viscosity and electric conductivity seem to increase clearly when the chemical potential increases.

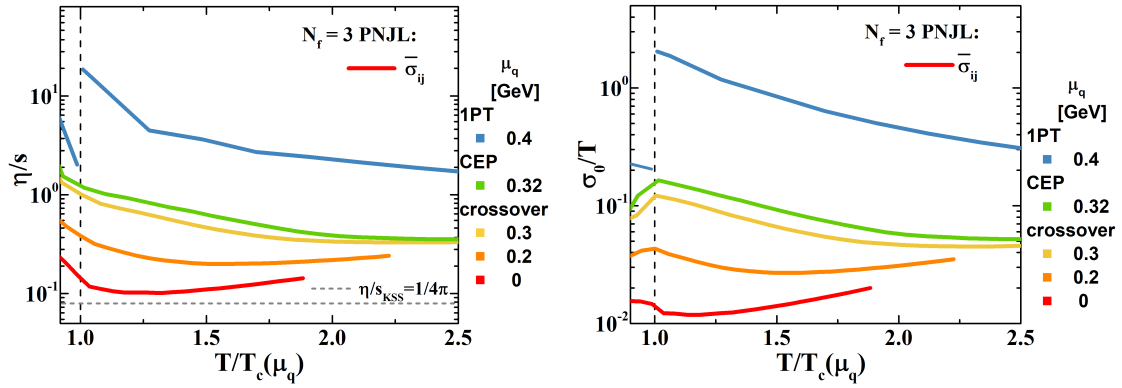

Fig. 5.12: Left: Shear viscosity at finite chemical potential. Right: Electric conductivity at finite chemical potential.

One can see a discontinuity at $\mu_q = 0.4\ GeV$ near the critical temperature, a sign of the first order phase transition that occurs at large μ. In the region of the CEP,

$\mu_q = 0.32\ GeV$, the η/S changes smoothly like for $\mu_q = 0.3\ GeV$. As a conclusion, the η/S cannot point out the position of the CEP but clearly shows if a first order phase transition occurs. In addition, the value of the η/S at finite μ is higher, meaning that the QGP is weakly coupled at large chemical potential on the whole range of temperatures. The electric conductivity also shows a discontinuity at $\mu_q = 0.4\ GeV$ in the vicinity of the first order phase transition region, but still does not point out the location of the CEP as the behaviour is smooth at $\mu_q = 0.32\ GeV$. The first order phase transition discontinuity occurring remains questionable as a consistent transport coefficient would be calculated only with hadronic contributions below $T = T_C$. The PNJL model should be supplied with a Hadron Resonance Gas model or a baryon model describing the transport coefficients below T_C.

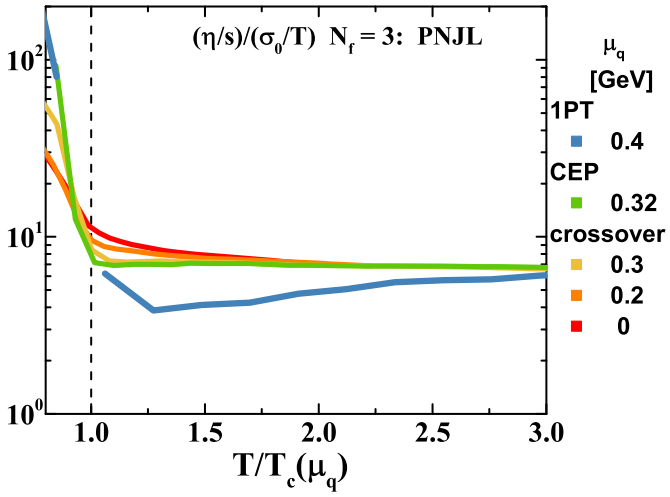

Fig. 5.13: ratio Shear viscosity to electric conductivity at finite chemical potential.

Another interesting quantity is the ratio $\frac{\eta/S}{\sigma_0/T}$. The fact that is it a ratio as for consequence that the temperature dependence near the phase transition suffers less from the approximations made on the evaluation of the cross sections or relaxation times. Fig. 5.13 shows that the ratio decreases slowly at low μ and sharply at large μ. A discontinuity appears at $mu_q = 0.4\ GeV$ again.

As a conclusion, using the entropy calculated from the equation of state in chapter4 and the correction to the one-fermion loop Eq.3.F.2, the shear viscosity and the electric conductivity now match the results of lattice QCD at $\mu = 0$, especially well in the region $1.25 - 2T_c$. The finite μ results show no sign of CEP from the shear viscosity and the electric conductivity, but a sign of first order phase transition from the discontinuity observed in those transport coefficients. However, the quark cross sections are not relevant below T_c in second and first order phase transitions where hadronic cross sections are relevant. In the cross over region, quark-hadrons cross sections should also be considered. This should improve the results regarding the electric conductivity which deviates from lattice results in the cross over region.

Chapter 6

Dynamical study of a first order phase transition

The studies that have been performed up to now were thermodynamic studies and only comparable with other theories like lQCD. To compare with experiments, the heavy ion collisions, one needs to study dynamically the phase diagram of strongly interacting matter. To do so, one can use an event generator, superposition of theoretical models reproducing an experimental heavy ion collision. The equation of state, determined thermodynamically, can be implemented into an event generator, especially if this event generator uses a hydrodynamical evolution to describe the expanding QGP. As the equation of state is needed to close the system of hydrodynamical evolution equations, one can study the dynamical consequences of a first order phase transition in the phase diagram of QCD. The event generator EPOS has been made to study the high beam energies collision and does not contain yet all the feature to describe consistently low energy beam collisions. Nevertheless, this work will still give an insight of the hydrodynamical evolution of an expanding QGP near a first order phase transition and will give perspectives on the possible improvements that can be done on EPOS in order to reach a better description of the low energy beam heavy ion collisions.

6.A Bjorken scenario

Heavy ion collisions are historically theoretically described using the Bjorken scenario [129], see Fig. 6.1.

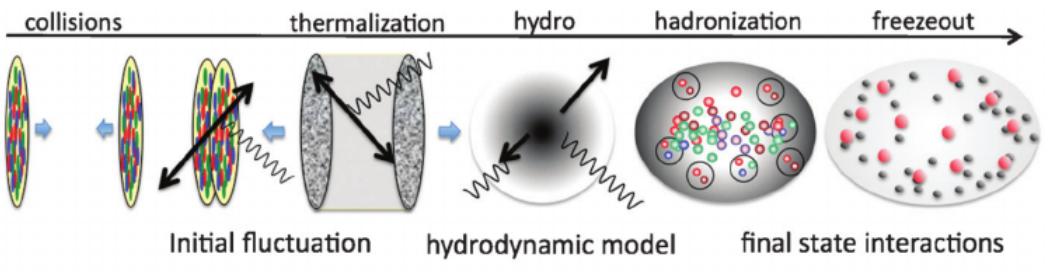

Fig. 6.1: Time evolution of a heavy ion collision [130]

This evolution can be summarised in four different stages:

- Initial condition and pre-equilibrium stage:

  The two nuclei which collide have an initial parton distribution. They collide and mutiple hard parton-parton scatterings happen. The system then starts to thermalise but fluctuations of energy density remains. This phase consists in establishing the initial conditions of the heavy ion collision from which the QGP emerges. Regarding the centrality of the collisions, it connects the impact parameter to the average number of particles participating to the collision and the average number of binary nucleon-nucleon collisions. The Glauber Model is often used for positioning the nucleons inside nuclei using a distribution function [131]. Microscopically, the pre-equilibrium state can be described in terms of gluons in the Color Glass Condensate model [132] or color flux tube in EPOS [133]. The hard probes in section 2.F are generated at this moment of the collision.

- QGP phase:

  At the end of this initial stage, when the system is pre-equilibrated, the quarks and the gluons are free in a so called plasma phase. This plasma phase starts to expand because of the pressure gradient provided by the fluctuations from the pre-equilibrium stage. This phase is generally characterised as a viscous fluid expansion [134]. The hydrodynamics evolution describes the evolution of the thermalised medium in expansion. The hydrodynamics evolution is directly related to the equation of state of the strongly interacting matter which implies that the evolution depends directly on the nature of the phase transition between the QGP phase and the hadronic matter. The hydrodynamics also depends on the transport coefficients of the medium and especially on the shear viscosity calculated in section 5.B, which affects the evolution of the QGP.

- Hadronic gas:

  From some energy and baryonic densities, depending on the ratio of the rate expansion over the number of particles collisions, the system gets out of equilibrium and cannot be described with a hydrodynamic evolution anymore but with the kinetic theory. The fluid is converted into particles via the Cooper Frye prescription [135],[136]. From this point, the system undergoes a hadronic gas expansion.

- Freeze-out:

  The system keeps expanding as a hadron gas and cools down. The temperature after which no more new hadron types are produced is known at the temperature of chemical freeze-out. The chemical composition of the medium does not change anymore [43]. Also a temperature of kinetic freeze-out is defined corresponding to the moment from which the momentum of the particles do not change anymore. At low energy, chemical and kinetic freeze-out occur roughly at the same moment. As the beam energy increases, the time between kinetic and chemical freeze-out increases. The chemical freeze-out appears first. The kinetic freeze-out appears at lower temperatures as the beam energy increases [43]. Eventually, hadrons behaves freely and those particles are the one recorded in the detectors.

This evolution can also be represented on the light cone, see Fig. 6.2.

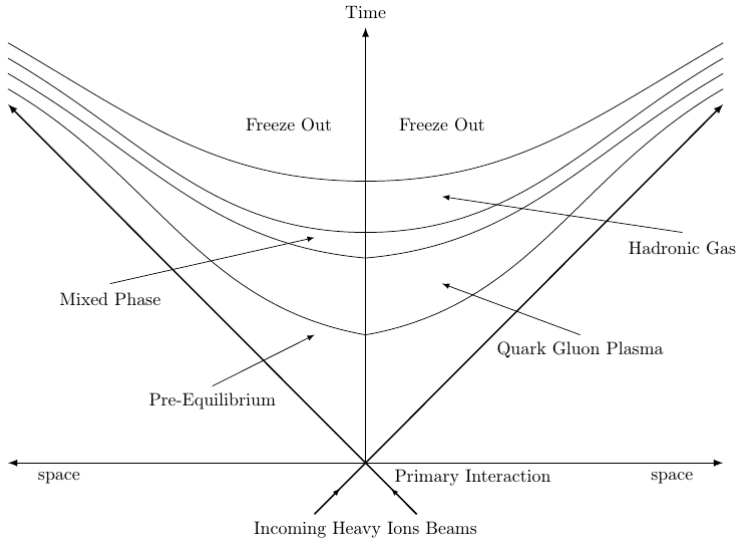

Fig. 6.2: space-time evolution of the heavy ion collision [54]

All those phases are found in the event generator used in order to study dynamically the QGP. Here is a short summary of how EPOS treat the different steps of the Bjorken scenario.

6.B The event generator EPOS

Parton-Based-Gribov-Regge Theory

EPOS is built from the Parton-Based-Gribov-Regge Theory (PBGRT) which gives the initial condition and the pre-equilibrium stage [133]. This theory used the analytic property of the S matrix (Lorentz invariance, unitarity, analyticity) in the high energy limit ($s \gg t$) to describe the amplitude of the elastic collisions. The asymptotic behaviour of those amplitudes can be described by the Regge theory [137]. In the limit of infinite s, the scattering looks like the exchange of an object in the t channel with a t dependent angular momentum, which prohibit to define it as a particle. This is the reggeon. It is interpreted as a superposition of amplitudes for the exchange of all possible particles in the t channel. The Pomeron is a special type of reggeon (see [137] for further details). The Regge theory describes very well the experimental results and the results predicted are recovered using the standard pQCD calculations. However, the unitarity of the S matrix is not respected anymore at very large energies. The cross section are proportional to s which disagrees with the Froissart-Martin bound [138].

This problem is cured by the Gribov-Regge theory which describes multiple scatterings between hadrons using a multiple pomeron exchange [54]. However, the conservation of the energy is not maintained on the level of cross section calculation. It works only for soft process.

In order to include all possible process, the Gribov-Regge theory is merged with the parton model for which the energy is conserved for hard process. The hadron exchange of the Gribov-Regge theory is substituted by a parton exchanged (quarks and gluons) at high energy.

The multiple parton-parton interactions can be converted into strings, using the phenomenological Lund model [139]. The medium can be separated into two phases: a phase of very large string density, the core and a phase of low string density, the corona, see Fig. 6.3. The core represents the QGP and expands hydrodynamically.

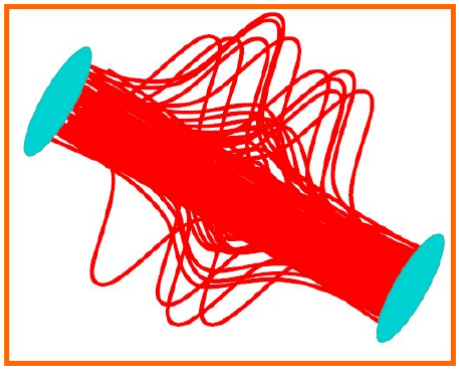

Fig. 6.3: Core corona separation in EPOS [140]

Hadronisation occurs within the fluid form and the conversion to kinetic theory is done with the standard Cooper Frye procedure. The strings in the corona hadronise afterwards and hadron-hadron rescattering appears.

6.C Observables and variables of the study

Few observables selected as probes of the QGP have been already presented in section 2.F. In this work, we are interested in comparing the data obtained from the same event generator (EPOS) with the same settings of collision, the only change being the eos: the standard eos of EPOS has a cross over on the whole T-μ plane ; the PNJL equation of state has a CEP and a first order phase transition at large μ.

The observables used for the comparison will be hadrons multiplicities and their ratio. The observables are generally shown as function of the centrality of the collision, the rapidity and the transverse momentum. The centrality tells how central are the collision: 0-5% being the most central and 95-100% being the most peripheral. The more central the collision, the higher the probability to have the formation of a QGP and the larger the size. The rapidity y is a variable that describes the dynamics of the system along the axis of collision:

$$y = \frac{1}{2} \ln \frac{E + p_z}{E - pz}. \tag{6.C.1}$$

Rapidity differences are invariant under longitudinal boost, which is the Lorentz transformation of interest because along the beam axis. The transverse momentum p_t is a variable

which is invariant under longitudinal boost that describes the dynamics of the system in the plan transverse to the collision. It is especially connected to collective effects.

6.D Converting the equation of state

The equation of state that has been calculated with the PNJL model, see section 4, is a function of the temperature and the chemical potential. The energy density and the baryonic density of the medium is then given by T and μ. However, in event generators and experiments, it is the other way around. The equation of state is a function of the energy density and the baryonic density which gives the temperature and the chemical potential of the medium. The PNJL equation of state must be inverted in order to be of use in an event generator. To do so, the property of monotonicity of E(T,μ) and N(T,μ) can be used to assign to each temperature and chemical potential a given energy density and baryonic density.

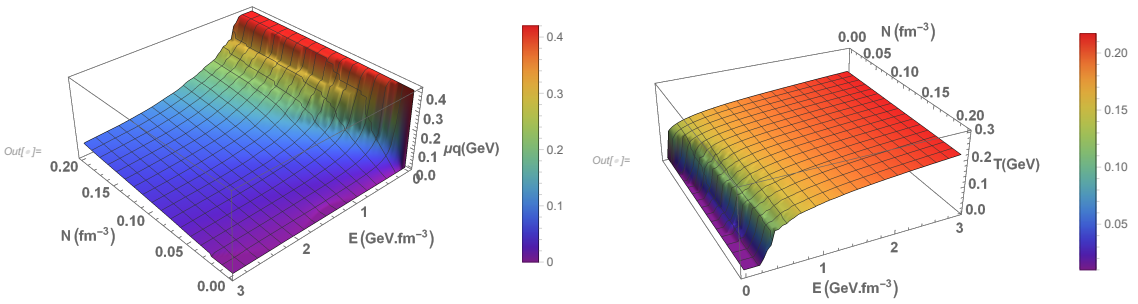

Fig. 6.4: PNJL equation of state: (left) quark chemical potential as function of the energy density and the baryonic density, (right) the temperature as function of the energy density and the baryonic density.

The temperature and the chemical potential as a function of the energy density and the baryonic density obtained from the PNJL equation of state is shown in Fig. 6.4. A jump appears at constant baryonic density and increasing energy density at $\mu_q = 0.32\ GeV$ and $T = 0.11\ GeV$, consequence of the first order phase transition, which does not appear in [141] where a cross over occurs in the whole $T - \mu$ plane, see Fig. 6.5.

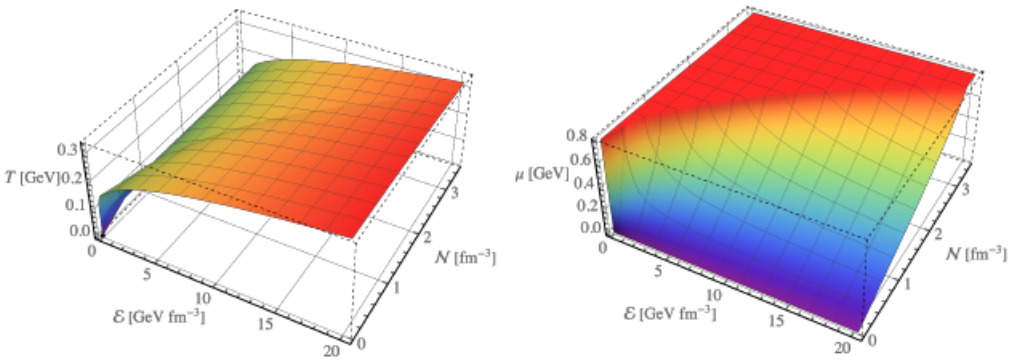

Fig. 6.5: Analytical equation of state [141] showing (left) the temperature as function of the energy density and baryonic density, (right) the chemical potential as function of the energy density and baryonic density.

In addition, the metastable states occurring in the chiral condensate, see Fig. 3.2, is expected to have dynamical consequences like the apparition of bubbles of large baryonic density in the plasma phase through the process of nucleation [35, 142].

6.E Influence of a first order phase transition on the hydrodynamical evolution of a heavy ion collision

6.E.1 Comparison of EPOS simulation for different collisional energies

In the event generator EPOS, the equation of state constraining the hydrodynamical evolution of the fluid is a cross over on the whole $T-\mu$ plan [143, 144]. By implementing the PNJL equation of state shown in Fig. 6.4 in EPOS, it becomes possible to see the influence of a first order phase transition on the hydrodynamical evolution of the fluid using the same event generator, initial condition and collision description. At zero chemical potential, both eos show a cross over within the error bars of the lattice equation of state. At finite but low density, both eos also share a cross over transition. The results at large energies, before the CEP, must then be similar. We choose the collisional energies 19.6 GeV, 14.5 GeV and 11.5 GeV in order to compare with the experimental data of the BES program, see section 2.F. The simulations are done with the EPOS version 3.2.59. The black line results contain 500k events from the results of [54], thesis devoted to this study and containing much more events than our red line results with 45k events. This difference in statistics is seen especially at large p_t, as the particle production is rare, where the data has fluctuations.

For Au-Au with $\sqrt{s} = 19.6\ GeV$, pions and kaons production have a similar behaviour with both eos, see Fig. 6.6. However, the EPOS simulation with the PNJL equation of state produced a little less particles. This feature also appears in the general mesons production. It is less clear for the baryons, especially at large p_t where the production is the same for both equation of state. One can also notice that for the strange hadrons,

kaons and Λ in Fig. 6.6, the difference appears is even more clearly and the production is much lower.

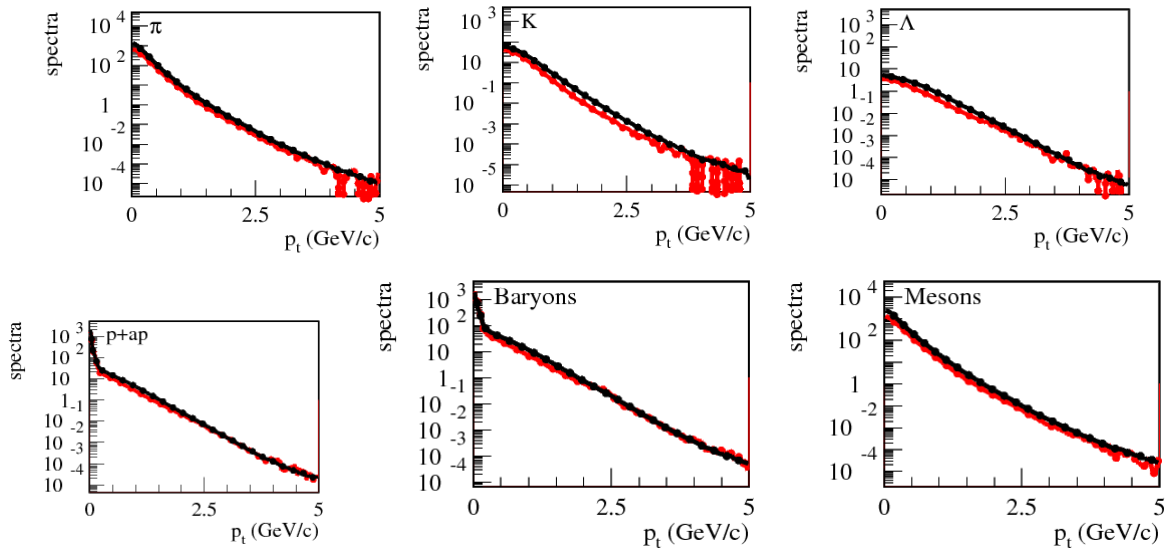

Fig. 6.6: p_T spectra for Au-Au $\sqrt{s} = 19.6GeV$ with a PNJL eos (red) and the standard epos eos (black)

For Au-Au with $\sqrt{s} = 14.5\ GeV$, the behaviour of the particle productions remains similar. However, the pions are now equally produced for both equation of state. The difference between strange hadrons production is much narrower though still lower with the PNJL eos. Regarding the protons, they are even more produced at large p_t and equally produced at low p_t, see Fig. 6.7.

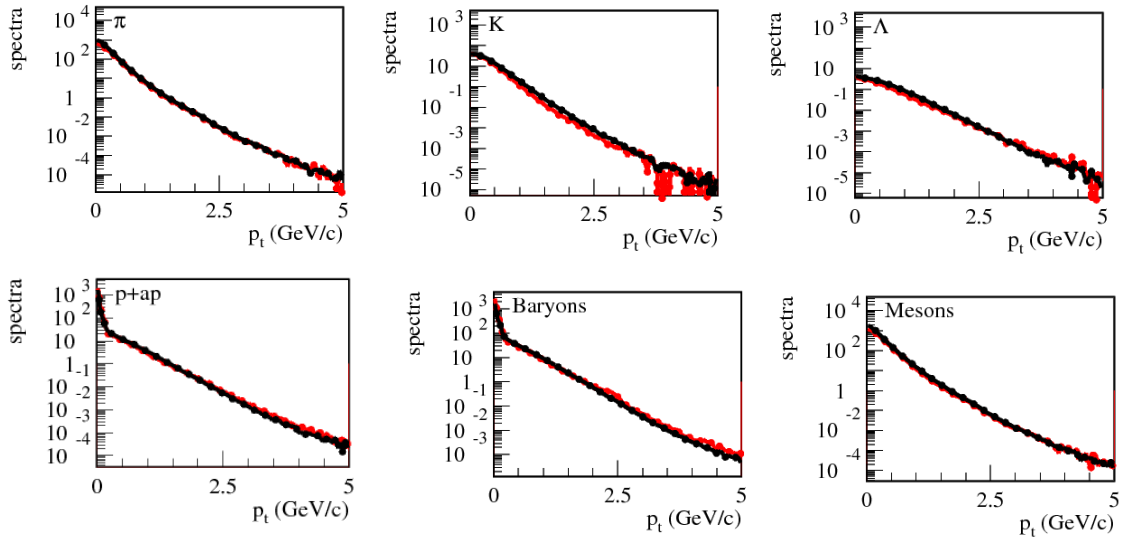

Fig. 6.7: p_T spectra for Au-Au $\sqrt{s} = 14.5GeV$ with a PNJL eos (red) and the standard epos eos (black)

The p_t spectra in log scale show that the behaviour is similar with both equations of state, but makes quantitative observations of the real differences complicated to see and therefore to conclude about. In order to clarify the conclusion, we plot the ratio of black (EPOS) and red (PNJL) lines of Figs. 6.6 and 6.7. This ratio is shown in Fig. 6.8. It confirms that apart for strange hadrons for which the ratio is similar for both energies, the ratios of identified particules produced with the PNJL eos over the identified particles produced by the EPOS eos are higher for $\sqrt{s} = 14.5\ GeV$ than for $\sqrt{s} = 19.6\ GeV$. It also confirms that the only ratios which shows that more particles are produced with the PNJL eos than with the EPOS eos, is that for the large p_t proton + antiproton and for baryon production at $\sqrt{s} = 14.5\ GeV$.

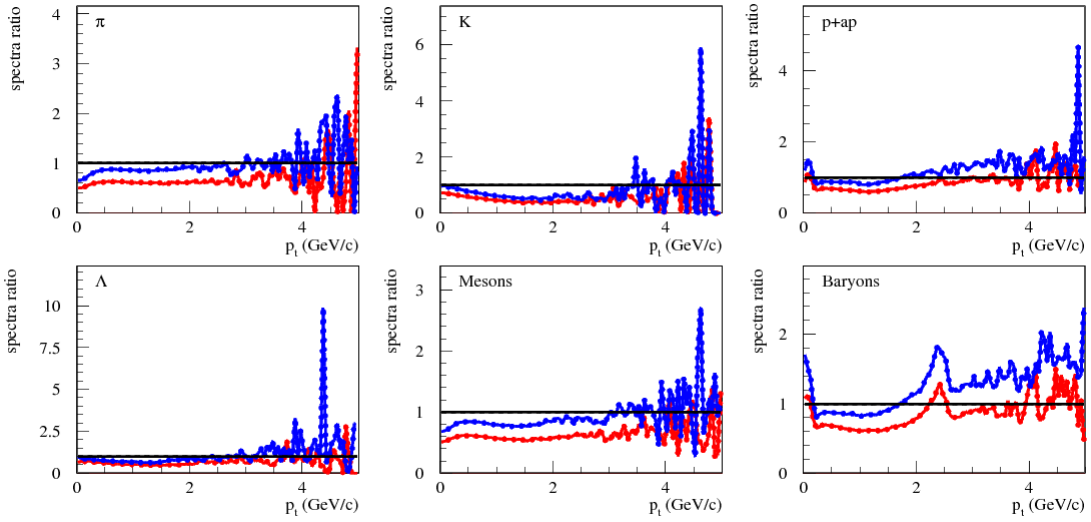

Fig. 6.8: ratio of the p_T spectra obtained from the PNJL eos over the epos eos for Au-Au $\sqrt{s} = 14.5GeV$ (blue) and $\sqrt{s} = 19.6GeV$ (red))

From those results, one cannot see the real influence of first transition but the influence of getting close of it. The cross over transition is characterised by a mixed phase of deconfined quarks and hadrons. The size of this transition region becomes smaller at large chemical potential if the equation of state has a CEP and a first order phase transition. Our results show that at $\sqrt{s} = 19.6\ GeV$, the simulation using the PNJL equation of state produced less particles, especially mesons and strange hadrons than the simulation using the standard EPOS eos. However, when decreasing the beam energy to $\sqrt{s} = 14.5\ GeV$, this difference seems to narrow and large p_t protons are even more produced with the PNJL eos than with the EPOS eos. In the literature, it is expected that a hydrodynamical expansion with an equation of state containing a first order phase transition produced more particles than in a case of a cross over[145, 146]. In the case of a first order phase transition, during the transition, the pressure remains constant while the energy density decreases. There is no pressure gradient and the system does not expand as efficiently as in the case of a cross over. This slow down in the expansion implies a bigger lifetime of the QGP and increase in the particle production [135].

The literature also expects that the discontinuity of the first order phase transition re-

sults in a store of energy that, when liberated after the transition, allows for the production of more massive particles like protons compare to light particles like pions [142, 147, 148]. Even though, the first order phase transition is not reached at $\sqrt{s} = 19.6\ GeV$ or $\sqrt{s} = 14.5\ GeV$, the evolution of the cross over toward a CEP and first order phase transition appears also through this phenomenon.

6.F Perspectives

Hence the reduction of the crossover region leads to a small increase of the particle production and especially of high p_t protons. A first order phase transition is also expected to lead to an increase of the particle production and especially more massive and energetic particles. The influence of the discontinuity of a first order phase transition on the hydrodynamical evolution of an expanding QGP has regained a recent interest with the study of the nucleation, in the case of first order phase transition [35, 142] and spinodal decomposition, in the case of second order phase transition [147, 148]: the apparition of bubbles of phase B (nucleation) or domains (spinodal decomposition) in a medium of phase A. The first perspective would be to generate an initial condition with EPOS at low energy beam and proceed to an hydrodynamical evolution of the expanding QGP only. By displaying the color map evolution of the hydro, one could see the formation of bubbles or domains showing the phase transition occurring. This has already been done in 1D [142] with the additional fact that fluctuations over the net baryon density are taken into account. It is not clear if a standard hydro only is enough to produce nucleation and spinodal decomposition.

In addition, EPOS has been designed to the study of a QGP formed from high collisional energies, ie vanishing chemical potential. In this conditions, the shear viscosity to entropy ratio is set to 0.08 [143], in agreement with the RHIC and LHC data and the literature [149]. However, the results of the chapter 5 shows that the η/S becomes much larger at finite μ and has even a discontinuity, see Fig. 5.13. This should make a large difference on the finite μ hydrodynamical evolution [150].

Part III

Postlude: Neutron stars and perspectives

Chapter 7

Description of neutron stars

This chapter is a preliminary work, guided by the motivation of a better understanding of the improvement that can be done on the PNJL model at finite μ and low temperatures using the constrains that can bring the physics of neutron stars. The knowledge of the equation of state and, generally speaking, of the phase diagram of strongly interacting matter plays a crucial role in the study of neutron stars. The (P)NJL models can be used for this study as the equation of state that helps describing the neutron star is limited to low temperatures and to a large chemical potentials, describing a matter dominated by quarks where the gluon contributions are negligible. However, the (P)NJL models suffer the lack of quark-quark interaction necessary to build nucleons in the hadronic phase, at moderate chemical potentials. We limit this work to a study of the mass-radius relation of a neutron star using the basic NJL model presented in chapter 3. This represents the opportunity of learning more about the equation of state expectations at large density and brings further improvements to our equation of state developed in chapter 4.

7..1 Neutron star creation

A neutrons star is a compact star formed after the supernovae explosion of a star at least eight times more massive than our sun[151]. A smaller mass would lead to a white dwarf formation and a mass larger than 25 solar mass would lead to a black hole formation [152]. Historically predicted by Landau [153] even before the prediction of the neutron by Chadwick [154], the first detection of neutron star happened however much later in 1968 [155] from pulsar, highly magnetized rotating neutron stars [156].

The scenario leading to the creation of a neutron star can happen for an isolated star or a binary system. In the case of binary systems, it can lead to a merger of compact double neutron star binary system emitting intense gravitational radiations. A possible end is the merging of the two stars producing again an even more powerful outburst of gravitational waves. Gravitational waves have been recently detected [157] and bring new constraints on the equation of state of strongly interacting matter, that predicts the maximal mass which a neutron star can reach before collapsing into a black hole. Neutron star that could be 2.6 times more massive that our sun [158] have been recorded thanks to the gravitational waves, while experimental measurements of pulsars [159] have set an upper limit of neutron star mass to be 1.97 time more massive than our sun. Those new constraints rule out many eos and force the theoreticians to better understand the phase diagram of strongly interacting matter.

7..2 Structure of a neutron star

A neutron star is usually separated into two main parts being the crust and the core. More details about the precise structure of the crust that is shared between an outer crust and an inner crust and the core also divided into an outer core and an inner core can be found in [160]. This is the usual description of a nuclear neutron star, but more exotic situations could also be possible:

- The quark star (strange star) made of quark matter [161], [162].
- The hybrid star, with an outer core of nuclear matter and an inside core of quark matter [163].

This is where the NJL model appears to be relevant as one of the models describing the equation of states of cold dense quarks.

7.A Equation of state and neutron stars

The size and the mass of a neutron star is determined at the hydrostatic equilibrium, when the attractive force coming from gravity and the repulsive force coming from the internal pressure compensate each other. One need three relativistic equations to describe the hydrostatic equilibrium[160]. The first one is the famous the Tolman-Oppenheimer-Volkoff (TOV) [164].

$$\frac{dP}{dr} = -\frac{Gm}{r^2}\left(1+\frac{P}{\rho c}\right)\left(1+4\frac{4\pi P r^3}{mc^2}\right)\left(1-\frac{2Gm}{c^2 r}\right)^{-1} \tag{7.A.1}$$

The second one describes the mass balance:

$$\frac{dm}{dr} = 4\pi r^2 \rho \tag{7.A.2}$$

The third one is a relativistic equation for the metric function $\phi(r)$ [160]:

$$\frac{d\phi}{dr} = -\frac{1}{\rho c^2}\frac{dP}{dr}\left(1+\frac{P}{\rho c^2}\right)^{-1} \tag{7.A.3}$$

To solve them, they must be supplemented by an equation of state $P = P(\rho)$, giving the pressure P as function of the density ρ. Equation 7.A.1 and 7.A.2 can be solved separately of Eq. 7.A.3, which will not be used in this part of the work. Consequently, the radius and the mass of the neutron star depends on the pressure of the medium, hence on the equation of state of the strongly interacting matter. The resolution of the TOV equation is done by imposing the following conditions at the center of the neutron star:

- $r = 0$
- $n(r = 0) = n_c$
- $P(r = 0) = P(n_c)$

- $m(r = 0) = 0$

where n is the density of the star and n_c is the density at the center of the star. The solution starts from the center of the star to the surface The radius, the mass, the pressure and the density are then iterated until the density reaches a value at which the change in mass is negligible. The central limit can then be varied in order to span the range of possible mass-radius configurations.

7.B Description of a neutron star using our approach

7.B.1 Constraint on the heavy ion matter equation of state to describe the neutron star matter

The physics of the neutron stars involves the four fundamental forces. The gravitational force has already been mentioned to derive the TOV equation, Eq. 7.A.1. The strong interaction is involved with the determination of the equation of state. The weak interaction implies the decay:

$$neutron \rightarrow proton + electron + antineutrino \tag{7.B.1}$$

Converting the neutron and the proton in terms of the fundamental constituents (u and d quarks) chemical potentials and neglecting the antineutrino, we can write:

$$2\mu_d + \mu_u = 2\mu_u + \mu_d + \mu_e \tag{7.B.2}$$

Which gives the following relations:

$$\mu_d = \mu_e + \mu_u \tag{7.B.3}$$

However, the β decays are just a possible reaction that conserves the baryon and electric charge. The possible transformations, including the strange chemical potential, are [151]:

$$\begin{aligned} \mu_u &= (\mu_b - 2\mu_e)/3 \\ \mu_d &= (\mu_b + \mu_e)/3 \end{aligned} \tag{7.B.4}$$

$$\mu_s = (\mu_b + \mu_e)/3 \tag{7.B.5}$$

which leads to:

$$\mu_d = \mu_s. \tag{7.B.6}$$

We have four unknowns, μ_d, μ_u, μ_s and μ_e, but only three equations. We then need another equation to close the system. We use the neutrality condition:

$$\frac{2}{3}n_q(\mu_u) - \frac{1}{3}n_q(\mu_d) - \frac{1}{3}n_q(\mu_s) - n_e(\mu_e) = 0 \tag{7.B.7}$$

This equation must be added to the gap equations, Eq. 3.D.18, giving m_u, m_d and m_s and all of them must be minimised at the same time. This is a set of four equations with four unknowns: m_u, m_d, m_s and μ_e.

7.C Mass-radius diagram

We test the TOV equation solver by considering the easiest case, the hadronic phase with the NJL model and the approximation of vanishing mass $m_s = m_u = m_d = 0$ in the QGP phase. The same algorithm is used as in section 6.D, in order to reverse the equation of state and to obtain the pressure as a function of the baryonic density by starting from the pressure and the baryonic density as a function of the chemical potential μ_q. The pressure obtained is shown in Fig. 7.1 left. The hadronic phase is not well described by the NJL model. The degrees of freedom should be baryonic (neutron) which is not the case here. Here we use a Douchin-Haensel type of equation of state [165], see Fig. 7.1 left, a well known hadronic equation of state in the neutron star community describing both the neutron star crust and the liquid core with a skyrme nucleon-nucleon interaction. This equation of state is interpolated with the NJL equation of state, see Fig. 7.1 left. A large increase appears in the pressure, sign of the phase transition between hadronic matter and QGP, compared to the pure hadronic equation of state of Douchin-Haensel.

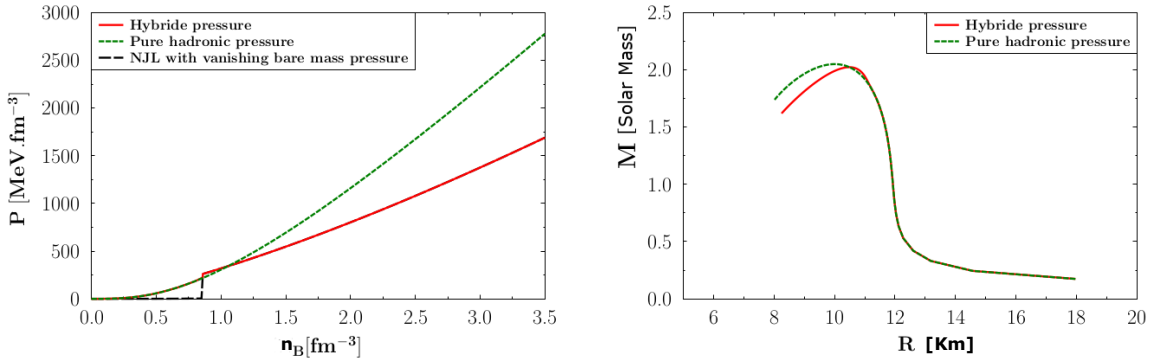

Fig. 7.1: Left: Hadronic pressure of Douchin-Haensel type [165] with skyrme nucleon-nucleoninteraction , NJL pressure and hybrid pressure as function of the baryonic density. Right: Neutron star mass-radius diagram from the hadronic equation of state and from the hybrid equation of state.

One can see that the difference of mass-radius relation between the two equation of state is very small for large radii, see Fig. 7.1 right. Increasing the maximal density the star can reach in the solution of the TOV equation, one has access to lower values of the

radius. However, the pressure is not strong enough anymore to balance the gravitational interaction and the mass has to drop.

A finite mass of the quark, and especially of the strange quark should not change a lot the behaviour of the mass-radius relation. However, the vector interaction of Eq. 3.B.27 has not been taken into account. By taking this repulsive interaction into account, the NJL pressure is expected to increase strongly, which could allow for more massive neutron star. In addition, the consideration of the baryons contribution in the NJL hadronic phase would allow a consistent, althought difficult, NJL treatment of the eos without any interpolation with a non NJL related hadronic equation of state.

7.D Mass of the strange quark

The next step is to move to the situation described in section 7.B.1, a neutral β-equilibrated matter, where the electrons balance the additional electric charge caused by the fact that the mass of the s quark is larger than the mass of the u and d quarks. However, the mass of the s quark behaves differently compared to the mass of the u and d quarks.

Fig. 7.2 shows the mass of the s quarks in different configurations, a s quark of vanishing mass in the QGP phase, the mass of the quark s in the case of symmetric matter suitable for heavy ion collision ($\mu_u = \mu_d$ and $\mu_s = 0$) and the the mass of the quark s in the case of asymmetric matter ($\mu_d = \mu_s$ and $\mu_u = \mu_d - mu_e$).

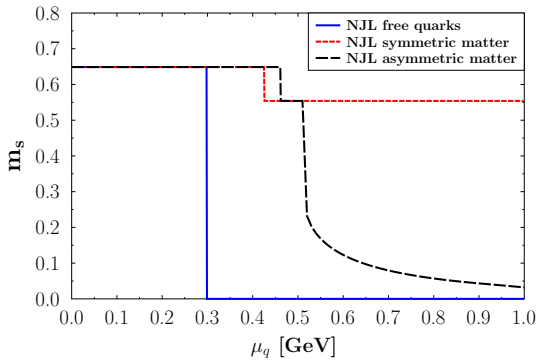

Fig. 7.2: Mass of the quark s in the case of free quarks in the QGP phase, symmetric matter and asymmetric matter as a function of the quark chemical potential at $T = 1\ MeV$.

The quark s, for asymmetric matter, seems to have a double phase transition. However, the first jump is built by determining the critical chemical potential and explicitly demanding the system to be in the hadronic phase before this critical chemical potential and in the QGP phase after. This is not the case of the second jump which is not here by construction. It comes naturally from solving the gap equations. One can wonder about its nature and the reason of its presence here. This double transition does not show up for u and d quarks, see Fig.7.3.

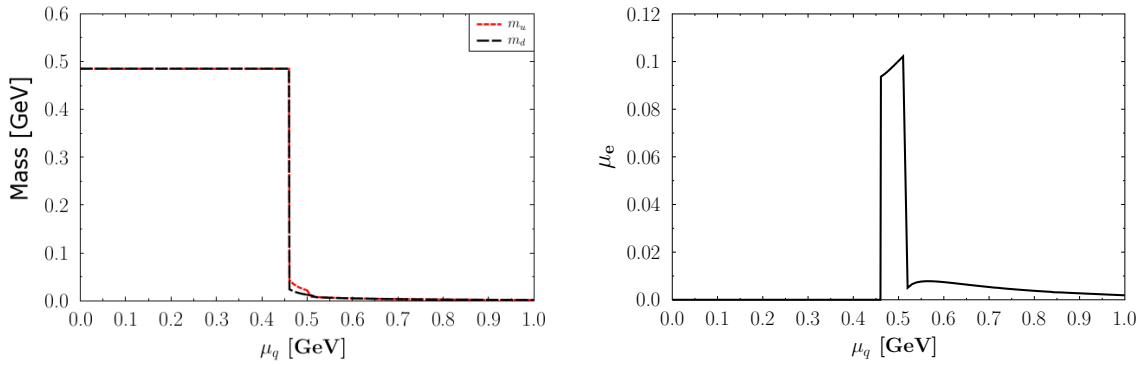

Fig. 7.3: Left: Mass of the quark u and d in the case of asymmetric matter as function of the quark chemical potential at $T = 1\ MeV$. Right: electron chemical potential as function of the quark chemical potential.

Chapter 8

Perspectives on the PNJL equation of state

By applying the PNJL equation of state to concrete studies and by comparing with other theories and experiments, more constraints are added and new ideas emerge to improve the PNJL model that has been designed all along this work.

- The neutron star literature reveals that the finite μ results can be described more consistently by adding the repulsive vector interaction, which has been neglected in the construction of the model. The way the vector interaction should be added has been introduced in the neutron star chapter 7.
- It also reveals that the baryons make a large contribution to the pressure at low temperature and finite chemical potential, to build a reasonable hadronic equation of state. To describe the nuclear phase, PNJL should also include baryons, and this should also apply to the heavy ion collision study.
- Even though the pressure and its first order derivatives are in agreement with the lattice results, very sensible observables like the speed of sound show differences. The chiral transition remains higher than the lattice results. The beyond mean field study does not include all the mesons and at least vector mesons and η mesons should be included in the contribution to the pressure to better describe this transition.
- The gap equations are not calculated beyond mean field. A consistent model should treat the pressure and the masses on the same level of approximation, which should also improve the description of the chiral transition mentioned above.

8.A Vector mesons

For vector mesons, the procedure is the same as in the scalar or pseudoscalar case, but the coupling is now γ_μ. The consequence is that the polarisation function is not scalar anymore but depends on the index μ and ν: $\Pi_{\mu\nu}$.

To determine the bound state equation which gives the mass, the current conservation equations are used [166]:

$$p_\mu \Pi^{\mu\nu} = 0 \tag{8.A.1}$$
$$p_\nu \Pi^{\mu\nu} = 0 \tag{8.A.2}$$

The polarisation function can be separated in a longitudinal part and transverse part:

$$L^{\mu\nu} = \frac{p^\mu p^\nu}{p^2} \tag{8.A.3}$$

$$T^{\mu\nu} = g_{\mu\nu} - \frac{p^\mu p^\nu}{p^2}. \tag{8.A.4}$$

The longitudinal part is chosen such that the scalar product $L^{\mu\nu}T_{\mu\nu}$ is orthogonal. $\Pi^{\mu\nu}$ is only function of the transverse part [167]:

$$\Pi^{\mu\nu} = T^{\mu\nu}\Pi_V \tag{8.A.5}$$

which means:

$$\Pi_V = \frac{\Pi^{\mu\nu}}{T^{\mu\nu}} = \frac{\Pi^{\mu\nu}g_{\mu\nu}}{T^{\mu\nu}g_{\mu\nu}} = \frac{1}{3}\Pi^{\mu\nu}g_{\mu\nu} \tag{8.A.6}$$

The polarisation Π_V does not have an index anymore and can be calculated as in the scalar and pseudoscalar case. The axial case is more complicated as coupling between axial and pseudoscalar modes must be taken into account [167]

8.B Baryons

The NJL literature provides the construction of the baryons based on a quark-diquark bound state. The Bethe-Salpeter equation used to build the mesons has to be slightly modified to be of use to describe the diquarks. In addition, the symmetries of the baryons bring several constraints on the diquark quantum numbers which can be used to make the bound state. This is where the Young diagrams formalism reveals to be a powerful tool to simplify the study.

8.B.1 Diquarks

The quark-quark bound state is constructed following the procedure of the quark-antiquark bound state. However, the antiquark in the quark-antiquark interaction must be replaced by its equivalent [168]:

$$\bar{q} = q^T C^{-1} \tag{8.B.1}$$

where the charge conjugaison Eq. 2.C.5 is performed on the quark such that Lorentz invariance is preserved. As for the mesons, the polarisation function must be calculated and is given by [83]:

$$\begin{aligned}\Pi^S_{ff'}(k_0, \vec{k}) = &-\frac{1}{\pi^2}[A(m,\mu,T) + A(m',\mu',T) \\ &+ [(m_f - m_{f'})^2 - (k_0 + \mu_f - \mu_{f'})^2 + \vec{k}^2]B_0(\vec{k}, m, \mu, m', \mu', k_0)]\end{aligned} \tag{8.B.2}$$

The coupling is [83]:

$$G_{Diq} = \frac{3}{4}G, \tag{8.B.3}$$

given by the Fierz transformations. The diquark must also be build such that the baryon to which it will give birth respects all the symmetries that it should. The baryon being a color neutral object. It is then required to be in the singlet irreducible representation of the $q \otimes q$ color space. Young diagrams gives the irreps of this product of tensor. According to Eq. 1.D.17, the antitriplet is the irrep leading to a singlet color baryon. The color is then in an antisymmetric representation.

In addition, the Pauli principle requires the baryon wavefunction to be antisymmetric under the exchange of any two quarks. As a consequence, the diquark needs to be in an overall antisymmetric tensorial product of representations. The color being in the antisymmetric irrep, the flavour-Dirac representation must be fully symmetric. According to Eq. 1.D.12, The flavour space can be in the antitriplet representation or in the sextet representation. The antitriplet leading to the octet of baryons and the sextet leading to the decuplet of baryons. A symmetric representation of the Dirac space will go with the sextet of flavour to build the decuplet of baryon and a antisymmetric representation of the Dirac space will go with the antitriplet of flavour to build the octet of baryons. Simply by symmetry consideration, the baryons must obey the table 8.1, [168, 83].

Interaction	color	flavour	Dirac
Scalar	$\bar{3}$	$\bar{3}$	0^+_A
Pseudoscalar	$\bar{3}$	$\bar{3}$	0^-_A
Vector	$\bar{3}$	$\bar{3}$	1^-_A
Axial	$\bar{3}$	6	1^+_S

Table 8.1: Summary of the symmetries to respect when building the baryons

The mass of the diquarks obtained are displayed in Fig.8.1.

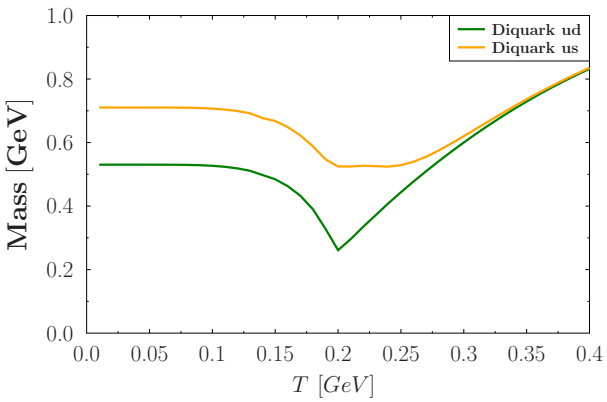

Fig. 8.1: Masses of the diquarks ud and us

8.B.2 Baryons

The advantage of using a quark-diquark bound state to build the baryons is that it allows for using the same equation than for the mesons. However, there is no free lunch and the price that must be paid is a quark exchange.

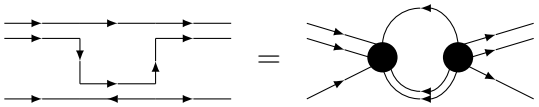

(8.B.4)

In the static approximation, the bound state equation is very similar to the mesons case [116]:

$$U(k^2) = \frac{2G_{q-D}^2}{1 + 4\frac{G_{q-D}^2}{m_q}\Pi(k^2)}. \tag{8.B.5}$$

The coupling constant is, however, different as it is now a quark-diquark coupling constant instead of the NJL interaction vertex. It is given by [116]:

$$\sqrt{\frac{4m}{\frac{\partial\Pi(k_0,0)}{\partial k_0}}} \tag{8.B.6}$$

In addition the division by the mass of the exchanged quark reminds the presence of the static approximation. The polarisation function is also more complicated [116]:

$$\begin{aligned}\Pi = 4m(\int \frac{p^2dp}{2\pi^2}\Bigg(&\frac{1}{2E_D}\frac{f_{BE}(T,-E_D)}{(-E_q-E_D+k0)(E_q-E_D+k0)} \\ &- \frac{1}{2E_D}\frac{f_{BE}(T,E_D)}{(-E_q+E_D+k0)(E_q+E_D+k0)} + \frac{1}{2E_q}\frac{f_{FD}(T,E_q)}{(-E_q+E_D+k0)(-E_q-E_D+k0)} \\ &- \frac{1}{2E_q}\frac{f_{FD}(T,-E_q)}{(E_q+E_D+k0)(E_q-E_D+k0)}\Bigg).\end{aligned} \tag{8.B.7}$$

The mass obtained is displayed in Fig 8.2.

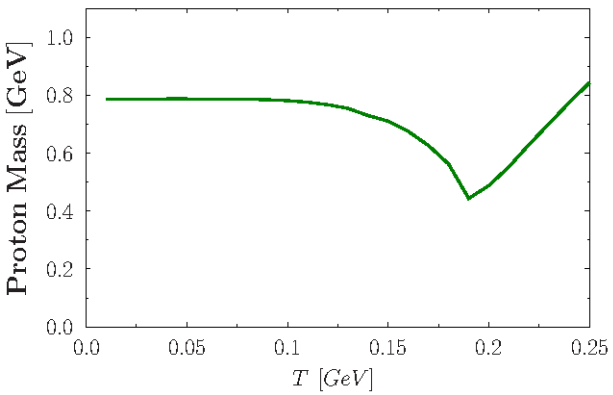

Fig. 8.2: Masses of the proton

The inconvenience of such an approach is that the static approximation, for which the mass of the quark must be large compared to the momentum, stops being valid when the mass of the quarks decreases, ie from $T \sim 0.2\ GeV$. The phase transition cannot be studied with this formalism. A solution to cure this weakness would be to include more diagrams in the quark diquark interaction.

Indeed, the Eq.8.B.4 comes from the resummation of all the possible diagrams of gluon exchange between three quarks. The diquark bound state include all the diagrams of the type:

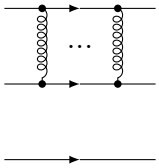

(8.B.8)

and the quark-diquark bound state with a quark exchange includes in addition all the diagrams of the form:

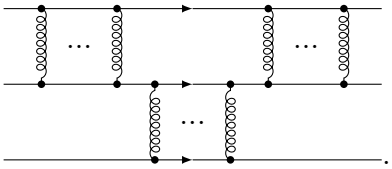

(8.B.9)

But they do not present all the possible diagrams. More should be taken into consideration like the three quark diagram:

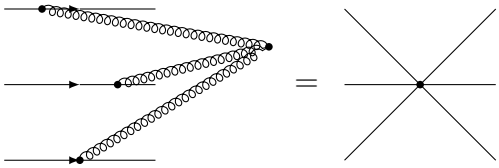

(8.B.10)

The three quark vertex is complicated to evaluate at it requires the calculation of a three quark polarisation function. The 6-quarks vertex is also not completely part of the Lagrangian as the 't Hooft Lagrangian includes a mixing of the three flavour when only two are present here. To include it, one might need to look for an additional term in the NJL Lagrangian that leaves all the symmetries of the model unbroken.

One can see in Fig 8.2 that the mass of the proton is not 0.938 GeV at 0 T and μ as it should be to agree with the experimental value. In general, what is done in the literature is a modification of the coupling constant Eq. 8.B.3 to obtain 0.938 GeV by considering the coefficient coming from the Fierz transformation, Eq. 8.B.3, as a free parameter. This coefficient is then fitted to reach $m_p = 0.938\ GeV$ [83]. This is however a freedom which is taken and the addition of more diagrams could also help to agree with the experimental result in a more natural way. Adding more diagrams in the calculation of the baryons is a perspective into what could be done in order to reach a better description of the three quark bound state, but more time are needed to perform all the necessary and complicated calculations.

8.C Vector interaction

In the NJL model described previously, from the Fierz transformation of the lagrangian, only the scalar and pseudoscalar interaction are taken into account. The vector and axial interactions should also be considered in the NJL model.

In the mean field approximation, the scalar interaction gives birth to the chiral condensate. The fact that the coupling is scalar implies that it couples to the mass which is also scalar. In the case of vector interaction, the coupling is γ_μ and it couples to the quadrivector p_μ. Howevere, the literature agrees on the fact that only the change in energy is important for the thermodynamics of the system and the vector condensate couples with γ_0 to the energy [11]. The chemical potential also couples to the energy with γ_0 and the vector interaction induces a change in the chemical potential value:

$$\bar{\mu} = \mu + 4G_v\langle\langle\psi^\dagger\psi\rangle\rangle \tag{8.C.1}$$

where:

$$\langle\langle\psi^\dagger\psi\rangle\rangle = \frac{N_C}{\pi^2}\int_0^{10\Lambda} dpp^2[f(E-\bar{\mu}_q,T) - f(E+\bar{\mu}_q,T)] \tag{8.C.2}$$

with $G_V = -\frac{1}{2}G$, given by the Fierz transformation. One can see from Eq. 8.C.1, that the vector interaction shifts the chemical potential.

Conclusion

This work presents several improvements and studies of the Nambu-Jona-Lasinio model and its Polyakov extension. These lead to a better description of the QCD at low energy and to many future possibilities to improve even more the model.

This achievement is due to a better PNJL equation of state. By considering beyond mean field contributions to the pressure, mesons give a non negligible contribution at low temperature and in the mixed phase. Including a re-parametrisation of the model in the QGP phase, the improved PNJL equation of state agrees with lattice results. At large chemical potential, the improved PNJL equation of state presents a Critical End Point and a first order phase transition and is in agreement with the pQCD results.

The study of the influence of the cut off in the calculation of the internal loops has lead to a better description of the transport coefficient at $\mu = 0$ and more trustful predictions at finite chemical potential. In particular, the shear viscosity over entropy ratio transport coefficient does not go beyond the KSS limit, considered has a real problem in the previous NJL calculations. This result also comes from the successful entropy matching with lattice results.

By inverting and implementing the PNJL equation of state obtained into the event generator EPOS, we study the hydrodynamical evolution of an expanding QGP near a first order phase transition. The cross over evolves to a first order phase transition for lower and lower beam energies only in the case of the PNJL equation of state. The ratio of identified hadrons production using the PNJL equation over the identified hadron production using the EPOS equation of state is globally higher for energy beam $\sqrt{s} = 14.5\ GeV$ than for energy beam $\sqrt{s} = 19.6\ GeV$. In particular, the high p_t proton production is higher with the PNJL equation of state than with the EPOS equation of state at $\sqrt{s} = 14.5\ GeV$.

In order to reach a better understanding of the physics of the strong interaction at large densities and low temperatures as encountered in neutron stars, a standard NJL model is used to determine a zero temperature and large chemical potential equation of state. This equation of state is needed to solve the Tolman-Oppenheimer-Volkoff equation and to determine the mass-radius relation of neutron stars. This study emphasises the need to add a baryonic contribution to the thermodynamic pressure of the NJL model at finite chemical potential and low temperature in order to be able to describe the hadronic phase. The baryonic pressure should also be added to our equation of state devoted to the heavy ion collision domain even though its contribution is expected to be less significant. To obtain a better description of the baryons within the PNJL model, more diagrams should be added in the calculation of the bound states equation to get closer to the

experimental values.

In order to obtain larger mass values for the neutron star, the repulsive vector interaction should also be added. This would be another features to add to equation of state and could modify the localisation and even the existence of our CEP and first order phase transition in the PNJL phase diagram.

This work leaves many possible way of improving the PNJL model in order to reach a consistent description of the physics of the strong interaction at low energy. It shows that by adding the baryons, the vector interaction and beyond mean field corrections, one can access a good description for neutron stars as well as for medium energy heavy ion reactions, though I had not the time to perform all the necessary and complicated calculations.

Résumé en français

Dans une optique de compréhension de la matière à l'échelle la plus fondamentale, le Modèle Standard regroupe trois des quatre interactions fondamentales de la physique : l'électromagnétisme, l'interaction faible et l'interaction forte. Si l'électromagnétisme, décrite théoriquement par la théorie de l'électrodynamique quantique, semble établie grâce à la puissance des calculs perturbatifs du fait que la constante de couplage est faible, l'étude de l'interaction forte, quand à elle, est loin d'être maîtrisée et reste un domaine en plein essor. Le domaine de l'interaction forte et la théorie de jauge $\mathrm{SU}(N_C = 3)$ associée, la ChromoDynamique Quantique, décrit les interactions de couleur entre les quarks et les gluons. Les quarks et les gluons ne sont jamais observables expérimentalement, comme état asymptotique. De manière générale, tout état coloré n'est pas observable. Seuls les états neutres en couleurs, les hadrons, comme les baryons (protons, neutrons) et les mésons (pions, kaons) le sont : c'est la propriété de confinement. A haute température ou potentiel chimique, les calculs perturbatifs prédisent que la constante de l'interaction forte devient faible et que la matière hadronique se déconfine en un plasma de quarks et de gluons. Le défi de la ChromoDynamique Quantique est que la constante de couplage de l'interaction forte est haute théorie à basse température et potentiel chimique et les méthodes perturbatives ayant déjà fait leur preuve pour l'électromagnétisme ne peuvent pas être utilisées. Dans ces conditions intervient la ChromoDynamique Quantique sur réseau qui est une théorie non perturbative consistant à discrétiser l'espace-temps sur un réseau et permettant d'étudier l'interaction forte à basse température. Elle n'est en revanche pas utilisable à potentiel chimique fini à cause du célèbre problème du signe. Dans ses conditions, des modèles effectifs approximant la ChromoDynamique Quantique sont utilisés pour étudier la ChromoDynamique Quantique à températures et potentiels chimiques finis et mieux comprendre le diagramme de phase de la ChromoDynamique Quantique. Ces modèles sont particulièrement importants afin de réaliser des prédictions théoriques permettant d'aider les expériences à contraindre les régions expérimentalement intéressantes. Ces prédictions ne sont que quantitatives compte tenu des approximations faites en amont mais peuvent permettre de déterminer ou tout au moins de donner une idée des énergies de collision permettant de reproduire les conditions expérimentales pour observer le possible point critique de la ChromoDynamique Quantique ainsi que les observables permettant de le détecter et le comportement attendu.

Cette thèse présente une étude d'un modèle effectif, le modèle de Polyakov-Nambu-Jona-Lasinio permettant de déterminer qualitativement le diagramme de phase de la matière interagissant fortement à basse température et potentiel chimique fini. Le modèle

de Polyakov-Nambu-Jona-Lasinio est un modèle dont les degrés de liberté sont les quarks. Les gluons sont gelés, approximation de la ChromoDynamique Quantique permettant de simplifier les équations à basses températures et potentiels chimiques finies. L'ajout d'un couplage minimal à la boucle de Polyakov permettant de rétablir un confinement approximatif (il n'existe pas à l'heure actuelle de théorie du confinement en tant que telle) en supprimant les quarks à basse température et potentiel chimique. D'autres modèles effectifs existent comme le modèle sigma (linéaire et non linéaire) ou le modèle des Quasi-Particules Dynamiques ou le modèle des Quarks et Mésons. Si le modèle NJL n'est pas reconnu comme étant une théorie effective constamment améliorable en allant chercher des corrections aux ordres supérieurs, il présente tout de même certains avantages. Ces avantages sont qu'il repose sur une densité Lagrangienne partageant à approximativement les symmétries que la densité Lagrangienne de la ChromoDynamique Quantique: la symmétrie chirale (la densité Lagrangienne peut être sous-divisé en deux densités Lagrangienne: une pour les particules droitières, une pour les particules gauchères, la symmétrie de saveur (pour les quarks légers: u, d, s), la symmétrie de couleur qui est globale dans NJL. La symmétrie de couleur est locale dans le Lagrangien ChromoDynamique Quantique et se traduit par l'échange de gluons entre quarks. Un autre avantage est le fait que les degrés de liberté de Nambu-Jona-Lasinio soient les quarks et les antiquarks. Beaucoup de modèles effectifs pour la basse énergie ont des degrés de liberté hadroniques et ne décrivent pas les quarks.

La première partie de cette thèse présente les outils mathématiques utilisés tout au long de ces travaux:

- Les birdtracks. C'est une formulation diagrammatique de la théorie des groupes permettant d'introduire notamment la transformation de Fierz dans les espaces de couleur/saveur et de Dirac. Ce formalisme permet aussi de recalculer les coefficients de Fierz avec une méthode élégante.

- Les diagrammes de Young. C'est un outil d'utilité notoire pour réaliser des décompositions de produit tensoriel en représentations irréductibles qui interviennent dans l'étude des états liés comme les diquark et les baryons et en particulier de déterminer les dimensions des représentation irréductibles et si elles sont symmétriques ou antisymmétriques. Ce formalisme peut être relié aux Birdtracks et aux opérateur symmetriques et anti-symmetrique.

- Des rappels de formules importantes de thermodynamique et théorie des champs à température finie qui seront réutilisés pour la détermination d'une équation d'état de la matière interagissante fortement.

La deuxième partie consiste en un résumé de la théorie ChromoDynamique Quantique et des applications des modèles Nambu-Jona-Lasinio et Polyakov-Nambu-Jona-Lasinio pour le calcul de la masse des quarks, des mésons et du diagramme de phase de la ChromoDynamique Quantique. Cette section présente un état de l'art du domaine permettant de saisir les enjeux des résultats de cette thèse. Différents aspects de la ChromoDynamique Quantique sont évoqués, sa densité Lagrangienne et ses symmétries sont tout d'abord présentés. Viennent ensuite les différents outils d'étude de cette densité Lagrangienne. L'approche perturbative, basée sur un développement de l'interaction en

puissance de la constante de couplage, fait intervenir des boucles internes aux ordres supérieurs nécessitant des intégrales divergentes. Une renormalisation de la théorie est donc nécessaires pour se jouer de ces divergences et impliquent un running de certaines grandeurs telles que la constante de couplage de l'interaction forte. La constante devient fonction de l'échelle d'énergie. Elle est faible pour les transferts d'impulsions élevés, c'est la liberté asymptotiques mais présentent un pôle de Landau à bas transfert d'énergie. La généralisation des méthodes perturbatives à températures et potentiels chimiques finies est évoquée, avec une courte présentation du formalisme boucles thermiques dures et des boucles denses dures. La ChromoDynamique Quantique devient non perturbative à partir d'une certaine échelle donnée par Λ_{QCD}. La chromodynamique quantique sur réseau est alors présentée et une attention est portée sur les prédictions faites par cette théorie quand à l'equétion d'état de la matière interagissant fortement à potentiel chimique nul. Enfin, les aspects expérimentaux du plasma de quarks et gluons sont présentés. Les sondes molles et dures permettant d'observer indirectement si le plasma a été créé lors de la collision d'ions lourds ou pas. Les expériences enregistrant ces observables sont aussi présentées en insistant particulièrement sur les expériences à basse énergie explorant la partie du diagramme de phase à potentiel chimique fini, leur programmes et les détecteurs utilisés ainsi que leur spécificité. Les accélérateurs sont aussi présentés et leur avantages techniques les uns par rapport aux autres sont discutés. Enfin le modèle de Nambu-Jona-Lasinio et l'extension de Polyakov sont présentés. Les piliers du modèle: la construction de la densité Lagrangienne à partir des symmétries, les équations de gap déterminant la masse des quarks, l'approximation du champs moyen et le grand potentiel sont expliqués. Des premiers résultats, état de l'art de ce que peut faire le modèle sont présentés. La construction des mésons est aussi expliquée en détails. Le diagramme de phase standard obtenu avec ce modèle est détaillé afin de mieux comprendre qu'elles sont les enjeux et les progrès possibles à faire sur ce modèle.

L'avant dernière partie présente les différents résultats phénoménologiques obtenus pendant ses trois années de thèse partagés sur quatre chapitres. Afin d'améliorer la qualité des prédictions, le modèle est poussé au-delà du champ moyen, incluant les contributions mésoniques à la pression du système et reparamétriser afin de décrire une transition confinement-déconfinement tenant compte phénoménologiquement de la présence des quarks dans le milieu. Certains degrés de liberté mésoniques sont donc naturellement inclus dans la fonction de partition. Cette correction du modèle de Nambu-Jona-Lasinio standard permet de corriger la pression à basse température. Le couplage avec la boucle de Polyakov supprime les quarks à basse température et potentiel chimique laissant une pression totale non nulle. La prise en compte naturelle d'une pression mésonique permet de retrouver une pression dans la phase hadronique. La correction du potentiel effectif du modèle de Polyakov-Nambu-Jona-Lasinio en prenant en compte la présence de quarks dans le milieu de façon phénoménologique permet quand à elle de corriger la pression à plus haute température. L'équation d'état qui en découle est en accord avec les résultats de la ChromoDynamique Quantique sur réseau concernant la pression et la première dérivée du grand potentiel. Elle est aussi en accord avec les résultats de ChromoDynamique Quantique perturbative à haute température et haut potentiel chimique. Le diagramme de phase obtenu présente un point critique et une transition du premier ordre. La comparaison de la ligne critique avec la ligne de freeze-out, à partir de laque-

lle les cellules d'hydrodynamique sont converties en particules, calculée par les modèles statistiques attestent de la possibilité d'étudier expérimentalement ces lignes critiques de transition de phase du diagramme de phase.

Les résultats obtenus sont utilisés dans le cadre d'applications pratiques tels que le calcul des coefficients de transport du Plasma de Quarks et de Gluons, ici la viscosité de cisaillement et la conductivité électrique. A partir du modèle amélioré pour déterminer l'équation d'état, les sections efficaces élastiques quark-quark et quark-antiquark sont calculés à température et potentiel chimique finie. Elles servent de base pour obtenir les coefficients de transport déterminés à partir de l'équation de Boltzmann dont le terme de collision est simplifié par l'approximation du temps de relaxation. La viscosité de cisaillement est particulièrement importante dans l'évolution hydrodynamique décrivant généralement l'expansion du plasma dans scénario théorique visant la description d'une collision d'ion lourd. La conductivité électrique informe sur le transport des charges dans le plasma. Grâce aux améliorations faites sur le modèle Polyakov-Nambu-Jona-Lasinio, les sections efficaces sont mieux calculées et la viscosité de cisaillement ne descend plus au-dessous de la limite de Kovtun-Son-Starinets, limite minimal de viscosité de cisaillement calculée par les modèles supersymmétriques pour un plasma très fortement couplé. Les résultats pour la viscosité de cisaillement et la conductivité électrique sont en accord avec les prédictions de la ChromoDynamique Quantique sur réseau à potentiel chimique nul. A potentiel chimique fini, les prédictions du modèle de Polyakov-Nambu-Jona-Lasinio présentent des coefficients de transport qui augmentent largement et présentent une discontinuité à très haut potentiel chimique, caractéristique d'une transition du première ordre.

Cette expansion hydrodynamique du plasma est aussi étudiée du fait qu'elle utilise une équation d'état. Elle permet une étude dynamique de l'influence d'une transition de phase du première ordre lors des collisions d'ions lourds. Grâce au générateur d'évènement EPOS développé à Subatech, la production de hadrons (pion, kaon, proton) prédite par simulation EPOS utilisant une équation d'état ayant un crossover sur l'ensemble du diagramme de phase comparée à une simulation EPOS avec l'équation d'état Polyakov-Nambu-Jona-Lasinio qui a un point critique et une transition du premier ordre à haut potentiel chimique permet de comprendre l'influence de la criticité de l'équation d'état sur la dynamique du plasma de quarks et de gluons. La conséquence observée est une augmentation des particules baryonique produites à haute impulsion transverse ainsi que des pions lorsque l'énergie de collision décroit, en utilisant l'équation d'état du modèle de Polyakov-Nambu-Jona-Lasinio contenant une transition du premier ordre et un point critique par rapport à la simulation utilisant l'équation d'état de EPOS qui n'a qu'un cross over sur tout le diagramme de phase. Cette différence n'est pas noté pour les particules étranges, mésons et baryons, pour lesquelles le ratio entre le résultat obtenu en utilisant l'équation d'état du modèle de Polyakov-Nambu-Jona-Lasinio et le résultat obtenu en utilisant l'équation d'état d'EPOS est sensiblement similaire.

L'étude de la relation masse-rayon des étoiles à neutron est aussi étudiée car impliquant l'utilisation d'une équation d'état utilisant des conditions de relation entre potentiel chimique des quarks u, d et s différentes. L'intérêt du modèle Nambu-Jona-Lasinio dans la description des étoiles à neutron est de pouvoir décrire des étoiles qui ne sont plus nucléaire mais où les quarks sont déconfinés du fait de la présence fantastique exercée. Ce

travail permet de mieux comprendre en quoi l'équation d'état peut être encore améliorer, notamment par l'ajout des baryons, contribution non négligeable à la thermodynamique du milieu à basse température et densité finie et du terme d'interaction vectorielle issu de la transformation de Fierz et non considéré de manière général dans l'ensemble de cette thèse. Ce travail sur les étoiles à neutron indique que l'interaction vectorielle joue un rôle répulsif important à potentiel chimique fini.

Enfin un chapitre de perspectives est présenté proposant plusieurs possibilité d'amélioration du modèle. Cette perspective explique comment ajouter l'interaction vectorielle, ajouter les diquarks et les baryons construits à partir de l'état lié quark-diquark et propose de considérer des diagrammes quark-quark-quark comme proposition pour améliorer la description des baryons. Les mésons vecteurs et axiaux sont abordés.

Bibliography

[1] Predrag Cvitanovic : *Group theory: Birdtracks, Lie's and exceptional groups*. 2008.

[2] Stefan Keppeler : Birdtracks for SU(N). *In QCD Master Class 2017*, 7 2017.

[3] Florian Cougoulic : *Nuclear effects in high-energy proton-nucleus collisions : transverse momentum broadening of energetic parton systems and soft anomalous dimension matrices*. Thèse de doctorat, Laboratoire de physique subatomique et des technologies associées, France, 2018.

[4] Michael E. Peskin et Daniel V. Schroeder : *An Introduction to quantum field theory*. Addison-Wesley, Reading, USA, 1995.

[5] B. Diu : *Physique Statistique*. Hermann, 2001.

[6] Renato Critelli, Jorge Noronha, Jacquelyn Noronha-Hostler, Israel Portillo, Claudia Ratti et Romulo Rougemont : Critical point in the phase diagram of primordial quark-gluon matter from black hole physics. *Phys. Rev. D*, 96(9):096026, 2017.

[7] Benjamin Svetitsky et Laurence G. Yaffe : Critical Behavior at Finite Temperature Confinement Transitions. *Nucl. Phys. B*, 210:423–447, 1982.

[8] Michael Oleszczuk et Janos Polonyi : Canonical versus grand canonical ensemble in QCD. 9 1992.

[9] J. Polonyi et K. Szlachanyi : Phase Transition from Strong Coupling Expansion. *Phys. Lett. B*, 110:395–398, 1982.

[10] Michel Le Bellac : *Thermal Field Theory*. Cambridge Monographs on Mathematical Physics. Cambridge University Press, 3 2011.

[11] R. Nebauer : *Proprietes Des Quarks Et Mesons A Temperature Et Densites Finies Dans Le Cadre Du Modele Njl*. Thèse de doctorat, Nantes U., 2000.

[12] The standard model. https://home.cern/science/physics/standard-model.

[13] S. Schael *et al.* : Precision electroweak measurements on the Z resonance. *Phys. Rept.*, 427:257–454, 2006.

[14] Roel Aaij *et al.* : Observation of $J/\psi p$ Resonances Consistent with Pentaquark States in $\Lambda_b^0 \to J/\psi K^- p$ Decays. *Phys. Rev. Lett.*, 115:072001, 2015.

[15] Francesco Giacosa : Heavy Glueballs: Status and Large-N_c Widths Estimate. *Acta Phys. Polon. Supp.*, 10:1021–1027, 2017.

[16] R.Keith Ellis, W.James Stirling et B.R. Webber : *QCD and collider physics*, volume 8. Cambridge University Press, 2 2011.

[17] Goran Senjanovic et Vladimir Tello : Strong CP violation: problem or blessing? 4 2020.

[18] Jack Dragos, Thomas Luu, Andrea Shindler, Jordy de Vries et Ahmed Yousif : Confirming the Existence of the strong CP Problem in Lattice QCD with the Gradient Flow. 2 2019.

[19] Murray Gell-Mann : A Schematic Model of Baryons and Mesons. *Phys. Lett.*, 8:214–215, 1964.

[20] R. Marty : *Simulation de l'expansion et la transition de phase d'un plasma de quarks et d'antiquarks, university of Nantes.* Thèse de doctorat, 2012.

[21] Steven D. Bass et Pawel Moskal : η and η mesons with connection to anomalous glue. *Rev. Mod. Phys.*, 91(1):015003, 2019.

[22] The dirac equation. http://www.damtp.cam.ac.uk/user/dt281/qft/four.pdf.

[23] The dirac equation. http:www.physics.ucc.ie/apeer/PY4106/Dirac_Equation.pdf.

[24] Tom Banks et A. Casher : Chiral Symmetry Breaking in Confining Theories. *Nucl. Phys. B*, 169:103–125, 1980.

[25] Andrei V. Smilga : *Lectures on quantum chromodynamics.* WSP, Singapore, 2001.

[26] Andrei V. Smilga et J. Stern : On the spectral density of Euclidean Dirac operator in QCD. *Phys. Lett. B*, 318:531–536, 1993.

[27] Alexandre Deur, Stanley J. Brodsky et Guy F. de Teramond : The QCD Running Coupling. *Prog. Part. Nucl. Phys.*, 90:1–74, 2016.

[28] H. Georgi : A Modern view of hadrons. *NATO Sci. Ser. B*, 351:1–42, 1995.

[29] H. Hansen, W. M. Alberico, A. Beraudo, A. Molinari, M. Nardi et C. Ratti : Mesonic correlation functions at finite temperature and density in the Nambu-Jona-Lasinio model with a Polyakov loop. *Phys. Rev.*, D75:065004, 2007.

[30] Gerard 't Hooft, C. Itzykson, A. Jaffe, H. Lehmann, P.K. Mitter, I.M. Singer et R. Stora, éditeurs. *Recent Developments in Gauge Theories. Proceedings, Nato Advanced Study Institute, Cargese, France, August 26 - September 8, 1979*, volume 59, 1980.

[31] Szabocls Borsanyi, Zoltan Fodor, Christian Hoelbling, Sandor D. Katz, Stefan Krieg et Kalman K. Szabo : Full result for the QCD equation of state with 2+1 flavors. *Phys. Lett. B*, 730:99–104, 2014.

[32] Philippe de Forcrand et Massimo D'Elia : Continuum limit and universality of the Columbia plot. *PoS*, LATTICE2016:081, 2017.

[33] Robert D. Pisarski et Frank Wilczek : Remarks on the Chiral Phase Transition in Chromodynamics. *Phys. Rev. D*, 29:338–341, 1984.

[34] Yuri L. Dokshitzer, Valery A. Khoze, Alfred H. Mueller et S.I. Troian : *Basics of perturbative QCD*. 1991.

[35] J.I. Kapusta et Charles Gale : *Finite-temperature field theory: Principles and applications*. Cambridge Monographs on Mathematical Physics. Cambridge University Press, 2011.

[36] Eric Braaten et Robert D. Pisarski : Soft Amplitudes in Hot Gauge Theories: A General Analysis. *Nucl. Phys. B*, 337:569–634, 1990.

[37] F.M. Steffens : The Temperature dependence of the QCD running coupling. *Braz. J. Phys.*, 36:582–585, 2006.

[38] R.A. Schneider : The QCD running coupling at finite temperature and density. 3 2003.

[39] Craig D. Roberts : Strong QCD and Dyson-Schwinger Equations. *IRMA Lect. Math. Theor. Phys.*, 21:355–458, 2015.

[40] N. Dupuis, L. Canet, A. Eichhorn, W. Metzner, J.M. Pawlowski, M. Tissier et N. Wschebor : The nonperturbative functional renormalization group and its applications. 6 2020.

[41] Gert Aarts : Introductory lectures on lattice QCD at nonzero baryon number. *J. Phys. Conf. Ser.*, 706(2):022004, 2016.

[42] Rajan Gupta : Introduction to lattice QCD: Course. *In Les Houches Summer School in Theoretical Physics, Session 68: Probing the Standard Model of Particle Interactions*, pages 83–219, 7 1997.

[43] Pierre Moreau : *Dynamical description of relativistic heavy-ion collisions out-of equilibrium*. Thèse de doctorat, Goethe U., Frankfurt (main), 2019.

[44] C. Davies, G. Batrouni, G. Katz, P. Lepage, P. Rossi, K. Wilson, Andreas S. Kronfeld et B. Svetitsky : Langevin simulations of lattice field theories using Fourier acceleration. *J. Statist. Phys.*, 43:1073–1075, 1986.

[45] Daniel Harlow, Jonathan Maltz et Edward Witten : Analytic Continuation of Liouville Theory. *JHEP*, 12:071, 2011.

[46] A. Bazavov *et al.* [HotQCD Collaboration] : Equation of state in (2+1)-flavor qcd. 2014.

[47] Szabolcs Borsanyi, Gergely Endrodi, Zoltan Fodor, Antal Jakovac, Sandor D. Katz, Stefan Krieg, Claudia Ratti et Kalman K. Szabo : The qcd equation of state with dynamical quarks. 2010.

[48] T.D. Lee et G.C. Wick : Vacuum Stability and Vacuum Excitation in a Spin 0 Field Theory. *Phys. Rev. D*, 9:2291–2316, 1974.

[49] H.A. Grunder, C.W. Leemann et F.B. Selph : Relativistic Heavy Ion Accelerators. *In 10th International Conference on High-Energy Accelerators*, pages 321–338, 1977.

[50] Mark G. Alford, Andreas Schmitt, Krishna Rajagopal et Thomas Schäfer : Color superconductivity in dense quark matter. *Rev. Mod. Phys.*, 80:1455–1515, 2008.

[51] Andreas Schmitt : *Dense matter in compact stars: A pedagogical introduction*, volume 811. 2010.

[52] Pavel Buividovich, Mikhail Polikarpov et Oleg Teryaev : Experimental signatures of superstrong magnetic fields in heavy-ion collisions. *In 15th Lomonosov Conference on Elementary Particle Physics*, pages 367–373, 2013.

[53] G. Agakishiev *et al.* : Strangeness Enhancement in Cu+Cu and Au+Au Collisions at $\sqrt{s_{NN}} = 200$ GeV. *Phys. Rev. Lett.*, 108:072301, 2012.

[54] Gabriel Sophys : *Formation of a Quark-Gluon-Plasma : understanding the energy and system size dependence.* Thèse de doctorat, Laboratoire de physique subatomique et des technologies associées, France, 2018s.

[55] Mingliang Zhou : Observation of long-range elliptic anisotropies in $\sqrt{s}$=13 and 2.76 TeV pp collisions with the ATLAS detector. *Nucl. Phys. A*, 956:769–772, 2016.

[56] Gabor David : Direct real photons in relativistic heavy ion collisions. *Rept. Prog. Phys.*, 83(4):046301, 2020.

[57] Chun Shen, Ulrich Heinz, Jean-Fran çois Paquet et Charles Gale : Thermal photons as a quark-gluon plasma thermometer reexamined. *Phys. Rev. C*, 89:044910, Apr 2014.

[58] Erwann Masson : *Mesure de la production de photons isoles dans les collisions proton-proton et proton-plomb au LHC avec l'experience ALICE.* Thèse de doctorat, SUBATECH, Nantes, 2019.

[59] A. Andronic *et al.* : Heavy-flavour and quarkonium production in the LHC era: from proton–proton to heavy-ion collisions. *Eur. Phys. J. C*, 76(3):107, 2016.

[60] Roland Katz : *A quantum approach to dynamical quarkonia suppression in high energy heavy ion collisions.* Thèse de doctorat, SUBATECH, Nantes, 2015.

[61] Georges Aad *et al.* : Observation of a new particle in the search for the Standard Model Higgs boson with the ATLAS detector at the LHC. *Phys. Lett. B*, 716:1–29, 2012.

[62] N. Abgrall *et al.* : NA61/SHINE facility at the CERN SPS: beams and detector system. *JINST*, 9:P06005, 2014.

[63] Nikolaos Davis : Searching for the critical point of strongly interacting matter in nucleus-nucleus collisions at CERN SPS. 2 2020.

[64] Maja Mackowiak-Pawlowska : NA61/SHINE results on fluctuations and correlations at CERN SPS energies. *In 28th International Conference on Ultrarelativistic Nucleus-Nucleus Collisions*, 2 2020.

[65] Grazyna Odyniec : The RHIC Beam Energy Scan program in STAR and what's next ... *J. Phys. Conf. Ser.*, 455:012037, 2013.

[66] Grazyna Odyniec : RHIC Beam Energy Scan Program: Phase I and II. *PoS*, CPOD2013:043, 2013.

[67] Qian Yang : The STAR BES-II and Forward Rapidity Physics and Upgrades. *Nucl. Phys. A*, 982:951–954, 2019.

[68] An international accelerator facility for beams of ions and anti-protons. Conceptual design report. 11 2001.

[69] Peter Senger : Probing dense QCD matter in the laboratory: The CBM experiment at FAIR. *Phys. Scripta*, 95(7):074003, 2020.

[70] T. Ablyazimov *et al.* : Challenges in QCD matter physics –The scientific programme of the Compressed Baryonic Matter experiment at FAIR. *Eur. Phys. J. A*, 53(3):60, 2017.

[71] Evgeny Syresin *et al.* : NICA Accelerator Complex at JINR. *In 10th International Particle Accelerator Conference*, page MOPMP014, 2019.

[72] Mikhail Kapishin : Studies of baryonic matter in the BM@N and MPD experiments at Nuclotron/NICA. *PoS*, CORFU2018:188, 2019.

[73] Anton Motornenko, Jan Steinheimer, Volodymyr Vovchenko, Stefan Schramm et Horst Stoecker : Equation of state for hot QCD and compact stars from a mean field approach. *Phys. Rev. C*, 101(3):034904, 2020.

[74] W. Cassing : QCD thermodynamics and confinement from a dynamical quasiparticle point of view. *Nucl. Phys. A*, 791:365–381, 2007.

[75] Lecture on the njl model. http://theory.gsi.de/∼ebratkov/LecturesWS1819/Lecture_NJL.pdf.

[76] A.C. Aguilar, D. Binosi et J. Papavassiliou : The Gluon Mass Generation Mechanism: A Concise Primer. *Front. Phys. (Beijing)*, 11(2):111203, 2016.

[77] Hideo Suganuma, Takumi Iritani, Arata Yamamoto et Hideaki Iida : Lattice QCD Study for Gluon Propagator and Gluon Spectral Function. *PoS*, LATTICE2010:289, 2010.

[78] Reinhard Alkofer et Hugo Reinhardt : *Chiral Quark Dynamics*. Springer-Verlag, 1995.

[79] R.L. JAFFE Véronique BERNARD et U.-G. MEISSNER : Strangeness mixing and quenching in the nambu-jona-lasinio model. 1988.

[80] Gerard 't Hooft : Symmetry breaking through bell-jackiw anomalies. 1976.

[81] Gerard 't Hooft : How instantons solve the u(1) problem. 1986.

[82] Nathan Isgur et H.B. Thacker : On the origin of the ozi rule in qcd. 5 2000.

[83] B.Sintes : *Etude des baryons avec le modèle de Nambu et Jona-Lasinio, university of Nantes*. Thèse de doctorat, 2015.

[84] S.P. Klevansky : The Nambu-Jona-Lasinio model of quantum chromodynamics. *Rev. Mod. Phys.*, 64:649–708, 1992.

[85] J. Hubbard : Calculation of partition functions. *Phys. Rev. Lett.*, 3:77–78, Jul 1959.

[86] Roman N. Zhokhov : Фазовые переходы под влиянием внешних условий в низкоразмерных моделях теории поля. Thèse de doctorat, Serpukhov, IHEP, 11 2015.

[87] D. Ebert : Bosonization in particle physics. *Lect. Notes Phys.*, 508:103–114, 1998.

[88] Andrei Smilga : *Digestible Quantum Field Theory*. Springer, Cham, 2017.

[89] P. Rehberg et S.P. Klevansky : One loop integrals at finite temperature and density. *Annals Phys.*, 252:422–457, 1996.

[90] A.Biguet : *Modeles Nambu-Jona-Lasinio pour l'etude des phases de la chromodynamique quantique - qualites des predictions et phases hautes densites, university of Lyon*. Thèse de doctorat, 2016.

[91] Alexander A. Osipov et Brigitte Hiller : Path integral bosonization of the 't Hooft determinant: fluctuations and multiple vacua. *Phys. Lett. B*, 539:76–84, 2002.

[92] Pedro Costa, H. Hansen, M.C. Ruivo et C.A. de Sousa : How parameters and regularization affect the PNJL model phase diagram and thermodynamic quantities. *Phys. Rev. D*, 81:016007, 2010.

[93] Tetsuo Hatsuda et Teiji Kunihiro : QCD phenomenology based on a chiral effective Lagrangian. *Phys. Rept.*, 247:221–367, 1994.

[94] Michael I. Buchoff *et al.* : QCD chiral transition, U(1)A symmetry and the dirac spectrum using domain wall fermions. *Phys. Rev. D*, 89(5):054514, 2014.

[95] Sayantan Sharma, Viktor Dick, Frithjof Karsch, Edwin Laermann et Swagato Mukherjee : The $U_A(1)$ anomaly in high temperature QCD with chiral fermions on the lattice. *PoS*, LATTICE2015:198, 2016.

[96] Pedro Costa, M.C. Ruivo, C.A. de Sousa, H. Hansen et W.M. Alberico : Scalar-pseudoscalar meson behavior and restoration of symmetries in SU(3) PNJL model. *Phys. Rev. D*, 79:116003, 2009.

[97] Kenji Fukushima : Relation between the Polyakov loop and the chiral order parameter at strong coupling. *Phys. Rev. D*, 68:045004, 2003.

[98] Peter N. Meisinger, Michael C. Ogilvie et Travis R. Miller : Gluon quasiparticles and the polyakov loop. *Phys. Lett. B*, 585:149–154, 2004.

[99] Kenji Fukushima, Marco Ruggieri et Raoul Gatto : Chiral magnetic effect in the PNJL model. *Phys. Rev. D*, 81:114031, 2010.

[100] Claudia Ratti, Michael A. Thaler et Wolfram Weise : Phases of QCD: Lattice thermodynamics and a field theoretical model. *Phys. Rev. D*, 73:014019, 2006.

[101] Lisa M. Haas, Rainer Stiele, Jens Braun, Jan M. Pawlowski et Jürgen Schaffner-Bielich : Improved Polyakov-loop potential for effective models from functional calculations. *Phys. Rev. D*, 87(7):076004, 2013.

[102] Volodymyr Vovchenko, Mark I. Gorenstein et Horst Stoecker : van der Waals Interactions in Hadron Resonance Gas: From Nuclear Matter to Lattice QCD. *Phys. Rev. Lett.*, 118(18):182301, 2017.

[103] J. Hufner, S.P. Klevansky, P. Zhuang et H. Voss : Thermodynamics of a quark plasma beyond the mean field: A generalized Beth-Uhlenbeck approach. *Annals Phys.*, 234:225–244, 1994.

[104] Gerard 't Hooft : A Planar Diagram Theory for Strong Interactions. *Nucl. Phys. B*, 72:461, 1974.

[105] Juan M. Torres-Rincon et Joerg Aichelin : Equation of state of a quark-meson mixture in the improved Polyakov–Nambu–Jona-Lasinio model at finite chemical potential. *Phys. Rev. C*, 96(4):045205, 2017.

[106] E. Beth et G. Uhlenbeck : The quantum theory of the non-ideal gas. II. Behaviour at low temperatures. *Physica*, 4:915–924, 1937.

[107] V. Vovchenko, Long-Gang Pang, H. Niemi, Iu. A. Karpenko, M.I. Gorenstein, L.M. Satarov, I.N. Mishustin, B. Kämpfer et H. Stoecker : Hydrodynamic modeling of a pure-glue initial scenario in high-energy hadron and heavy-ion collisions. *PoS*, BORMIO2016:039, 2016.

[108] Claudio Bonati, Massimo D'Elia, Francesco Negro, Francesco Sanfilippo et Kevin Zambello : Curvature of the pseudocritical line in qcd: Taylor expansion matches analytic continuation. 2018.

[109] Aleksi Kurkela et Aleksi Vuorinen : Cool quark matter. *Phys. Rev. Lett.*, 117(4):042501, 2016.

[110] A. Vuorinen : The Pressure of QCD at finite temperatures and chemical potentials. *Phys. Rev. D*, 68:054017, 2003.

[111] K. Redlich J. Cleymans, H. Oeschler et S. Wheaton : Comparison of chemical freeze-out criteria in heavy-ion collisions. 2006.

[112] A. V Friesen, Yu. V. Kalinovsky et V. D. Toneev : Quark scattering off quarks and hadrons. *Nucl. Phys.*, A923:1–18, 2014.

[113] P. Rehberg, S. P. Klevansky et J. Hufner : Elastic scattering and transport coefficients for a quark plasma in SU-f(3) at finite temperatures. *Nucl. Phys.*, A608: 356–388, 1996.

[114] M. Tanabashi *et al.* : Review of Particle Physics. *Phys. Rev. D*, 98(3):030001, 2018.

[115] Rudy Marty, Elena Bratkovskaya, Wolfgang Cassing, Jörg Aichelin et Hamza Berrehrah : Transport coefficients from the Nambu-Jona-Lasinio model for $SU(3)_f$. *J. Phys. Conf. Ser.*, 509:012052, 2014.

[116] Eric Blanquier : *Le modèle de Polyakov, Nambu et Jona-Lasinio et ses applications pour décrire les particules sub-nucléaires*. Thèse de doctorat, Toulouse III U., 2013.

[117] Lecture models for heavy-ion collisions (part ii):transport models. http://http://theory.gsi.de/ẽbratkov/LecturesSS2019/Lecture_TransportModels_Part2.pdf.

[118] Hamza Berrehrah, Pol-Bernard Gossiaux, Jörg Aichelin, Wolfgang Cassing et Elena Bratkovskaya : Dynamical collisional energy loss and transport properties of on- and off-shell heavy quarks in vacuum and in the Quark Gluon Plasma. *Phys. Rev. C*, 90(6):064906, 2014.

[119] Hamza Berrehrah : *Quarkonia propagation and collectivity in a Quark Gluon Plasma: Towards the suppression of J/ψ suppression at high temperatures*. Thèse de doctorat, SUBATECH, Nantes, 12 2011.

[120] Rudolph C. Hwa et Xin-Nian Wang, éditeurs. *Quark-gluon plasma 4*. World Scientific, Singapore, 2010.

[121] P. Kovtun, Dan T. Son et Andrei O. Starinets : Viscosity in strongly interacting quantum field theories from black hole physics. *Phys. Rev. Lett.*, 94:111601, 2005.

[122] Ryogo Kubo : Statistical mechanical theory of irreversible processes. 1. General theory and simple applications in magnetic and conduction problems. *J. Phys. Soc. Jap.*, 12:570–586, 1957.

[123] P. Chakraborty et J.I. Kapusta : Quasi-Particle Theory of Shear and Bulk Viscosities of Hadronic Matter. *Phys. Rev. C*, 83:014906, 2011.

[124] J.L. Anderson et H.R. Witting : Relativistic quantum transport coefficients. *Physica*, 74(3):489 – 495, 1974.

[125] Chihiro Sasaki et Krzysztof Redlich : Transport coefficients near chiral phase transition. *Nucl. Phys. A*, 832:62–75, 2010.

[126] M. Albright et J.I. Kapusta : Quasiparticle Theory of Transport Coefficients for Hadronic Matter at Finite Temperature and Baryon Density. *Phys. Rev. C*, 93(1):014903, 2016.

[127] Lata Thakur, P.K. Srivastava, Guru Prakash Kadam, Manu George et Hiranmaya Mishra : Shear viscosity η to electrical conductivity σ_{el} ratio for an anisotropic QGP. *Phys. Rev. D*, 95(9):096009, 2017.

[128] Olga Soloveva, Pierre Moreau et Elena Bratkovskaya : Transport coefficients for the hot quark-gluon plasma at finite chemical potential μ_B. *Phys. Rev. C*, 101(4):045203, 2020.

[129] J.D. Bjorken : Highly Relativistic Nucleus-Nucleus Collisions: The Central Rapidity Region. *Phys. Rev. D*, 27:140–151, 1983.

[130] Chiho Nonaka et Masayuki Asakawa : Modeling a Realistic Dynamical Model for High Energy Heavy Ion Collisions. *PTEP*, 2012:01A208, 2012.

[131] Michael L. Miller, Klaus Reygers, Stephen J. Sanders et Peter Steinberg : Glauber modeling in high energy nuclear collisions. *Ann. Rev. Nucl. Part. Sci.*, 57:205–243, 2007.

[132] Edmond Iancu : The Color glass condensate. *Nucl. Phys. A*, 715:219–232, 2003.

[133] H.J. Drescher, M. Hladik, S. Ostapchenko, T. Pierog et K. Werner : Parton based Gribov-Regge theory. *Phys. Rept.*, 350:93–289, 2001.

[134] Paul Romatschke : New Developments in Relativistic Viscous Hydrodynamics. *Int. J. Mod. Phys. E*, 19:1–53, 2010.

[135] Yu.M. Sinyukov, S.V. Akkelin, Iu.A. Karpenko et Yogiro Hama : Kinetics versus hydrodynamics: Generalization of Landau/Cooper-Frye prescription for freeze-out. *Acta Phys. Polon. B*, 40:1025–1036, 2009.

[136] Fred Cooper et Graham Frye : Single-particle distribution in the hydrodynamic and statistical thermodynamic models of multiparticle production. *Phys. Rev. D*, 10:186–189, Jul 1974.

[137] Jeffrey R. Forshaw et D.A. Ross : *Quantum chromodynamics and the pomeron*, volume 9. Cambridge University Press, 1 2011.

[138] Marcel Froissart : Asymptotic behavior and subtractions in the Mandelstam representation. *Phys. Rev.*, 123:1053–1057, 1961.

[139] Bo Andersson, G. Gustafson, G. Ingelman et T. Sjostrand : Parton Fragmentation and String Dynamics. *Phys. Rept.*, 97:31–145, 1983.

[140] Benjamin Guiot et Klaus Werner : Hard probes and the event generator EPOS. *J. Phys. Conf. Ser.*, 589(1):012008, 2015.

[141] Lipei Du et Ulrich Heinz : (3+1)-dimensional dissipative relativistic fluid dynamics at non-zero net baryon density. *Comput. Phys. Commun.*, 251:107090, 2020.

[142] Masakiyo Kitazawa, Grégoire Pihan, Nathan Touroux, Marcus Bluhm et Marlene Nahrgang : Critical fluctuations in a dynamically expanding heavy-ion collision. *In 28th International Conference on Ultrarelativistic Nucleus-Nucleus Collisions*, 2 2020.

[143] K. Werner, B. Guiot, Iu. Karpenko et T. Pierog : Analysing radial flow features in p-Pb and p-p collisions at several TeV by studying identified particle production in EPOS3. *Phys. Rev. C*, 89(6):064903, 2014.

[144] K. Werner, Iu. Karpenko, T. Pierog, M. Bleicher et K. Mikhailov : Event-by-Event Simulation of the Three-Dimensional Hydrodynamic Evolution from Flux Tube Initial Conditions in Ultrarelativistic Heavy Ion Collisions. *Phys. Rev. C*, 82:044904, 2010.

[145] Qing-feng Li, Jan Steinheimer, Hannah Petersen, Marcus Bleicher et Horst Stocker : Effects of a phase transition on HBT correlations in an integrated Boltzmann+Hydrodynamics approach. *Phys. Lett. B*, 674:111–116, 2009.

[146] P. Batyuk, Iu. Karpenko, R. Lednicky, L. Malinina, K. Mikhaylov, O. Rogachevsky et D. Wielanek : Correlation femtoscopy study at energies available at the JINR Nuclotron-based Ion Collider fAcility and the BNL Relativistic Heavy Ion Collider within a viscous hydrodynamic plus cascade model. *Phys. Rev. C*, 96(2):024911, 2017.

[147] Christoph Herold, Marlene Nahrgang, Igor Mishustin et Marcus Bleicher : Formation of droplets with high baryon density at the QCD phase transition in expanding matter. *Nucl. Phys. A*, 925:14–24, 2014.

[148] Jan Steinheimer et Jorgen Randrup : Spinodal amplification of density fluctuations in fluid-dynamical simulations of relativistic nuclear collisions. *Phys. Rev. Lett.*, 109:212301, 2012.

[149] Ulrich Heinz, Chun Shen et Huichao Song : The viscosity of quark-gluon plasma at RHIC and the LHC. *AIP Conf. Proc.*, 1441(1):766–770, 2012.

[150] Bohao Feng, Carsten Greiner, Shuzhe Shi et Zhe Xu : Viscous effects on the dynamical evolution of QCD matter during the first-order confinement phase transition in heavy-ion collisions. *Phys. Lett. B*, 782:262–267, 2018.

[151] N.K. Glendenning : *Compact stars: Nuclear physics, particle physics, and general relativity.* 1997.

[152] Max Camenzind : *Compact objects in astrophysics : white dwarfs, neutron stars, and black holes.* 2007.

[153] 8 - on the theory of stars. *In* D. TER HAAR, éditeur : *Collected Papers of L.D. Landau*, pages 60 – 62. Pergamon, 1965.

[154] J. Chadwick : The Existence of a Neutron. *Proc. Roy. Soc. Lond. A*, 136(830):692–708, 1932.

[155] A. Hewish, S.J. Bell, J.D.H Pilkington, P.F. Scott et R.A. Collins : Observation of a rapidly pulsating radio source. *Nature*, 217:709–713, 1968.

[156] T. Gold : Rotating neutron stars as the origin of the pulsating radio sources. *Nature*, 218:731–732, 1968.

[157] B.P. Abbott *et al.* : Observation of Gravitational Waves from a Binary Black Hole Merger. *Phys. Rev. Lett.*, 116(6):061102, 2016.

[158] R. Abbott *et al.* : GW190814: Gravitational Waves from the Coalescence of a 23 Solar Mass Black Hole with a 2.6 Solar Mass Compact Object. *Astrophys. J. Lett.*, 896(2):L44, 2020.

[159] Paul Demorest, Tim Pennucci, Scott Ransom, Mallory Roberts et Jason Hessels : Shapiro Delay Measurement of A Two Solar Mass Neutron Star. *Nature*, 467:1081–1083, 2010.

[160] D.G. Yakovlev P.Haensel, A.Y.Potekhin : *Neutron Star 1.* Springer, 2007.

[161] A.R. Bodmer : Collapsed nuclei. *Phys. Rev. D*, 4:1601–1606, 1971.

[162] Edward Witten : Cosmic separation of phases. *Phys. Rev. D*, 30:272–285, Jul 1984.

[163] K. Schertler, C. Greiner, J. Schaffner-Bielich et M.H. Thoma : Quark phases in neutron stars and a 'third family' of compact stars as a signature for phase transitions. *Nucl. Phys. A*, 677:463–490, 2000.

[164] J.R. Oppenheimer et G.M. Volkoff : On Massive neutron cores. *Phys. Rev.*, 55:374–381, 1939.

[165] F. Douchin et P. Haensel : A unified equation of state of dense matter and neutron star structure. *Astron. Astrophys.*, 380:151, 2001.

[166] Tetsufumi Hirano, Naomi van der Kolk et Ante Bilandzic : Hydrodynamics and Flow. *Lect. Notes Phys.*, 785:139–178, 2010.

[167] S.P. Klevansky et Richard H. Lemmer : Spectral density functions and their sum rules in an effective chiral field theory. 7 1997.

[168] Michael Buballa : NJL model analysis of quark matter at large density. Other thesis, 2005.

DOCTORAT MATIERE BRETAGNE MOLECULES LOIRE ET MATERIAUX

UNIVERSITÉ DE NANTES

Titre : Dynamique et thermodynamique du Lagrangien NJL

Mots clés : PNJL, Hadronisation, diagramme de phase, interaction forte, QCD, QGP

Résumé : Cette thèse présente une étude du modèle PNJL permettant de déterminer le diagramme de phase de la matière QCD à basse température et potentiel chimique fini. Le modèle est poussé au-delà du champ moyen, incluant les contributions mésoniques à la pression du système et reparamétriser afin de décrire une transition confinement-déconfinement tenant compte phénoménologiquement de la présence des quarks dans le milieu. L'équation d'état qui en découle est en accord avec les résultats de la QCD sur réseau. Les résultats obtenus sont utilisés dans le cadre d'applications pratiques tels que le calcul des coéfficients de transport du Plasma de Quarks et de Gluons ou encore l'expansion hydrodynamique du plasma qui fait intervenir l'équation d'état et permet une étude dynamique de l'influence d'une transition de phase du première ordre lors des collisions d'ions lourds. Ce travail se termine par une étude de la relation masse-rayon des étoiles à neutron impliquant aussi l'utilisation d'une équation d'état. Ce travail permet de mieux comprendre en quoi l'équation d'état peut être encore améliorer, notamment par l'ajout des baryons, contribution non négligeable à la thermodynamique du milieu à basse température et densité finie.

Title : Dynamics et thermodynamics of the NJL Lagrangian

Keywords : PNJL, Hadronisation, phase diagram, strong interaction, QCD, QGP

Abstract : This thesis presents a study of the PNJL model that allows for a determination of the phase diagramme of the QCD matter at low temperature and finite chemical potential. The model goes beyond mean field, including mesonic contributions to the pressure of the medium and is reparametrised in order to describe confinement-deconfinement phase transition phenomenologically taking into account the presence of quarks in the medium. The equation of state calculated from the model turns out to be in agreement with the lattice results. The results obtained are used for practical applications like the determination of the transport coefficients of the Quark Gluons Plasma or the hydrodynamic expansion of the plasmas which requires the equation of state and allows for a dynamic study of the influence of the first order phase transition on the heavy ion collisions. This work ends with the study mass-radius relation of neutron stars that also makes use of the equation of state. This work allows for a better understanding of the manner in which the equation of state could be improved, especially by adding the baryonic contribution to the medium, non negligible at low temperature and finite densities.